A Study of Drug Transport in the Vitreous Humor: Effect of Drug Size; Comparing Micro- and Macro-scale diffusion; Assessing Vitreous Models; and Obtaining In Vivo Data

by

Rhiad Tariq Christopher Gajraj

A thesis submitted in conformity with the requirements
for the degree of Masters of Applied Sciences

Chemical Engineering and Applied Chemistry
University of Toronto

A Study of Drug Transport in the Vitreous Humor: Effect of Drug Size; Comparing Micro- and Macro-scale diffusion; Assessing Vitreous Models; and Obtaining In Vivo Data

Rhiad Gajraj

Masters of Applied Sciences

Chemical Engineering and Applied Chemistry
University of Toronto

2012

Abstract

Treatment of vision impairing diseases involves drug transport through the vitreous humor. Diffusion cells were used to measure macro-scale (mutual) diffusivity (D_m) to understand how solute size affects diffusion through the vitreous humor of rabbit and porcine eyes. Solutes examined included timolol maleate, dexamethasone sodium phosphate (DMSP), sodium fluorescein, and FITC-dextrans (4, 40, and 150kDa). Diffusivity was inversely dependent on solute size. The D_m's of small solutes in the vitreous were 30 – 65% of that in PBS, while the D_m's of large solutes were 40 – 60% of that in PBS. Extrapolations to the human eye produced similar results using diffusivities based on either species. We used Diffusion Ordered NMR Spectroscopy to measure micro-scale (self) diffusivity (D_s) of DMSP through vitreous humor. The D_s and D_m were significantly different in PBS, but similar in vitreous. A method for obtaining in vivo imagery and data of vitreous fluorophore distribution is also presented.

Acknowledgments

I would like to acknowledge the 20/20 NSERC Ophthalmic materials Network for their financial support of this project. I am forever grateful to Professor Yu-Ling Cheng for her academic guidance and supervision, and for my first set of golf clubs. I would like to send special thanks to Prof. Shelley Boyd and Dr. Christine Zhao for their assistance with the in vivo aspect of this project. I wish to express my appreciation for Dr. Darcy Burns' help, patience and guidance in the use of NMR technology for measuring self diffusivity. I must thank my family, relatives and friends for their love and support, and for always believing in me. Lastly, but certainly not least, I would like to say thank you to my close "buddies" for the many intellectual and downright silly conversations we've had throughout these last two years. The numerous moments of enlightenment, and the many laughs I enjoyed were all a welcome relief from the mental stress often derived from research.

Table of Contents

List of Tables

List of Figures

List of Appendices

1 Background

1.1 Ocular Anatomy

The eye is an isolated sensory organ with its anatomy divided into an anterior and posterior segment. The anterior segment is composed of the cornea, lens, iris, ciliary body and aqueous humor, while the posterior segment comprises the photoreceptive retina, posterior sclera, choroid and vitreous humor (see Figure 1). The lens divides the two segments, and is common to both.

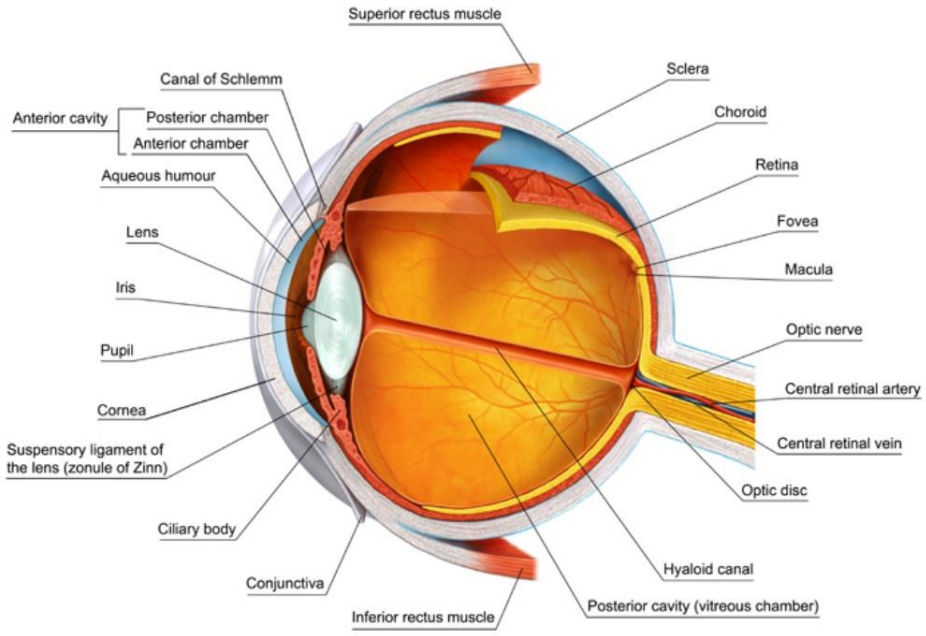

Figure 1 The anatomy of the eye (reproduced with permission from [1]).

1.1.1 The Cornea

The cornea forms the strongest refractive entity of the eye, contributing two-thirds of the refractive power of this organ [2]. It is completely avascular and is composed of three main layers. These layers, beginning at the anterior of the cornea, are the epithelium, the stroma and the endothelium. The stroma makes up 90% of the cornea's structure and is composed of collagen fibers, proteoglycans and approximately 78% water. The stroma is composed of collagen fibers and proteoglycans. Without interweaving, the collagen fibers are laid down at

right angles to each other. This arrangement allows for the transmittance of 99% of incident visible radiation [3].

1.1.2 The Lens

The lens is the transparent biconvex epithelial tissue that is responsible for accommodation and refraction of light. This structure is avascular and is made up of a dense inner cortex and an elastic outer capsule. The bulk of the lens is made up of elongated lens fiber cells which are precisely aligned to maintain transparency and a high refractive index.

1.1.3 The Iris

The iris is a colored muscular tissue attaching peripherally to the ciliary body. It controls the amount of light entering the pupil. The iris also divides the anterior segment into the anterior and posterior chambers. The stroma of the iris contains the dilator and sphincter muscles. The dilator muscle relaxes the iris to increase the amount of light that enters the pupil, while the sphincter muscle constricts the iris to achieve the opposite effect.

1.1.4 The Ciliary Body

The ciliary body is located between the choroid and iris. It is divided into two sections, the anterior pars plicata and the posterior pars plana. The pars plicata comprises the ciliary muscles and ciliary processes. The ciliary muscles are attached to the zonules of the lens by the ciliary processes. These muscles pull on the zonules to change the shape of the lens in order to adjust the accommodation. In addition to connecting the ciliary muscles to the zonules, the ciliary processes also produce the aqueous humor that flows into the anterior chamber through the pupil.

1.1.5 Aqueous Humor

The aqueous humor (also referred to as the “aqueous”) is a flowing fluid that fills the anterior chamber, the space between the cornea and iris. This fluid is produced by the ciliary processes and is ejected through the trabecular meshwork into the canal of Schlemm which leads into episcleral veins. The ciliary processes of the human eye produce aqueous humor at a rate of 2 to 2.5 μL/min [2]. The production of the aqueous humor results in the intraocular pressure (IOP) of the eye. The disruption of this flow results in glaucoma, a disease that causes the IOP to become

abnormally high. The composition of the aqueous humor is similar to that of blood plasma. A major function of the aqueous is to provide nutrients for the cornea and lens.

1.1.6 The Retina

The retina is the light sensory tissue which lines the posterior two-thirds of the eye. It contains the photochemicals and neurologic connections which convert the light entering the eye to neural impulses that are relayed to the brain via the optic nerve. The retina is supplied with blood by a layer of large choroidal vessels and capillaries. Immediately inside this vascular layer is the retina pigment epithelium (RPE) layer and the inner neurosensory layer (rods, cones and ganglion cells). The RPE is a single layer of tightly joined cells which forms a barrier that prevents the diffusion of some substances between the choroid and the neurosensory layer. The photoreceptor cells of the retina are the rods and cones. The rods, the majority of which are in the periphery of the retina, are responsible for peripheral and low luminance vision. The cones, clustered mainly in the macula, provide color vision and central detailed vision. Inner to the rods and cones is the bipolar layer which serves as neural transmitters to the ganglion cell layer. The ganglion cell layer is the last neural connector which converges to form the optic nerve that ultimately transmits the neural impulses.

1.1.7 The Choroid

The choroid is the dense network of blood vessels that covers the retina. These blood vessels are of two types. The first category is the choriocapillaris, which are small capillaries that form the innermost layer of the choroid. The second group of blood vessels is composed of larger arteries and veins, which are posterior to the choriocapillaris. The blood flow from the choroid provides nutrients to the RPE.

1.1.8 The Sclera

The sclera is the white colored part of the eye. This tissue is composed mainly of collagen fibers. However, unlike the collagen fibers of the cornea’s stroma, those of the scelra are arranged in a disorganized manner. This haphazard arrangement results in the opacity of the sclera. The main function of this tissue is to provide a protective layer for the internal components of the eye.

1.1.9 The Vitreous Humor

The vitreous humor, sometimes referred to as “the vitreous body” or just “the vitreous”, is a transparent, gel-like structure that accounts for about four fifths of the eye’s volume [4], [5]. Towards the anterior segment of the eye, it is bordered by the lens, zonules and ciliary body (see Figure 1). In the posterior segment, the vitreous humor is enclosed by and adjoins the retina. It serves as a mechanical buffer for the surrounding tissues, and assists in the maintenance of intraocular pressure. Transparency of the vitreous body provides an uninhibited path for light to be transmitted to the retina.

1.2 Ocular Diseases

Many sight threatening diseases occur within the posterior segment causing vision impairment and even irreversible blindness [6], [7]. Some of these diseases include age-related macular degeneration (AMD), retinitis pigmentosa, endophthalmitis, and diabetic retinopathy. Currently, an estimated two million Americans [8] and one million Canadians [9], aged 50 and older, suffer from AMD. The number of people affected with AMD in the U.S. has been projected to increase to 3 million by 2020 [10]. One of the most important complications in intraocular surgery is postoperative endophthalmitis, which is bacterial in origin [11]. This disease has an incidence of 0.05-0.33% in those that undergo intraocular surgery, with more than 50% of all such cases suffering irreversible vision loss [11]. About 30 – 40% of patients suffering from acquired immune deficiency syndrome (AIDS) subsequently develop vision loss due to cytomegalovirus retinitis [11], a disease that causes inflammation of the retina. Based on data from the US National Health and Nutrition Examination Survey, there is a 28.5% prevalence of diabetic retinopathy among diabetic patients in the US, with 4.4% that have progressed to the vision threatening level [12]. A major complication of diabetic retinopathy is diabetic macular edema characterised by a breakdown in the blood-retinal barrier that results in intraretinal accumulation of fluid. Of those that suffer from diabetic retinopathy, 29% have clinically significant macular edema [13].

1.3 Drug Therapy

Treatment of ocular diseases is often difficult as the eye is well protected from systemic access by the blood-retinal and blood aqueous barriers [6], [11], [14]. Due to lachrymal flow and

aqueous humor efflux, topical drug delivery has very poor treatment efficiency with only about 3 – 5 % of the applied dosage being delivered to the anterior segment, and negligible amounts actually reaching the posterior segment [6], [7], [15], [16]. The blood-retinal and blood-aqueous barriers make it difficult to achieve therapeutic levels via systemic drug administration [6], [7], [17]. Also, compared to other larger organs, the eye is one of the smaller organs of the body receiving a proportionally smaller blood supply. High drug concentrations are therefore required in systemic administration for therapeutic amounts to penetrate the blood-retinal barriers, which in turn increases the risk of adversely affecting non-targeted tissues in the body [16]. It is therefore clear that systemic and topical modes of administration are not effective means of treating posterior segment diseases. More direct approaches such as intravitreal and transscleral delivery [6], [18–20] are used instead.

Intravitreal injection of drug solutions and surgical insertion of drug delivery systems into the posterior segment allow drugs to be administered directly into the vitreous humor. Clinical studies have shown that therapeutic tissue levels are attained via intravitreal drug delivery [6], [21]. In the case of injections, patients must endure the discomfort of repeated deliveries. Vitreous implants such as the Vitrasert® ganciclovir implant offer sustained drug release kinetics [6], [16], [21]. However, such devices must be implanted by intraocular surgery, and must be periodically replaced. The use of these systems has potential side effects similar to those associated with intravitreal injections, which include cataract, retinal detachment, haemorrhage and endophthalmitis.

Transscleral drug delivery, which is safer and less invasive, involves the placement of sustained drug release devices into the surrounding tissues of the posterior segment of the eye. Transscleral approaches can be subconjunctival, retroseptal, perilimbal or via the posterior sub-Tenon's [16], [22]. In recent years, this method has been explored with great interest. For example, clinical trials have been conducted for the sub-Tenon's infusion of triamcinolone acetonide [23–26]. Despite the great interest in transscleral drug delivery, it is still not as clinically effective as intravitreal drug delivery in treating retinal diseases [23]. A study on the delivery of prednisolone via subconjunctival injection reported that the bioavailability within the vitreous ranged from 0.01-0.1% [27].

1.4 Pharmacokinetic Models

Many drugs that are used to treat vitreoretinal diseases have a narrow therapeutic range above which they become toxic [28], [29]. Tools that can accurately predict the biodistribution of a drug for transscleral or intravitreal drug delivery would help determine drug concentrations at the targeted tissue site for a given dosage, and would therefore be valuable in the design of both drugs and drug delivery systems. Many have attempted to predict drug distribution in the eye by using advanced computer software to develop ocular pharmacokinetic (PK) models that can be used to simulate the distribution and elimination of solutes from the posterior eye [7], [15], [17], [30–36]. Such models are already being used to guide the development of drug delivery strategies, and to better understand the clearance mechanisms of the eye's physiology. For example, developers of the intravitreal drug delivery device Iluvien™ [19], used to treat diabetic macular edema (DME), have referred to intravitreal drug distribution models for guidance on where this device should be placed in the vitreous humor. These models indicated that placing the device at the inferior vitreous humor close to the equator (see Figure 2) would ensure that most of the drug reaches the retina for treatment of DME. Delivering Iluvien™ this way takes advantage of the posteriorly directed vitreous humor flow, which minimizes drug flow towards the anterior chamber thus preventing drug exposure of the trabecular meshwork.

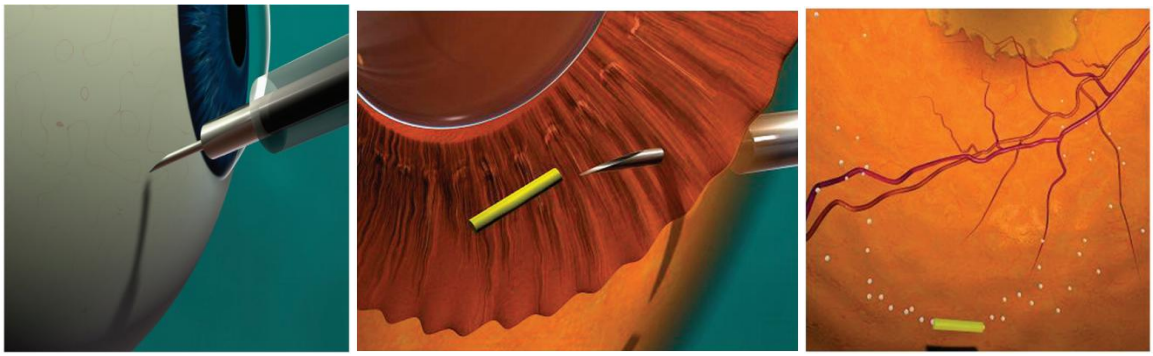

(a) (b) (c)

Figure 2 Delivery of Iluvien™ to the posterior segment (reproduced with permission from [19]) (a) Site of insertion, (b) Interior view of the delivery of the Iluvien™ insert, (c) Location of Iluvien insert at inferior vitreous humor.

Drug distribution models consist of:

1. the governing equations and boundary/initial conditions that describe the transport and reaction processes of interest within the region of interest, such as the sclera, choroid, retina, vitreous; and
2. the values of parameters that are required in the governing equations, e.g., drug diffusivity, hydraulic conductivity, retinal permeability

Several models have been reported, and researchers continue to refine models to better account for all aspects of the ocular anatomy and physiology [7], [35]. However, due to limited available data for real drugs, most of these models use data for drug surrogates such as sodium fluorescein. The real value of ocular PK modeling will not be realized until it can be used to predict the biodistribution of real drugs. Progression is currently hindered by the limited availability of data on ocular transport parameters of drugs, i.e., the diffusivity within the vitreous humor and permeability across posterior segment tissues such as the sclera, choroid and retina.

The diffusivity of drugs in the vitreous humor will be the focus of this thesis. This parameter is the common governing factor for both intravitreal and transscleral drug delivery. Since intravitreal drug delivery involves direct administration within the vitreous humor (see Figure 3), the transport of drugs is governed by both convection and diffusion [7], [15], [32]. It has been shown that diffusion is the primary contributor for the transport of molecules within the vitreous humor, but that the effect of convection becomes more pronounced for large molecules [32]. In transscleral delivery, the drug must permeate inwards across the posterior segment tissues starting from the episcelra or from the suprachoroidea [37], and emerge into the vitreous through the RPE layer (see Figure 3) . The sclera is the thickest of all the posterior segment tissues [38], with its thinnest region at the equator [22], [39]. This feature makes the equatorial region the prime position for drug instillation. However, the downside to equatorial placement is that drug molecules that do permeate into the vitreous humor must still be transported over a considerably large distance to reach targeted areas, such as the macula, in order to treat diseases like DME and AMD. This aspect of transscleral administration makes transport in the vitreous humor a prominent factor for this drug delivery method.

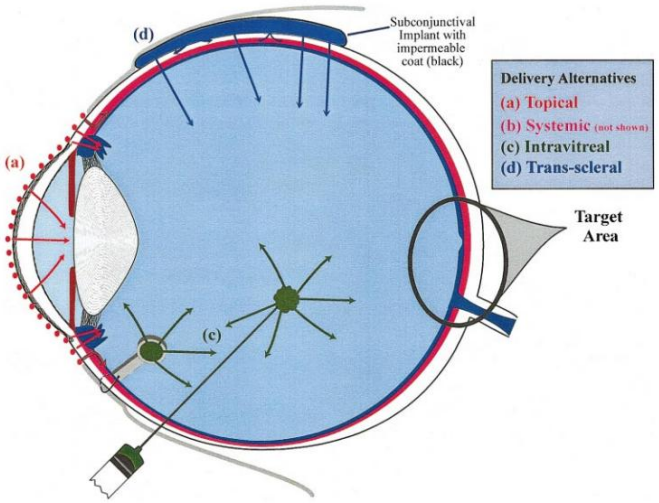

Figure 3 Drugs delivered through intravitreal and transscleral routes must diffuse through the vitreous to reach the target site (reproduced with permission from [16]).

1.5 Characteristics of the Vitreous Humor

1.5.1 Physical and Chemical Properties

The vitreous humor contains 99% water, yet it behaves like a gel. This is due to a meshwork of long, thin, nonbranching collagen fibrils that are suspended in a network of hyaluronan that stabilize the collagen conformation and reinforce the vitreous structure [38], [40] (see Figure 4). The human vitreous weighs about 4g and has a volume of approximately 4ml [40].The average viscosity of the human vitreous has been reported to range from 300 to 2000 times that of water [41] and the intravitreal pH has been estimated to range from 7 to 7.4 [42].

1.5.2 Macromolecular Structures

Collagen and hyaluronan (also referred to as hyaluronic acid) comprise the majority of the non-aqueous composition of the vitreous humor [4], [40], [43]. Type II collagen is the primary collagenous constituent of the vitreous contributing 80% of the total vitreous collagen [5]. This protein consists of three polypeptide chains (α-chains) which form a right handed triple helix [43], [44]. These fibrils are unbranched and are assumed to be anchored at the basal laminae of the retina at one end and attached to the basal laminae of the ciliary epithelium at the other end

[38]. The diameter of the vitreous collagen fibrils vary from 10 to 30 nm in all species examined [5], [44].

Hyaluronan is the major glycosaminoglycan (GAG) found in the vitreous humor [5] . GAGs are polysaccharides composed of repeating disaccharide units, each composed of hexosamine (usually N acetyl glucosamine or N- acetyl galactosamine) glycosidically linked to either uronic acid or galactose [5], [44]. Vitreous hyaluronan has a molecular weight that varies from 3000 to 4500 kDa [38]. The volume of the unhydrated dry molecule is 0.66 cm^3/g, whereas its volume in physiological salt solution is 2000 to 3000 cm^3/g. In their hydrated form, these molecules occupy a large volume and become entangled above 300 -500 µg/ cm^3 [38]. This entanglement forms the network of hyaluronan that contributes to the gel-like structure of the vitreous body [38]. However, the interaction between collagen fibrils and hyaluronan is what primarily accounts for the viscoelastic properties of the vitreous gel (see Figure 4). It is believed that the hyaluronan molecules are bound to the collagen fibrils via the GAGs of chondroitin sulphate proteoglycan and heparan sulphate proteoglycan [5], [45]. The macromolecular composition of the vitreous body varies across species [38]. The hyaluronan concentration of the human vitreous is similar to that of the rhesus monkey (192 µg/ml). However, this concentration is less than that of bovine vitreous (496 ±44 µg/ml) [46]. Collagen concentration is greater in the human vitreous (300 µg/ml) compared to that in bovine vitreous (60 µg/ml) [5].

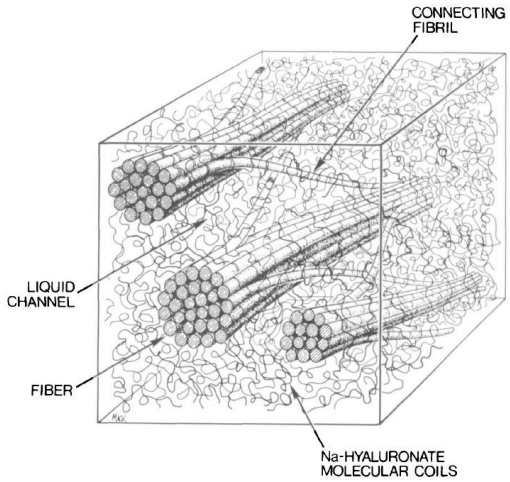

Figure 4 Schematic diagram of the ultrastructure of the adult human vitreous humor. Collagen fibrils aggregate into bundles and form fibers. Hyaluronan and water molecules fill the interfibrillar space (reproduced with permission from [47]).

1.5.3 Anatomical Elements

The vitreous humor is heterogeneous in consistency, thus giving rise to a number of distinct regions within the vitreous (see Figure 5). An S-shaped channel free of collagen fibrils extends from the optic disc to the posterior lens [4]. This conduit is Cloquet's canal and represents the remainder of the hyaloid artery that supplies a dense network of blood vessels around the lens in the embryonic stages [45]. Cloquet's canal is 1 to 2 mm wide in the region adjacent to the lens, while posteriorly towards the optic nerve, its width is about 4 to 5 mm [4]. The outer layer of the vitreous humor is known as the vitreous cortex, and is composed of densely packed collagen fibrils, cells and proteins [4]. It has an average thickness of 200 μm but is generally thicker in the region next to the ciliary body and lens than in the region adjacent to the retina [45]. The hyaloid (or hyaloid membrane) is an aggregation of collagen fibrils that forms the anterior surface of the vitreous body, thus forming the boundary between the aqueous and vitreous humor [38], [40]. The vitreous collagen is most dense in the anterior cortex where it fuses with the basement membrane of the pars plana epithelium and the inner limiting membrane of the anterior retina. This point of anchorage is called the vitreous base, and it is the strongest point of attachment to the surrounding posterior segment tissues [38], [45]. Without covering the fovea and optic nerve head, the cortex forms ring-like attachments to the retina around these structures to form the premacular and prepapillary holes respectively [4], [45]. These two features also serve as strong attachments for the vitreous body [4].

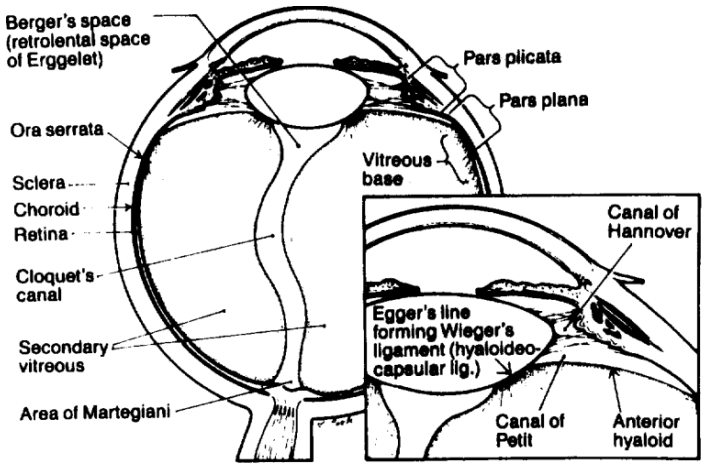

Figure 5 Schematic diagram of the vitreous humor's anatomy according to classical anatomic/histological studies (reproduced with permission from [5]).

1.5.4 Vitreous Subdivisions

Cloquet's canal represents the remainder of the embryonic hyaloid artery, and the first of the vitreous humor that develops; this region is therefore referred to as the primary vitreous. All remaining elements outside the canal comprise the secondary vitreous [4], [45]. Some investigators also regard the vitreous humor as being divided into a gel phase and a liquid phase, respectively called the gel vitreous and liquid vitreous [38] (see Figure 6). The gel vitreous contains the collagen fibrils and is essentially the vitreous cortex. The liquid vitreous is contained within the vitreous cortex and is composed mainly of water and hyaluronan. These liquid and gel components can be separated by filtration making it possible to assess the amount of each phase in the vitreous body [40], [45]. In many species, which include those commonly used for ophthalmic studies, such as cattle, dogs, cats and rabbits, the entire vitreous space is filled with gel vitreous throughout their lifespan. However, for humans, some monkeys (rhesus, owl) and in all birds and fishes, the vitreous body is filled with both gel and liquid vitreous [38].

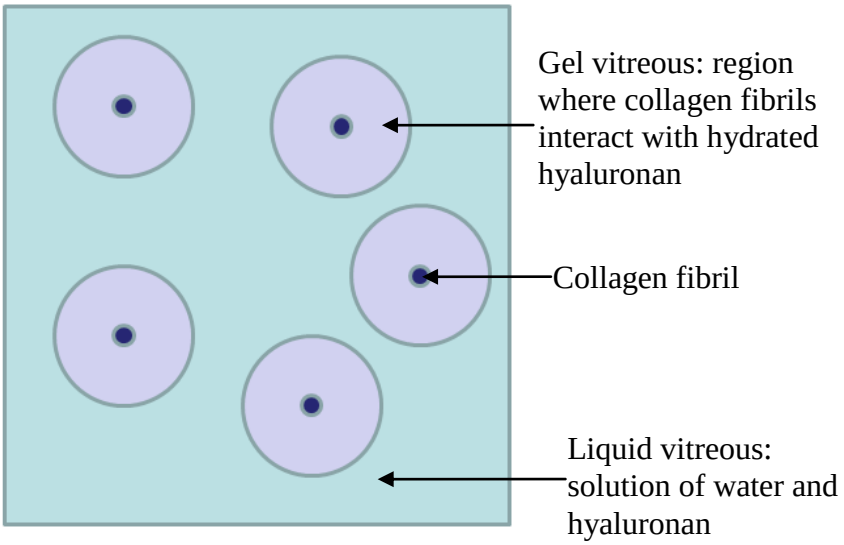

Figure 6 Schematic showing representation of gel vitreous and liquid vitreous (adapted from [45]).

1.5.5 Aging of the Vitreous Humor

As the vitreous humor ages, it undergoes liquefaction [38], [43–45] as shown in Figure 7. Liquefaction is prominent in the central vitreous where collagen concentration is the lowest [43]. The mechanism of liquefaction is not clearly understood, but it is believed to involve

conformational changes of the collagen [43–45]. Beyond the age of 20 years, the total vitreous collagen no longer increases and has been found to remain constant. However, the collagen concentration in the gel vitreous was shown to increase after the ages of 40 to 50 [38]. Since the total collagen content of the human vitreous body does not change, yet the collagen concentration of the gel vitreous increases, it has been posited that the volume reduction of the gel phase is due to the aggregation of the collagen fibrillar network [38], [45]. The predominant cell type of the vitreous body is the hyalocytes [38], [44]. These cells are thought to be responsible for the production of hyaluronan, which is the major macromolecular constituent of the vitreous liquid phase [4], [38], [48]. Studies have shown that there is a decrease in these vitreous cells with the progression of age. For each region of the vitreous body studied, the quantity of cells in younger animals (rabbit and cattle) exceeded that of older ones [40], [44].

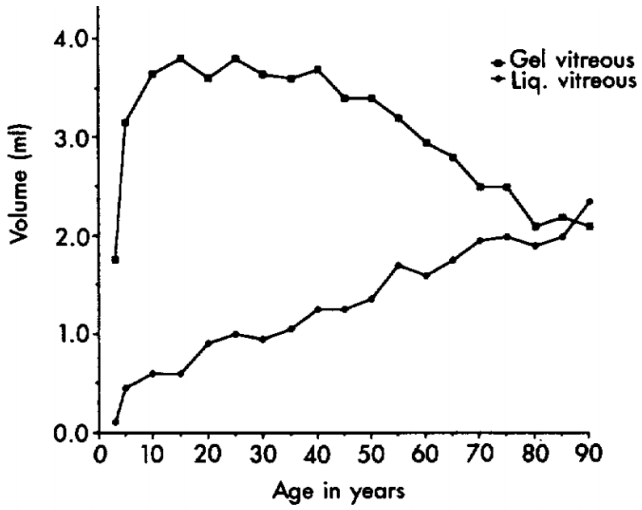

Figure 7 Liquefaction of human vitreous. The volumes of gel and liquid vitreous in 610 fresh, unfixed human eyes were measured post-mortem, and the results were plotted versus the age of the donor (reproduced with permission from [5]).

1.6 Drug Transport in the Vitreous Humor

Much work has been done in trying to understand the effect of the physicochemical properties of drugs on permeability through ocular tissues such as the cornea [49], [50],sclera [39], [49–52], conjunctiva [50], choroid [51], [53], and retina [54]. Most of these studies determine permeability with the use of diffusion cells in conjunction with assay methods such as UV-visible spectrophotmetry or high performance liquid chromatography. The effect of the

physicochemical properties of drugs on their transport through the vitreous humor has received comparatively little attention. Table 1 summarizes studies that have examined the transport of various molecules through the vitreous humor by measuring their diffusion coefficients.

Many different techniques have been used to determine diffusion coefficients of drugs. A common in vivo method, using human subjects, is to administer sodium fluorescein orally or intravenously, and then measure the change in fluorescein concentration in the vitreous along the optical axis with time using slit lamp fluorophotometry [55–57]. The diffusion coefficient is then obtained by fitting a time dependent function to the concentration profiles. Despite the fact that multiple studies have examined diffusion of sodium fluorescein through human vitreous humor, there is significant variation in the diffusion coefficients reported (see Table 1). This may be attributed to a difference in the interpretation of fluorescence data. Engler et al. [56] accounted for the presence of the fluorescein metabolite, fluorescein glucuronide, whereas Lund-Anderson et al. [55] and Zeimer et al. [57] did not. Magnetic resonance imaging (MRI) is an effective tool for obtaining dynamic 3-D imagery of the dispersion of a paramagnetic agent. This technique has been used to visualize in vivo the distribution of gadolinium-labeled albumin [58] in rabbit vitreous humor that was administered by intravitreal injection. The diffusion coefficient of this compound was estimated by fitting an equation to the distribution data, which described radial diffusion from a spherical source with known initial concentration and radius. A major disadvantage with MRI is that it only applies to paramagnetic compounds. However, MRI provides the greatest detail of distribution with the ability to achieve three dimensional resolutions. Vitreous fluorophotometry, on the other hand, can only provide one dimensional data along the optical axis.

One commonality among these studies [55–58] is that the mathematical models used to fit the data did not account for convection within the vitreous humor. Whether there is significant bulk flow in the vitreous humor has been debated since the late 1800s. Earlier authorities [38], [40] have regarded the vitreous humor as a mostly stagnant gel thereby taking diffusion to be the primary means of drug transport in this part of the eye. Earlier pharmacokinetic models did not account for convective drug transport. Tojo and Isowaki [59] modeled the vitreous humor as a discretized cylindrical body, and simulated average concentration profiles for intravitreal drug delivery of ganciclovir and dexamethasone *m*-sulfobenzoate using different implant designs.

Their simulations showed a good match with average vitreous humor concentration obtained in vivo for rabbits, but their study lacked spatial resolution of the drug concentration. Friedrich et al. [36] were the first to use finite element analysis to simulate ocular drug distribution. They modeled intravitreal drug delivery in a rabbit eye using fluorescein and fluorescein glucuronide as drug surrogates, and assumed that the vitreous humor is stagnant. Their simulations were in good agreement with in vivo data obtained by Araie and Maurice [60] which showed that the elimination of fluorescein is dominant through the retina, while fluorescein glucorinide has low retinal permeability.

A review by Hayreh [61] features an impressive collection of studies that have investigated the transport of probe molecules by vitreous fluid flow. Different conclusions were drawn from different species. In rabbits, there has been evidence of significant fluid flow from the vitreous humor posteriorly along the central retinal artery into the orbit, as well as flow directed into the anterior chamber. The observation is different in primates (rhesus monkey and man) where Hayreh concludes that there is no posterior drainage of vitreous humor, but anteriorly directed flow has been demonstrated. The Peclet number indicates the relative importance of flow versus diffusion in transport of a solute through a fluid. Using a flow velocity based on the measured hydraulic conductivity of bovine vitreous humor, and using the measured diffusivity of acid orange 8 (364Da) through bovine vitreous humor, Xu et al. [14] found that convection can contribute about 30% of the total transport of this molecule within the human eye. Recently, more physiologic pharmacokinetic models have accounted for convection in the vitreous humor [7], [15], [17], [31–35]. Kim et al. [17] used a finite element mathematical model to predict how gadolinium-diethylenetriaminopentaacetic acid (Gd-DTPA) distributes in rabbit vitreous humor for release from an intravitreal polymer-based implant. Their model accounted for fluid flow and simulated concentration profiles that agreed well with in vivo data obtained using MRI. A Peclet number of 0.09 was calculated for Gd-DTPA which reflected a dominant contribution of diffusion to transport versus that of convection. What is certain is that according to the Peclet number, convection becomes more dominant with larger drug sizes and with smaller eye models [14]. Stay et al. [32] conducted a theoretical analysis for two different sized molecules, one small (300 to 600Da) and one large (e.g. antibodies). Peclet numbers of 1.1 and 54.3 were calculated for the small and large molecules, respectively, demonstrating that convection becomes more important for larger sized molecules.

The eye is not normally stationary, but instead undergoes a series of extremely rapid angular rotations ($300^{o}s^{-1}$ or more) known as saccades [62]. There has been recent interest in understanding how saccadic eye rotations induce flow in the vitreous humor [63–65]. Stocchino et al. [64] investigated flow of the vitreous humor experimentally by measuring the fluid velocity of aqueous solutions of glycerol (model vitreous) contained in a Perspex model of the posterior chamber during sinusoidal torsional oscillations. They showed that saccadic motion can contribute a significant mixing effect in eyes with liquefied vitreous humor. This mixing can enhance convection as indicated by the Peclet number values of 10^3 to 10^6 that Stocchino et al. calculated for the transport of fluorescein. This convection contribution is significantly higher than that estimated by Xu et al. and Kim et al..

Siggers and Ethier [62] present a good review of studies that have examined the effect of saccades on vitreous humor fluid dynamics [62]. As done by Stocchino et al. [64], all of these studies model the vitreous humor using an incompressible fluid contained in a chamber subjected to motorized rotations. However, whether the findings of these studies can be extended to the dynamics of intact vitreous humor is questionable due to the lack of two features that are difficult to capture: the non-Newtonian nature of the vitreous humor; and, more importantly, the hindrance of free rotational flow due to the firm attachment of the vitreous humor to the vitreous base, and to the prepapillary and premacular holes (see section 1.5.3). The anchorage of the vitreous humor to the surrounding posterior segment tissues challenges the notion that this fluid can freely rotate with a degree of freedom similar to that in experiment models reported in [62]. Additionally, the results of these models match theoretical calculations, but are yet to be supported by in vivo data. Nevertheless, such models can provide valuable information either in the case of vitreous liquefaction that occurs with advanced age (see section 1.5.5), or for understanding the dynamics of vitreous substitutes that are used to replace the vitreous humor following vitrectomies.

The complication of convection is not present in studies done in vitro [14], [41], [66], [67] that use steady state permeation and transient lag time to back out diffusion coefficients. Typically, the vitreous humor is placed between two diffusion half cells, with one half cell (donor) containing drug solution and the other (receptor) filled with solvent. Due to a high concentration gradient, a pseudo steady state flux ensues due only to diffusive drug transport. The change in

receptor drug concentration is tracked using UV-visible spectrophotometry or HPLC, and from a plot of receptor concentration vs. time, the mutual diffusion coefficient can be estimated.

There are some complications in in vitro studies. The integrity of the vitreous humor is inevitably compromised to some degree due to the method of extraction from the eye, and as a result of being removed from its natural nurturing environment. The vitreous must therefore be used quickly after extraction. Also, because of the fluid nature of the vitreous humor, and unlike other posterior segment tissues, the vitreous must be contained within an additional middle compartment, normally a ring, which is sandwiched between two permeable membranes thus adding extra diffusion resistance (see Figure 11 in section 2.3.1.1). Unlike in vivo methods that are limited to fluorescent or paramagnetic compounds, the diffusion cell method can be used to study both real drugs and drug surrogates of different properties. Nevertheless, in vivo data will be ideal for validating mathematical models. If such models show good agreement with in vivo distribution profiles for fluorescent or paramagnetic surrogates, then they can be extended to simulate the distribution of actual drugs.

One of the earliest studies that reported diffusion coefficients in the eye for a small solute is that by Kaiser and Maurice [68]. They measured the diffusivity of fluorescein through the lens of both rabbit and bovine eyes by using fluorophotometry to measure the rate of diffusion from a point source. They also measured fluorescein diffusivity in agar gel to be 6×10^{-6}cm^2/s and found it to be independent of agar concentration. Even though agar gel is different from the vitreous humor, this diffusivity has been used in mathematical models [7], [32], [60] to represent fluorescein diffusivity in the vitreous humor. Araie and Maurice [60] used this diffusivity value to calculate a theoretical rate constant for the loss of fluorescein from the vitreous humor of rabbit eyes, but found it to be lower than what was measured experimentally. They admitted that perhaps a better match would have been achieved with a more accurate measurement of fluorescein diffusivity. The accuracy would certainly be improved by measuring the diffusivity of fluorescein through actual vitreous humor.

As Table 1 shows, the current pool of diffusion data is based on different vitreous systems i.e. human, rabbit, porcine, and on aqueous media. Diffusivities were also measured using different experiment techniques, some of which are based on different diffusion theories. The data

available, therefore, is not sufficient to allow for proper analysis of how diffusivity of drugs may correlate with their physicochemical properties. A study that measures the diffusivity of a collection of solutes for transport through the same vitreous system would improve our understanding of how drug diffusion in the vitreous humor depends on physicochemical properties. This knowledge would provide strategic guidance in drug development for improved administration and efficacy of therapy.

Stay et al. [32] suggested that the diffusion coefficient for 300–600 Da molecules in the vitreous humor is 60–75% of that in water. Such a relationship between the two diffusion media would be useful for approximating a drug's diffusivity in the vitreous humor based on its diffusivity in water, since it is easier to measure the latter. However, Stay et al.'s approximation was only based on three molecules: acid 8 orange, fluorescein, and dexamethasone sodium m-sulfabenzoate(DMSB). This relationship needs to be explored further not just for small molecules, but also for molecules that mimic larger drugs such as Lucentis or Macugen.

Table 1 Summary of existing data on the diffusivity (*D*) of compounds in the vitreous humor.

Ref.	Experiment Type	Diffusion media	Compound	Method	Diffusivity measured(cm^2/s)
[55]	In vivo	Human vitreous	Fluorescein (332Da)	Mathematical model was fit to distribution data obtained from slit lamp fluorophotometry	$7.4\pm3.4x10^{-6}$ (normal subjects); and $9.6\pm2.0x10^{-6}$(diabetic subjects)
[56]	In vivo	Human vitreous	Fluorescein (332Da)	Mathematical model was fit to distribution data obtained from slit lamp fluorophotometry	$4.91\pm2.08x10^{-6}$
[57]	In vivo	Human vitreous	Fluorescein (332Da)	Mathematical model was fit to distribution data obtained using a Fluorotron®	$13x10^{-6}$
[58]	In vivo	Rabbit vitreous	Gd-labeled albumin (~75kDa)	Mathematical model was fit to distribution data obtained from MRI	$8\pm3\ x10^{-7}$
[69]	In vivo	Rabbit vitreous	FITC-Dextran(4.4 and 9.3 kDa)	Intravitreal infusion of FITC-dextrans followed by serial sampling of vitreous humor using microdialysis. Time lag for spherical system used to estimate *D*	For 4.4 kDa - 7.56×10^{-6} For 9.3kDa - 6.18×10^{-6}
[14]	In vitro	1. Bovine vitreous 2.Water	Acid 8 Orange (364Da)	Two-chamber diffusion cell apparatus used for *D* in vitreous, and Wilke-Chang correlation used for *D* in water	$3.4x10^{-6}$ in vitreous; and $6.5x10^{-6}$ in water
[41]	In vitro	1. Saline solution 2.Mixtures of saline and hyaluronan 3. Porcine vitreous	Dexamethasone(392Da)	Two-chamber diffusion cell apparatus used for *D* in vitreous and in other media	$7.2\pm3.3\ x10^{-5}$ in saline; For hyaluronan solution: $4.7\pm 1.1\ x10^{-5}$ in 30µg/ml , and $2\pm 0.5\ x10^{-5}$ in 180µg/ml; and $1.8\pm0.6\ x10^{-5}$ in vitreous.
[70]	In vitro	1. Phosphate buffered saline(PBS) 2.Balanced salt solution(BSS) 3.Porcine vitreous	1.Alexa 488 (~0.5kDa) 2.Green Fluorescent Protein(GFP) (~29kDa)	Fluorescence correlation spectroscopy	For Alexa 488 in: PBS – $3.0\ x10^{-6}$; BSS – $3.1\ x10^{-6}$; Liquid vitreous – $3.3\ x10^{-6}$; and Gel vitreous – $3.1\ x10^{-6}$. For GFP in: BSS – $1.3\pm0.012\ x10^{-6}$; Liquid vitreous – $1.4\pm0.011\ x10^{-6}$ Gel vitreous – $1.2\pm0.016\ x10^{-6}$
[66]	In vitro	1.Rabbit vitreous 2. Aqueous solution (unspecified)	Dexamethasone sodium *m*-sulfobenzoate (~600Da)	Two-chamber diffusion cell apparatus used for *D* in vitreous	$5.1x10^{-6}$ in vitreous; and $7x10^{-6}$
[67]	In vitro	Rabbit vitreous	Ganciclovir(255Da)	Two-chamber diffusion cell apparatus used for *D* in vitreous	$9.89\ x10^{-6}$

1.7 Micro-scale versus Macro-scale Mutual Diffusivity:

Diffusion fundamentally occurs due to Brownian motion of the species of interest, and can be classified into two types depending on the system being studied. “Binary” or “mutual” diffusion occurs with two chemically distinct species (solute and solvent) and arises due to a net flux of solute molecules down a concentration gradient of that solute within the diffusion medium. Fick’s Law explicitly describes mutual diffusion, and is used to calculate mutual diffusivity. The other diffusion classification is referred to as intradiffusion, and is characterized by diffusion in a ternary system where there are three distinguishable species [71]. One species is chemically distinct from the other two, which differ only in their isotopic composition. For clarity, we will refer to the chemically distinct species as the solvent, and the other two isotopically different species as the solute. Since the less occurring isotopes of chemical species have a radioactive signature that allows them to be traced, this type of diffusion is sometimes referred to as “tracer diffusion”. In the limit where the system contains just the solute molecules so that there is diffusion of solute molecules among themselves, this case of intradiffusion is appropriately referred to as “self diffusion”. In contrast to mutual diffusion, with no concentration gradient to direct the diffusion of the solute molecules , their displacement due to intradiffusion is purely statistical [72].

Early studies that have measured both mutual diffusivity and intradiffusivity have used diaphragm cells [73], [74]. In the case of mutual diffusion, the system is setup so that the donor compartment has a solution of the solute in the solvent, while the receptor compartment has just solvent. This configuration achieves a concentration gradient that then drives solutes from the donor compartment to the receptor compartment. Conversely, to examine intradiffusion, both the donor and receptor compartments are filled with solutions of equal concentrations. However, in the donor chamber, a portion of the solute is replaced by its isotopically-labelled form (tracer) taken to be a new species whose concentration may be separately measured. With this configuration, equivalent and opposite concentrations between tracer solutes and normal solutes are assumed to be established resulting in equimolar counterdiffusional fluxes relative to the volume-fixed frame of reference. Essentially, intradiffusivity is treated as mutual diffusivity allowing for its value to be measured by Fick’s Law [75] . Since the chemical difference between the tracer and normal solute is negligible, then the intradiffusivity should be the same as the

mutual diffusivity, especially since the former is measured in the same way as the latter. However, unlike in the case of mutual diffusion where there is only interchange between solute and solvent species, for intradiffusion, there is also interchange between tracer and normal solutes which is taken to account for the difference between the two diffusion mechanisms [73].

In all studies featured in Table 1, the systems examined were for two distinct components; the drug or drug surrogate of interest, and the diffusion medium. Therefore, in accordance with the above definition, all diffusivities reported are mutual diffusivities. There have been occurrences where separate independent studies have measured the mutual diffusivity of a solute in diffusion media of varying viscosities and arrived at conflicting conclusions regarding the dependence of diffusivity on medium viscosity. The major difference between these studies was the experiment technique used. Gisladottir et al. [41] conducted diffusion cell experiments to measure the mutual diffusion coefficient of dexamethasone for transport through the vitreous humor, and through aqueous media of different viscosities. Their study concluded that the rate of diffusion fell with increased viscosity as suggested by the Stokes-Einstein equation. However, Barton et al. [70] challenged the claim that molecular diffusivity varies with viscosity of the vitreous humor. Using fluorescence correlation spectroscopy, Barton et al. showed that the diffusion coefficients of two fluorescent molecules of different molecular weights were similar in physiological salt solutions, homogenized porcine vitreous, and intact porcine vitreous gel (see Table 1). Contrary to Gisladottir et al.'s conclusion, Barton et al. suggested that the increased rate of molecular diffusion in the vitreous chamber after vitrectomy or vitreous degeneration is not a consequence of a reduction in viscosity, but is more likely a result of increased fluid circulation. The difference in the observations of these studies should, instead, be attributed to the use of different experiment methodologies that use different theories to calculate diffusion coefficients.

In all studies featured in Table 1, except for that by Barton et al., diffusion occurs due to a concentration gradient. In such cases, Fickian diffusion theory is applied to calculate the mutual diffusion coefficients of the solutes examined. Barton et al. used fluorescence correlation spectroscopy (FCS), a technique that measures molecular dynamics and interaction. FCS is based on the detection of intensity fluctuations of homogenous fluorescent molecules in a small volume that is defined by a focused laser beam. Analysis of the data using a correlation function gives the average number of fluorescent particles and average diffusion time [76]. The main difference

between these two techniques is the time scale and consequent length scale over which diffusivity is observed. FCS operates best on a time scale of microseconds to milliseconds, which translates to a diffusion distance on the scale of microns. Diffusion cell experiments last for minutes to hours which correspond to a diffusion length of millimeters. This difference in time and length scale leads to a categorization of mutual diffusion. In the case of FCS, and other techniques that use small time and length scales, micro-scale mutual diffusivity is measured; while for large time and length scales, macro-scale mutual diffusivity is determined [77]. For simplicity, we refer here to these mechanisms as microdiffusivity and macrodiffusivity. Barton et al.'s assertion is therefore based on microdiffusivity, and not macrodiffusivity, which applies to Gisladottir et al.'s findings. No study has explicitly examined both types of mutual diffusivities for a specific solute in the same vitreous system. It would be worthwhile to do so to determine whether they are interchangeable in the context of drug transport in the vitreous humor.

A new technique that is seeing increasing usage for measurement of microdiffusivity is diffusion ordered nuclear magnetic resonance spectroscopy (DOSY NMR). DOSY NMR experiments have been developed primarily for the analysis of homogenous mixtures [78]. The majority of studies that have used this technique report the measured diffusivity as self diffusivity. According to the aforementioned definition, here, the use of self diffusivity is a misnomer. However, in keeping with the accepted terminology of this field, we have elected to be consistent by also referring to diffusivities measured with this technique as self diffusivities. Also, as was done by Kwak et al [77], from here onwards, we will refer to macro-scale mutual diffusivity simply as mutual diffusivity. Conventional NMR produces one dimensional spectra where chemical species are resolved according to their chemical shift. DOSY NMR experiments produce spectra that are resolved along two dimensions, with the conventional chemical shift in one dimension, and self-diffusion coefficients in the other (see

Figure 8). This technique is non-invasive and non-destructive with the added advantage of the specificity of NMR which permits the identification of each component in a single experiment.

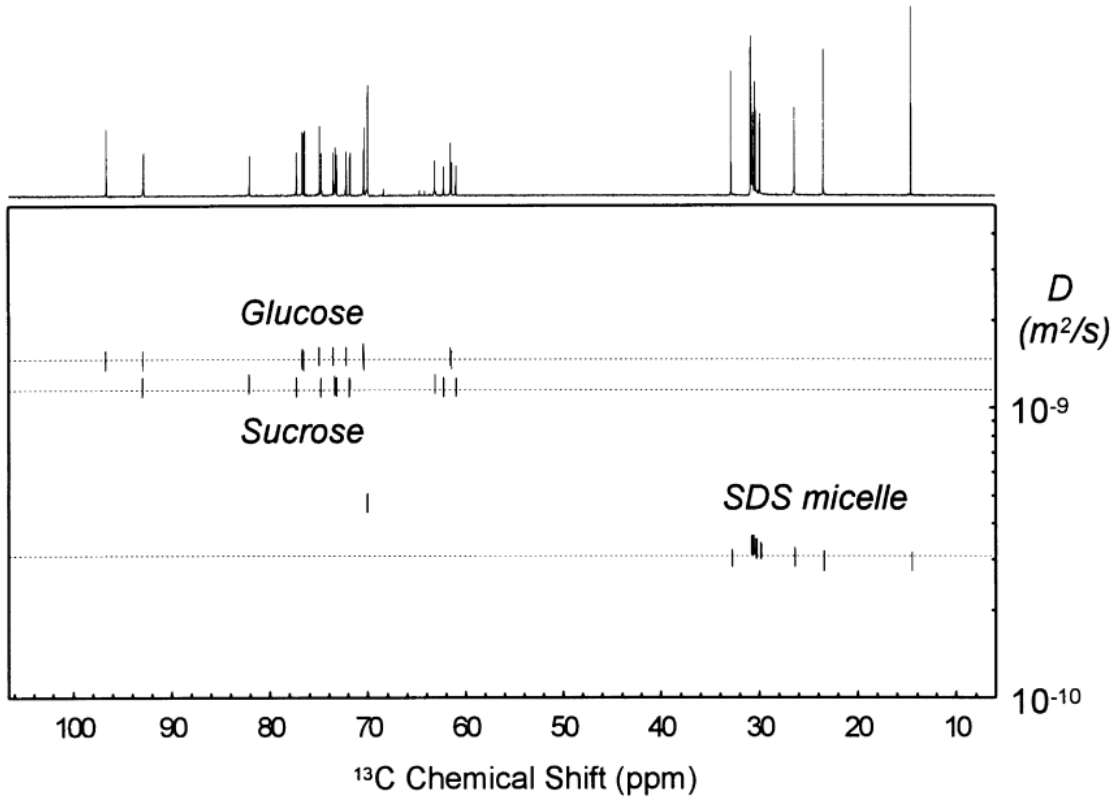

Figure 8 ^{13}C DOSY NMR Spectra of a mixture containing glucose, sucrose and sodium dodecyl sulfate. The dotted lines show the average self diffusivity of each component. The 1D NMR spectrum of the mixture is shown at the top (reproduced with permission from [79]).

However, one major requirement for DOSY NMR is that the sample must have a spin-active nucleus – any nucleus that has a magnetic moment such as ^{13}C, ^{1}H, or ^{19}F. Since DOSY NMR measures self-diffusion coefficients, it can provide information about molecular size via the Stoke's Einstein equation which has proven useful for the classification of components in complex mixtures [80–82]. This technique is also used to elucidate gelatinous systems by measuring the diffusion coefficients of polymer probes of different molecular weights at various concentrations and relating them to the structure and dynamics of the matrix investigated [83], [77], [84]. More relevant to this work is the use of this technique for the measurement of self-diffusivity in bio-gel systems. Colsenet et al. [85] used DOSY NMR to investigate the structure of whey protein gels of different protein concentrations by measuring the self diffusion coefficients of poly(ethylene glycol)s (PEGs) of varying molecular weights. Lafitte et al. [86] also used PEGs of different molecular weights in the same way to characterize the structure of

purified pig gastric mucin. Burstein et al. [87] used DOSY NMR to study what affects the transport of small solutes through calf articular cartilage by measuring the self diffusivity of water, cations (Na^+, Li^+) and the trifluoroacetate anion.

An in-depth explanation of DOSY NMR has been presented by Antalek [88] and Johnson [79]. Briefly, the diffusivity of any chemical specie with a spin active nucleus can be tracked by applying a magnetic field gradient (gradient pulse) as a function of position to the sample for a short time which encodes the spins. In the encoding stage, the gradient labels the position of the spins by producing a spatially dependent phase angle. A specific time passes before the spins are decoded where a second magnetic field gradient is applied which imparts a phase opposite to that of the first gradient, again as a function of position. Between the encode and decode steps, the nuclei will change position as defined by their self diffusivity. As a result, there will be a phase change associated with each nucleus. Consequently, the NMR signal that results from the net magnetization of all magnetic moments within the sample will decrease relative to the signal detected prior to the application of the magnetic gradient. This reduction in the NMR signal is used to measure the self diffusivity of the species of interest. The ratio (R) of the NMR signal with the diffusion-sensitizing magnetic field gradient strengths (g) to that without is related to the self diffusivity (D_s) by the Stejskal-Tanner equation written as

$$\boldsymbol{R = -exp\left(\gamma^2 g^2 \delta^2 \left(\Delta - \frac{\delta}{3}\right) D_s\right)} \qquad \textbf{Eq. 1}$$

where γ is the gyromagnetic ratio specific to the spin-active nucleus, δ is the duration of the magnetic field gradient strength and Δ is the time between successive gradient pulses. In a DOSY NMR experiment, the R is measured for different values of g while all other variables are fixed. DOSY software fits Eq. 1 to the measured data to obtain D_s.

DOSY NMR has thus far not been used to measure self-diffusivity of drugs in the vitreous humor. Given the complex nature of this tissue, the specificity of this technique makes it amenable for this application and would prove valuable in exploring any agreement between mutual diffusivity and self diffusivity of drugs in the vitreous humor.

1.8 Thesis Scope

Transport studies on the vitreous humor have thus far only looked at one or two solutes, and most studies have examined drug surrogates. To date, there has been no study that investigated exclusively the effect of physicochemical properties of drugs on their transport in the vitreous humor. As a starting point, we examine how solute size (molecular weight and radius) affects the transport of both ocular drugs and drug surrogates. The ocular drugs are timolol maleate (TM), a β-blocker used to treat glaucoma; and dexamethasone sodium phosphate (DMSP), a glucocorticosteroid used to treat inflammatory conditions. The chosen drug surrogates are sodium fluorescein (Na-F) and three fluorescein isothiocyanate (FITC)-conjugated dextrans (FD) with molecular weights of 4, 40, and 150kDa abbreviated as FD4, FD40 and FD150 respectively. The mutual diffusion coefficients of these solutes were measured in vitro for transport through phosphate buffered saline (PBS), rabbit vitreous humor (RVH) and porcine vitreous humor (PVH) using diffusion cells in conjunction with UV-visible spectrophotometry. These solutes cover the molecular weight range (300 – 150kDa) of drugs relevant for ocular treatment.

Many in vitro studies use vitreous humor sourced from porcine and rabbit eyes as substitutes for human vitreous humor. It would therefore be worthwhile to assess the extent of agreement between the drug diffusivities measured for each animal species since findings based on either one are extrapolated to the human eye [14]. Rabbits are also popular choices for in vivo transport studies as shown in Table 1. As mentioned earlier, mathematical models are validated based on agreement between simulated drug distribution profiles and in vivo profiles. Since in vivo profiles of some drug surrogates exist in the literature for rabbit eyes [55–57], these can be used to validate mathematical models that simulate drug distribution profiles for geometries that mimic the rabbit's eye. Drug diffusion coefficients in rabbit vitreous humor is a key parameter in the mass balance equations that constitute these models, so those measured in this study would prove valuable for both model development and subsequent validation.

Measuring the diffusivity of drugs in the vitreous humor is difficult. Since the vitreous humor is about 99% water it would seem reasonable to estimate vitreous humor drug diffusivity based on the diffusivity measured for an aqueous medium. In this study, we examine the validity of such rule-of-thumb correlations by measuring the mutual diffusivity of the solutes in PBS and comparing them to those measured for the vitreous humor.

Some studies ignore the difference between micro-scale and macro-scale mutual diffusivity. Whether the two types of diffusivities can be used interchangeably in the context of transport in the vitreous humor has never been checked experimentally. DOSY NMR was used to measure the micro-scale mutual diffusivities of DMSP in PBS and in both rabbit and porcine vitreous. These were compared to the macro-scale mutual diffusivities that were measured using the diffusion cells.

Ocular pharmacokinetic models are validated if the predicted drug distribution profiles agree well with in vivo biodistribution profiles. This document presents preliminary experiments that demonstrate in vivo acquisition of distribution profiles of Na-fluorescein in rabbit vitreous humor at different time points.

2 Experimental Materials and Methods

2.1 Materials

Dexamethasone sodium phosphate, timolol maleate, sodium fluorescein and FITC-dextrans(4, 40, and 150kDa) were purchased from Sigma-Aldrich, and used as received. Dubelcco's phosphate buffered saline (PBS) was purchased from Medical Sciences Store, University of Toronto.

Jacketed diffusion cells, Neoflon rings, clamps and a three-cell stir station were all purchased from Permegear Inc.(Hellertown, PA, USA). Filter membranes were purchased from Fischer Scientific. Wilmad® NMR tubes, and Wilmad® coaxial inserts were all purchased from Sigma-Aldrich. Table 2 provides details on the specifications of the equipment used in this study.

Table 2 Specifications for equipment used in diffusion cell and DOSY NMR experiments.

Equipment	Specification
Side-by-side diffusion cell	Compartment volume of 3.4ml with cross-sectional diffusion area of 1.13 cm^2
Neoflon ring	12 mm ID x 28mm OD x 4.42mm thick
3-station stirrer for side-by-side cells	115 v, 60hz, 600 rpm, 51cm long
Filter membranes	25mm diameter and 50nm pore size
Wilmad® NMR tube	Precision type, 5 mm diameter, 7 in. length, 600MHz frequency rating
Wilmad® 32mm coaxial insert stem	32mm length, reference capacity of 40 µL, sample capacity of 339 µL

2.2 Vitreous Humor Extraction

No animals were sacrificed for in vitro experiments. All eyes were obtained from abattoirs and the vitreous humor was extracted and used within three days. Porcine eyes were obtained from Quality Meat Packers Ltd.(Toronto, ON), and New Zealand albino rabbit eyes were procured from Abate Rabbit Packers Ltd. (Arthur, ON). Only one eye was collected from each animal. All eyes were kept on ice in a well insulated container until they were ready for use.

The pig eye was prepared by first removing excess muscle tissue and then sterilizing the exterior surface with 70% alcohol. The cornea was punctured using a 25 gauge needle and the aqueous humor was withdrawn into a 1 ml syringe and discarded. A razor blade was used to make an incision at the limbus and the cornea was then cut away with curved scissors. The lens was removed using forceps, and a cut was then made along the posterior retina/choroid/sclera (RCS) from the limbus to the optic nerve. The RCS was splayed open and the vitreous humor (~ 3 to 3.5 ml) was deposited into a 15 ml tube (see Figure 9). It was often necessary to use tweezers to detach the vitreous base from the ora serrata. The vial containing the vitreous humor was then immediately stored on ice in a well insulated container.

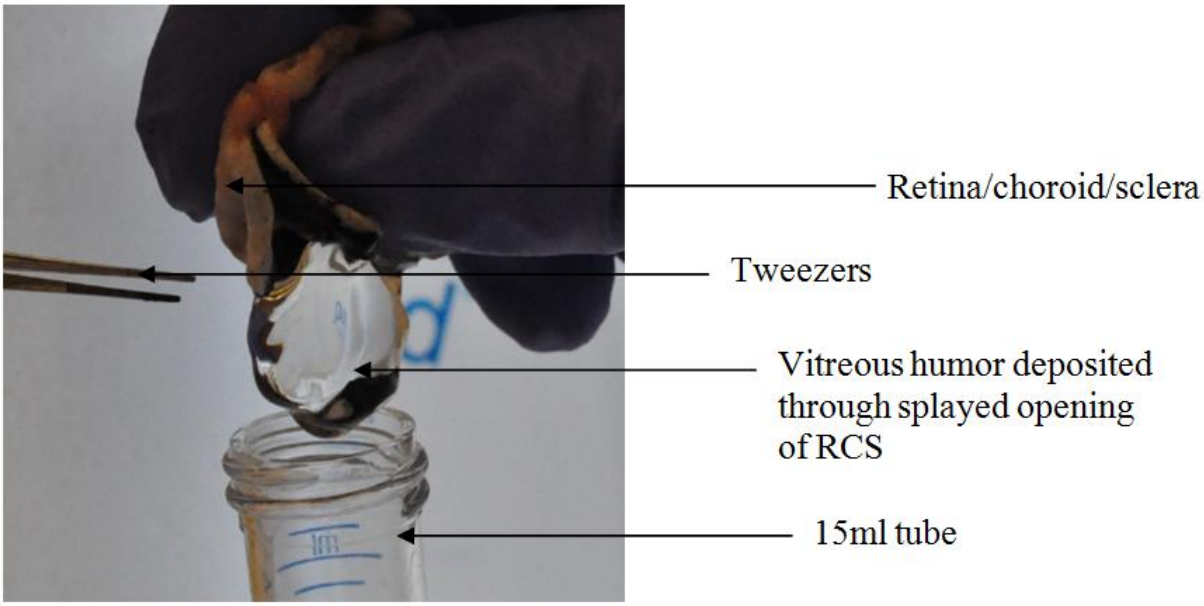

Figure 9 Extracting vitreous humor from a porcine eye.

For rabbit vitreous extraction, the only procedural difference was that after removal of the anterior segment and lens, the vitreous humor was expelled through the limbal opening by squeezing the posterior segment between the thumb and index finger (see Figure 10). Since the volume of rabbit vitreous (~ 1 ml) is less than that of porcine vitreous, rabbit vitreous was collected in 1.5ml vials.

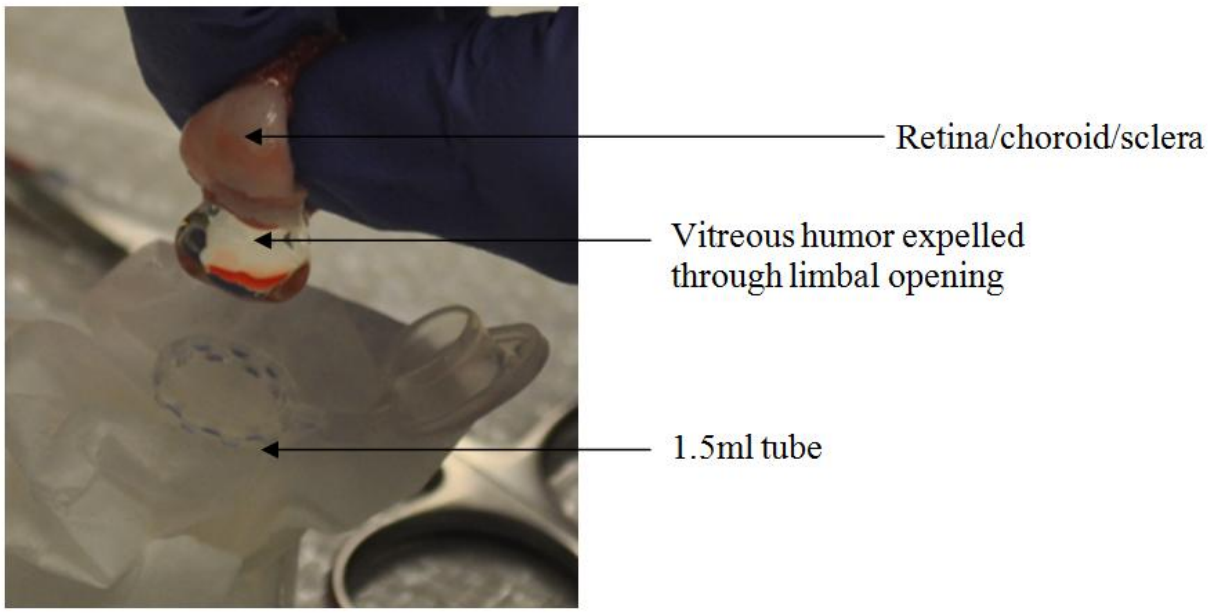

Figure 10 Extracting vitreous humor from a rabbit eye.

2.3 In Vitro Study

2.3.1 Mutual Diffusion Experiments

2.3.1.1 Diffusion Cell Setup

A Neoflon ring was sandwiched between two filter membranes (see Figure 11) that were first soaked in PBS to purge air from the membrane pores. This assembly was mounted to the jacketed side-by-side diffusion cell and served as the diffusion media compartment. In all experiments, the diffusion medium (PBS or vitreous humor) was first warmed to 37^{o}C. The ring was customized to include a shaft that spanned from the outer edge to the inner edge as shown in Figure 11. Through this shaft, 0.5 ml of the diffusion medium was loaded into the ring using a 16 gauge needle. A plastic tube wrapped in paraffin film was then used to seal the shaft. The donor compartment was filled with 3.4 ml of a solution of the drug or drug surrogate in PBS (see Table

3 for concentrations) while the receptor compartment was charged with 3.4 ml of fresh PBS with pH of 7.4. Three of these diffusion cell assemblies were housed on a stir station that included manifolds to which the cell jackets were connected to receive circulated water from a temperature controlled water bath (see Figure 12). Each compartment was thus constantly stirred and maintained at 37^{o}C. At appropriate time intervals (see Table 3), 0.1 ml samples were collected from the receptor compartment and refrigerated. The sample was replaced with 0.1 ml PBS to maintain receptor volume. Solute concentration in the samples were assayed by UV-visible spectrophotometry (see Appendix i for calibration curves). Diffusion experiments were also conducted with just the two filter membranes, without a diffusion medium, to assess their contribution to the overall diffusion resistance.

Table 3 Details of mutual diffusion experiments. The chosen run times allowed for pseudo steady state to be established.

		Diffusion media			
		PBS		Vitreous humor	
Solute	Donor conc.(mg/ml)	Run time (minutes)	Sample frequency (minutes)	Run time (minutes)	Sample frequency (minutes)
Na-F	2.5	180	30	180	15
TM	2.5	135	15	240	15
DMSP	2.5	135	15	240	15
FD4	10	180	15	420	30[a]
FD40	20	240	15	480	30[b]
FD150	20	240	15	480	30[b]

[a]Samples were collected 2 hours after starting experiment.

[b]Samples were collected 4 hours after starting experiment.

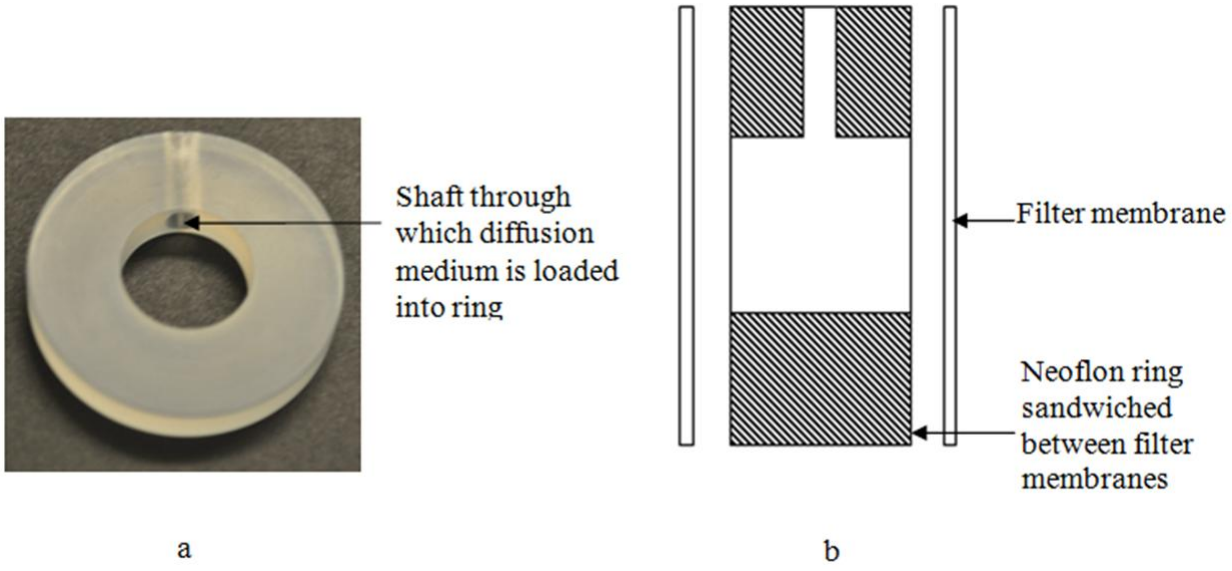

Figure 11(a) Customized Neoflon ring in which the diffusion medium was contained (b) Schematic showing arrangement of ring and filter membranes.

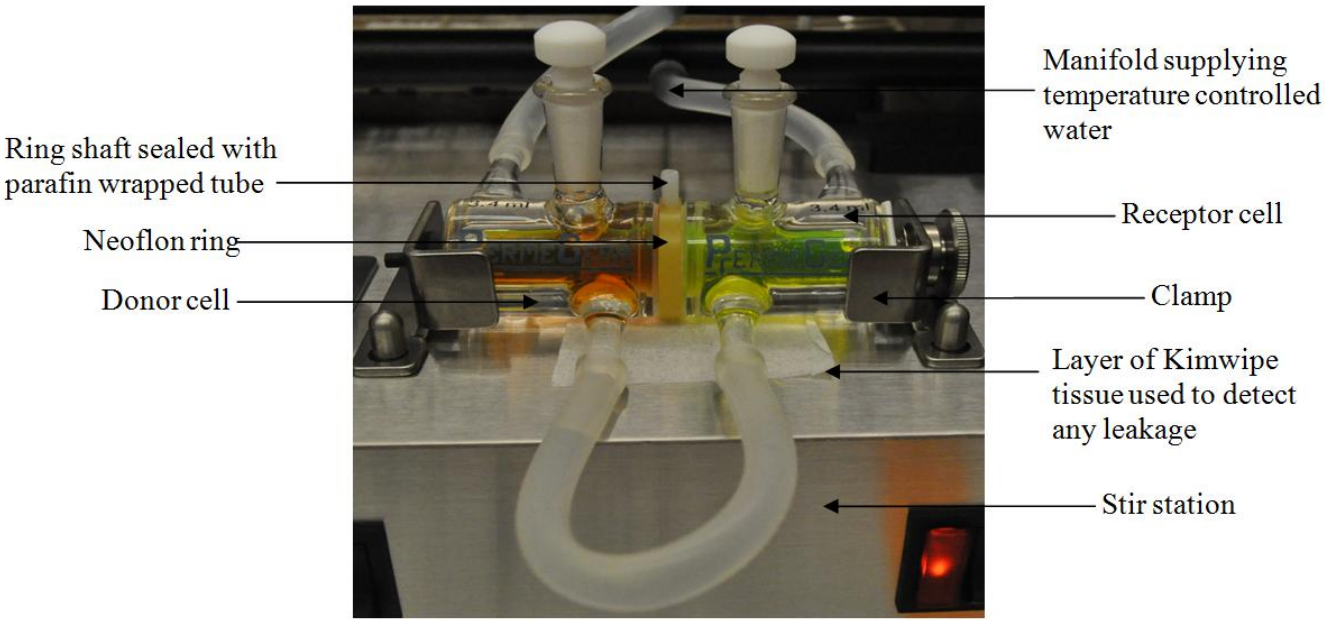

Figure 12 Setup of constantly stirred jacketed diffusion cell.

2.3.1.2 Calculating Mutual Diffusivity

Receptor concentration vs. time profiles for all n experiments were constructed on one plot, and a linear regression was performed on data in the pseudo steady state region (see Appendix ii). To ensure that the chosen region of a plot represented pseudo steady state, a normal probability plot was constructed (see Appendix ii) for the data in that region. If the normal probability plot exhibited an apparent linear profile for the majority of the regressed data, then this indicated that the region of the concentration profile taken to represent pseudo steady state was acceptable. The x-intercept of the extrapolated linear region of the curve gives the lag time (τ). The mutual diffusion coefficient (D_m) was calculated using τ and the diffusion path length (l), in this case the ring thickness, using the following equation:

$$\tau = \frac{l^2}{6D_m} \qquad \textbf{Eq. 2}$$

Six experiments were analyzed for each solute for diffusion in each medium with the exception of FD40 for diffusion in rabbit vitreous where only four experiments yielded acceptable results (positive time intercept for the concentration profile).

2.3.2 Self Diffusion Experiments

2.3.2.1 Sample Preparation

Solutions of DMSP with 1 w/v% concentration were prepared with PBS, porcine vitreous and rabbit vitreous. This drug concentration was chosen to amplify the signal-to-noise ratio during DOSY NMR analysis. For both PBS and porcine vitreous 10 mg of DMSP was dissolved in 1 ml of the medium. Since the volume of rabbit vitreous that could be extracted was smaller than that of porcine vitreous, 5 mg of the drug was dissolved in 0.5 ml of this medium. The vial was vortexed until the DMSP was visually observed to be dissolved. A 16 gauge needle and 1 ml syringe were then used to transfer 0.5 ml of the drug solution to a NMR tube. A coaxial insert, containing a 0.4 ml solution of 100 mg/ml trifluoroacetic acid (TFA) in deuterated water, was then inserted into the NMR tube (see Figure 13). With this arrangement, the solution in the coaxial insert was kept separate from that in the NMR tube. The coaxial insert minimized the occurrence of convection and allowed the self diffusivity of TFA to be measured simultaneously with that of the DMSP. Measuring a consistent TFA self diffusivity across samples was used as a

means to check that the same conditions were maintained for each experiment. Also, a close match between the measured TFA self diffusivity in water and with that in literature ($0.97\times10^{-5}cm^2/s$ [87]) meant that the DOSY NMR setup and the parameters used for the experiments produced reliable measurements for self diffusivity of DMSP in the diffusion media examined.

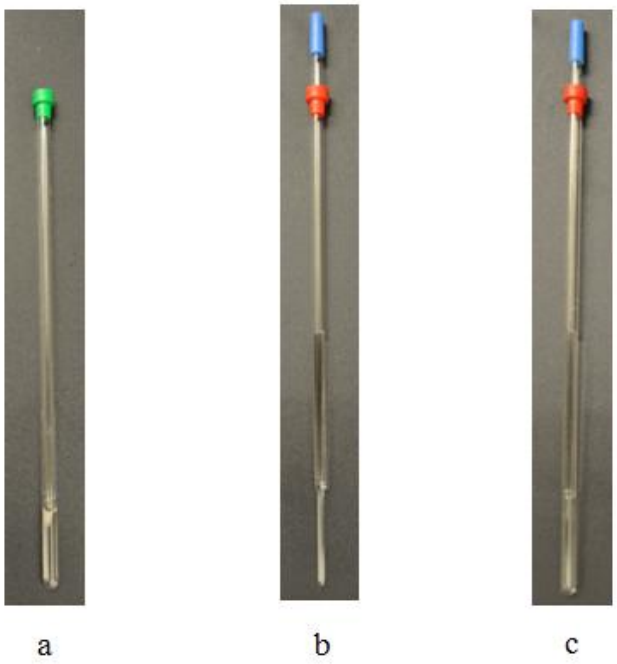

Figure 13(a) 5mm NMR sample tube containing drug solution (b) NMR tube coaxial axial insert containing TFA solution (c) NMR sample tube containing coaxial insert.

2.3.2.2 Self Diffusivity Measurement

All spectra were obtained on a Varian VnmrS NMR spectrometer operating at 376.095 MHz (^{19}F) equipped with an autotuneable field gradient probe. Measurements were carried out at 37^{o}C and with gradient strengths that ranged from 0.95 to 47.25 G/cm over 11 increments. The probe was calibrated for gradient non-uniformity, and these calibrations were used in all subsequent diffusion analyses. Using a 3 s relaxation delay, 64 scans were collected for each spectrum using the D-one-shot pulse sequence as supplied in the VnmrJ 3.2A pulse sequence library. Self diffusion coefficients were calculated using the VnmrJ 3.2 software. Briefly, for the different field gradient strengths, a Stejskal-Tanner plot of R vs k was constructed, where $k = \gamma^2 g^2 \delta^2(\Delta-\delta/3)$, and the self diffusivity was measured by fitting Eq. 1 to the plot (see section 1.7). For all

experiments a Δ of 50 ms and δ of 2 ms were used. Six samples were analysed for pig vitreous humor, five for PBS and four for rabbit vitreous humor.

2.4 In vivo study

2.4.1 Animal model and fluorophore

Experiments were performed on a male adult New Zealand albino rabbit. The animal was obtained from the vivarium of the Keenan Research centre at St Michael's Hospital. Sodium fluorescein, chosen as the drug surrogate, was obtained from Sigma-Aldrich.

2.4.2 Fluorometer

The Fluorotron Master™ (Ocumetrics, Mountain View, CA) was used to scan the rabbit's eye to measure the fluorophore distribution in the vitreous humor. After aligning the eye with the lens of the Fluorotron Master™, a blue light is emitted through the optics of the system along the eye's optical axis. This incident light excites the fluorophore molecules which in turn emit fluorescent light that is detected by the system. The level of fluorescence is measured at the point where the incident ray and fluorescent ray intersect. The Fluorotron ™ moves this point of focus in steps of 0.25 mm along the eye's optical axis and measures the fluorescence intensity at each step. Fluorescence intensity is recorded by a program which then converts the reading to the corresponding concentration to generate a profile of fluorophore concentration (ng/ml) vs distance (mm) from the retina. The intensity conversions are based on the manufacturer's calibration done using standard solutions of Na-F in de-ionized water. .

2.4.3 Vitreous Fluorophotometry

A 2.97 kg rabbit was anaesthetized with 1 ml of ketamine 10% and 1.5 ml of xylazine 2% at dosages of 35 mg/kg and 10 mg/kg respectively. In order to keep the animal sedated, ketamine and xylazine were subsequently infused throughout the experiment at a rate of 2 ml/hr with a volume ratio of 1:1. The pupils of both eyes were dilated by topical application of Mydriacyl® 1% and Mydfrin® 2.5%. Fluorescent baseline scans were then obtained for both eyes. Using a 30 gauge needle, 15 µL of 0.2% of Na-F was injected into the central part of the vitreous 3 mm behind the limbus in the superior temporal region of the left eye (see Figure 14). This Na-F dosage is the same as that used by Araie and Maurice [60].The needle was inserted 7.5 mm into

the vitreous at an angle of 40^{o} from the optical axis. In order to see the initial shape of the fluorophore deposition, the vitreous of the left eye was scanned using a bioimaging instrument known as the Spectralis® HRA2 (see Figure 15). The Spectralis® HRA2 uses a confocal scanning laser technology to obtain images of the retina. This technology was, for the first time, used for obtaining a 2D image of the fluorophore distribution in the vitreous. Fluorophotometric readings of the left eye were then obtained 2.5 hr, 3.5 hr and 4 days after Na-F injection. Following the Spectralis® HRA2 scans of the left eye, the right eye was injected with 15 µL of 0.2% Na-F in the same way as was done for the left eye. Fluorotron ™ scans of the right eye were then performed 5 min, 50 min, 1.5 hr and 4 days after injection.

a b

Figure 14(a) Na-fluorescein injected into eye 3 mm behind the limbus using a 30 gauge needle (b) Na-fluorescein in vitreous humor is visible after injection.

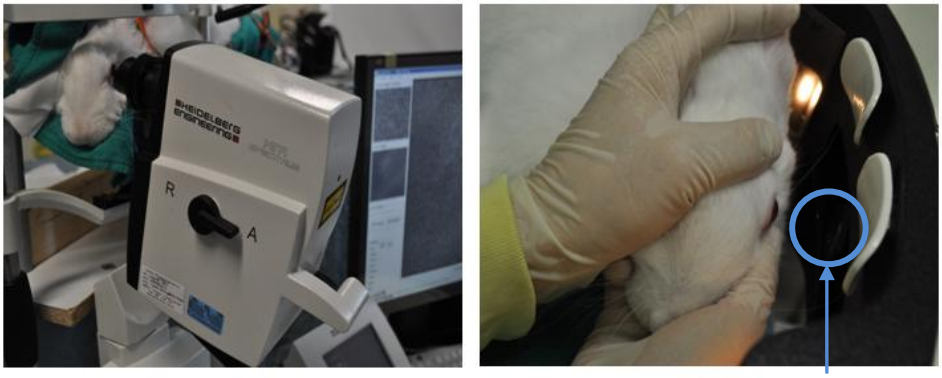

a b

Figure 15(a) Rabbit's vitreous being scanned using Spectralis ® HRA-2 (b) Rabbit's vitreous being scanned with Fluorotron ™. The eye must be held stationary and facing the lens of the Fluorotron ™ for the duration of the scan.

3 Results

3.1 In vitro studies

3.1.1 Mutual Diffusion Experiments

Since filter membranes (FM) were used to contain the PBS and vitreous humor within the Neoflon ring, it was necessary to assess the diffusion resistance from these membranes. Steady state permeation experiments were conducted with two membranes fixed between the donor and receptor cells. The lag time was used as a proxy for the diffusion resistance and was recorded for six pairs of membranes. As Table 4 shows, the lag time for diffusion through the filter membranes was significantly lower than those for diffusion through the combined media and filter membranes. Filter membrane lag times ranged from 4% to 23% of those for PBS + FM; 1% to 9% of those for PVH + FM; and 1% to 11% of those for RVH + FM. Therefore, the diffusion resistance from the filter membranes was neglected, and the diffusivity of the solutes through PBS and vitreous humor was determined using the steady state permeation method.

Table 4 Lag times (minutes, mean ± S.E.) for diffusion of solutes through different media for n = 6 except where noted.

Solute	FM	PBS + FM	PVH + FM	RVH + FM
Na-F	0	34 ± 15	96 ± 27	85 ± 41
TM	1 ± 0.5	27 ± 4	91 ± 23	68 ± 31
DMSP [a]	2 ± 0.4	36 ± 4	88 ± 11	57 ± 43
FD4	15 ± 3	65 ± 6	173 ± 69	142 ± 36
FD40 [a]	9 ± 5	66 ± 9	242 ± 85	131 ± 70
FD150	7 ± 3	69 ± 17	124 ± 89	167 ± 96

[a]Lag time for diffusion through rabbit vitreous+FM was based on n = 4

The mutual diffusivities of the solutes examined for transport through PBS, porcine vitreous and rabbit vitreous are reported in Table 5. Diffusivity in the vitreous humor is lower than in PBS for

all solutes which is expected since the former is more viscous than the latter. The mutual diffusivity of the solutes in porcine vitreous ranged from 30–56% of their value in PBS. The mutual diffusivity of DMSP in rabbit vitreous was unusually high at 64% of the value in PBS, while diffusivities for the other solutes ranged between 40% and 50% of their values in PBS. Comparison between mutual diffusivities in porcine and rabbit vitreous obtained for each solute shows significant overlap in their standard error. Assuming normal distribution of the mean diffusivity, a t-test was done for both diffusivities obtained for each solute (see Appendix v). For a 95% confidence interval, the difference in mutual diffusivity between either vitreous was found to be statistically insignificant in all cases.

Table 5 Physicochemical properties of the solutes examined and mutual diffusivities (mean ± S.E.) measured for each solute in different media.

Solute	MW (Da)[a]	Radius (nm) [a]	pKa [a]	$K_{o/w}$ [a]	D_m in PBS ($\times10^{-6}cm^2/s$)	D_m in porcine vitreous ($\times10^{-6}cm^2/s$)		D_m in rabbit vitreous ($\times10^{-6}cm^2/s$)	
						Absolute	As % of PBS D_m	Absolute	As % of PBS D_m
Na-F	376	0.50	9.12	0.10	16 ± 7.0	5.7 ± 1.6	36	6.4 ± 3.1	40
TM	432	0.48	9.4	1.94	20 ± 3.1	5.9 ± 1.5	30	8 ± 3.7	40
DMSP	516	0.58	6.4	0.29	15 ± 1.6	6.2 ± 0.7	41	9.6 ± 7.3	64
FD4	4000	1.3	6.4	0.17	8.4 ± 0.8	3.1 ± 1.2	37	3.8 ± 1.0	45
FD40	40000	6.4	6.4	0.33	8.3 ± 1.1	2.2 ± 0.8	27	4.1 ± 2.2	49
FD150	150000	8.3	6.4	0.39	7.9 ± 2.0	4.4 ± 3.2	56	3.3 ± 1.9	42

[a]All pKa values were obtained from [51], [89–91]. Molecular radii were cited from [50], [52] with the exception of that for DMSP which was calculated with the Stokes-Einstein equation using its measured self diffusivity in PBS at 37°C. Octanol/water partition coefficients ($K_{o/w}$) values were culled from [51], [92–94] except for that of FD40 and FD150 which were measured at room temperature using the shake flask method (see Appendix iii).

Figure 16 shows an inverse relation between the mutual diffusivity of the solutes and their molecular weight. A closer look shows, however, that this inverse relation is not observed for the small molecules (Na-F, TM and DMSP) for transport in all media. The same can also be said for the large molecules (FD4, FD40 and FD150) for transport in the vitreous humor. Figure 17 also suggests an inverse relation between mutual diffusivity and molecular radius. The inverse relationship holds well for the transport of all molecules in PBS, but deviates among the small molecules, and among the large molecules for transport in the vitreous humor (see Table 5).

The Stokes-Einstein equation relates solute diffusivity at infinite dilution, D_o, to its size where

$$D_o = \frac{k_B T}{6\pi\mu R_h} \qquad \textbf{Eq. 3}$$

The solute is modeled as an equivalent spherical particle with radius R_h (taken as the molecular radius) diffusing through a quiescent fluid with dynamic viscosity μ at absolute temperature T, and k_B is the Boltzmann constant. The relation is only an approximate one since the structure of the solute is not accounted for, and, in the case of the vitreous humor, the dynamic viscosity of the solvent is not uniform. The radius is related to the molecular weight (MW) and density ρ in the following way

$$R_h = \left(\frac{3}{4}\frac{MW}{\pi\rho}\right)^{\frac{1}{3}} \qquad \textbf{Eq. 4}$$

Eq. 3 and Eq. 4 suggests that diffusivity should scale linearly with the reciprocal of the molecular radius (MR^{-1}), or scale linearly with the reciprocal of the cubed root of the molecular weight ($MW^{-1/3}$). For diffusion in PBS, linear regression of the mutual diffusivity with $MW^{-1/3}$ (see Figure 18) gave a R^2 value of 0.84 , which was similar to the R^2 value of 0.89 obtained for regression of the mutual diffusivity with MR^{-1} (see Figure 19). Similarly, for porcine vitreous, there was an insignificant difference between the correlations of mutual diffusivity with $MW^{-1/3}$ ($R^2 = 0.68$), and of mutual diffusivity with MR^{-1} ($R^2 = 0.71$). For rabbit vitreous, the correlations of mutual diffusivity with $MW^{-1/3}$ ($R^2 = 0.73$) and with MR^{-1} ($R^2 = 0.71$) were similar.

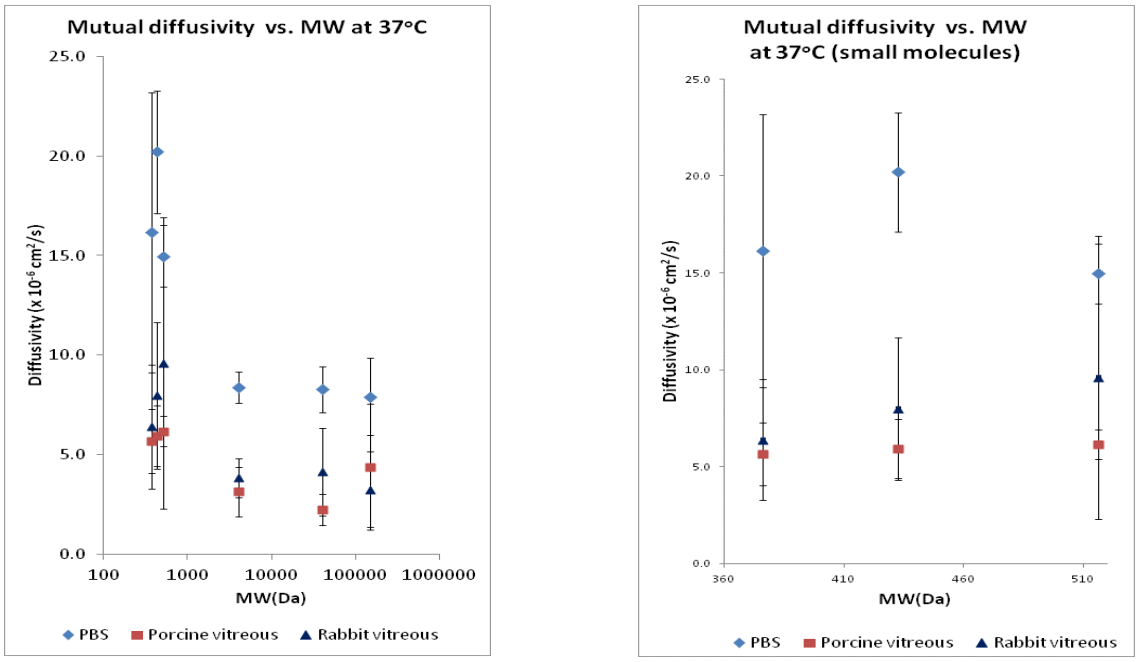

(a) (b)

Figure 16 Mutual diffusivity vs. molecular weight for all solutes (a) and for the small solutes (b)

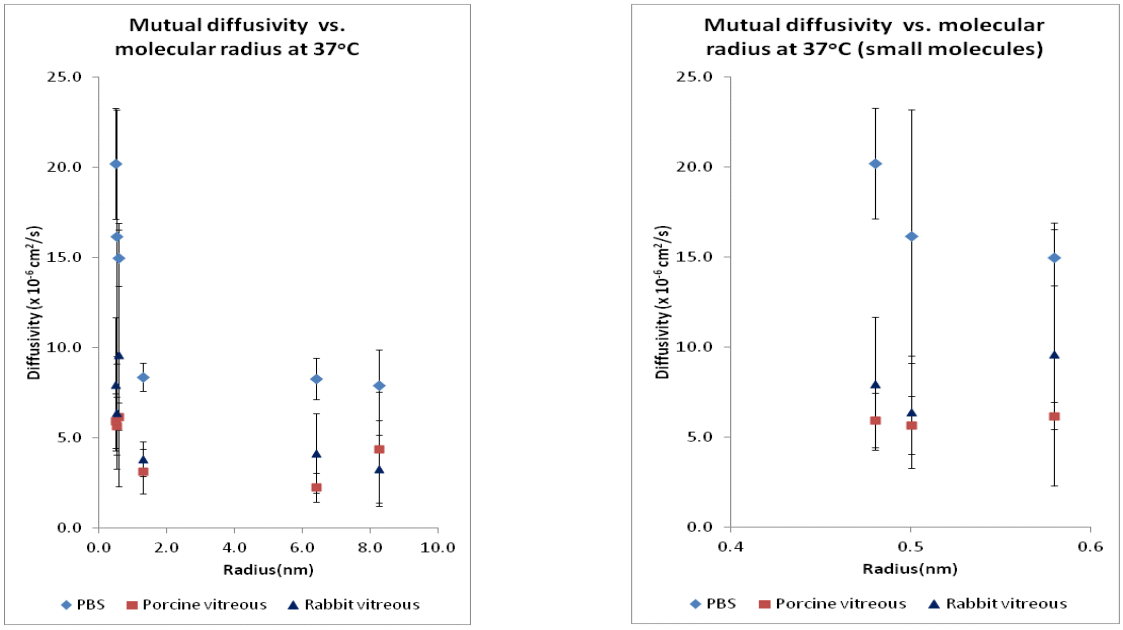

(a) (b)

Figure 17 Mutual diffusivity vs. molecular radius for all solutes (a) and for the small solutes (b)

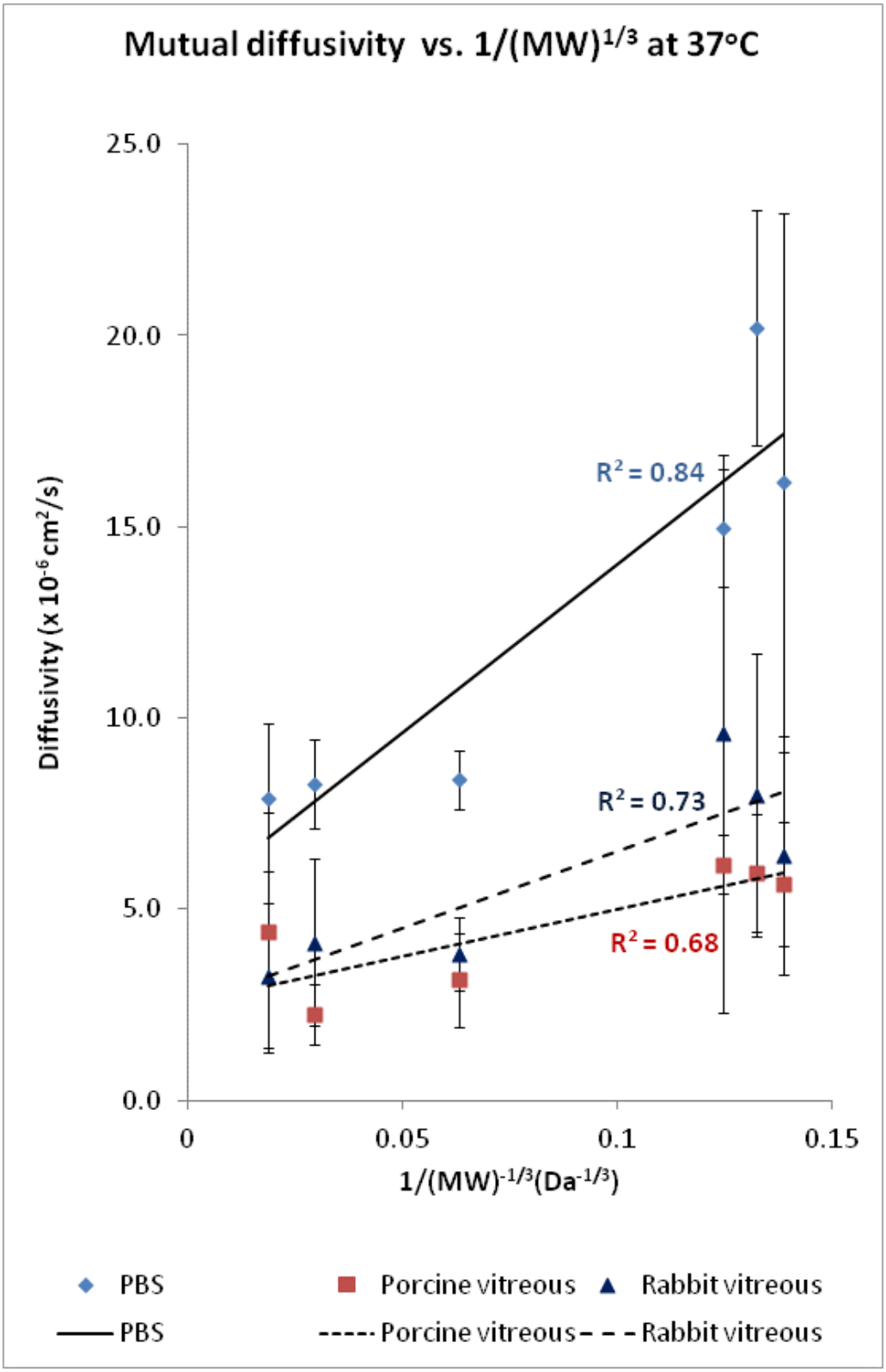

Figure 18 Correlation between mutual diffusivity and molecular weight

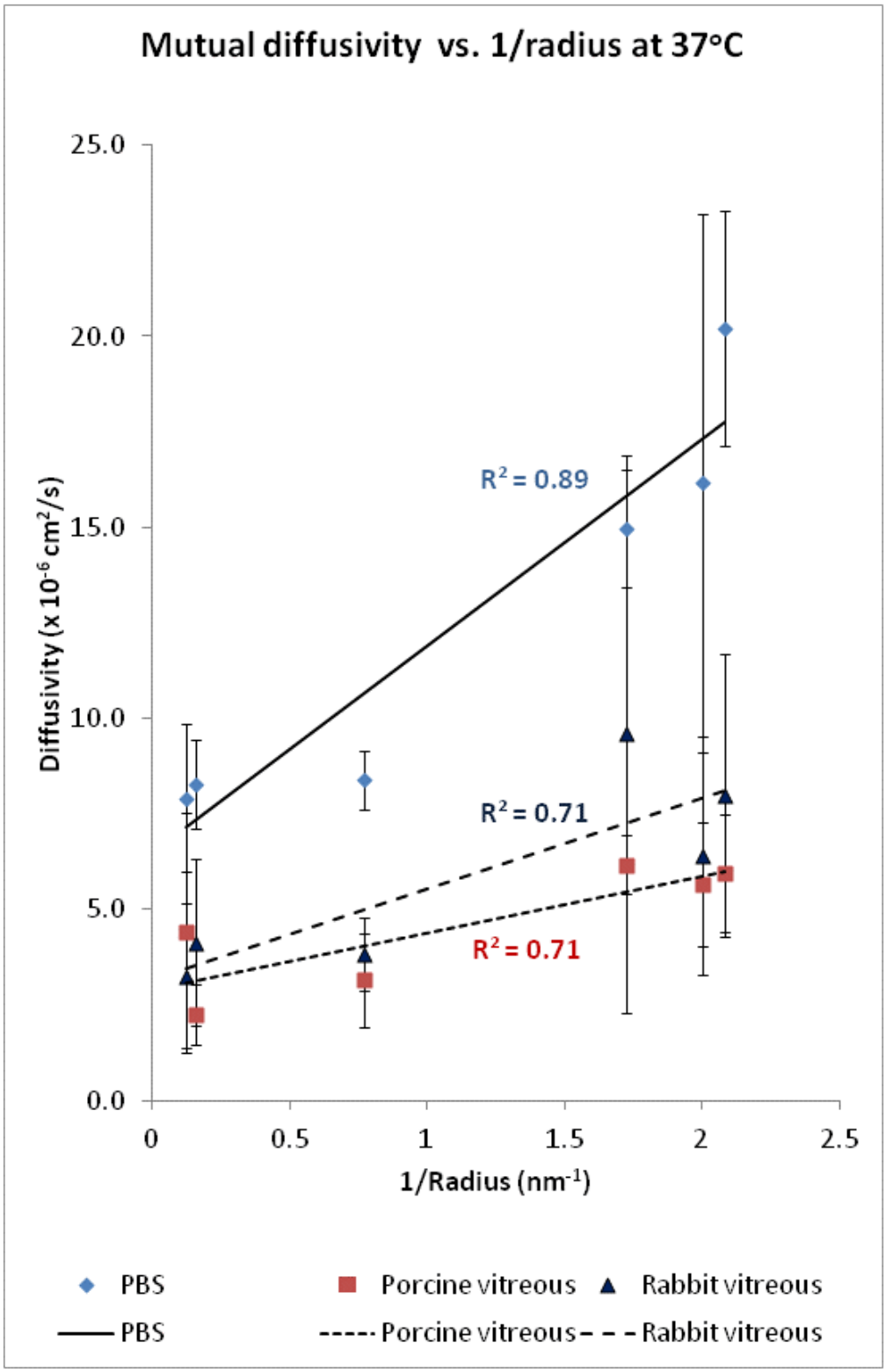

Figure 19 Correlation between mutual diffusivity and molecular radius

3.1.2 Self Diffusion Experiments

Table 6 shows the self diffusivities that were measured for DMSP in PBS and vitreous humor (refer to Appendix iv for an example of the chemical shift spectrum, Stejskal-Tanner plot, and DOSY NMR spectrum). TFA self diffusivity was consistent throughout all experiments with a value of $1.2\pm0.1\times10^{-5}$ cm^2/s confirming that all samples were subjected to the same experimental conditions. Also, the close match between the measured TFA self diffusivity in water and that reported in literature ($0.97\times10^{-5}cm^2/s$ [87]) confirmed that the DOSY NMR setup and the parameters used for the experiments produced reliable measurements for self diffusivity of DMSP in all diffusion media examined. DMSP self diffusivity was found to be lower than its mutual diffusivity in both PBS and vitreous humor. There was no significant difference among the self diffusivities measured in all diffusion media. Using t-tests, the sample mean D_s and sample mean D_m were compared for diffusion in each media (see Appendix v). For a 95% confidence interval, the difference in the sample means for both vitreous models was found to be statistically insignificant. However, mutual diffusivity and self diffusivity were found to significantly differ for diffusion in PBS.

Table 6 Self diffusivities ($\times10^{-6}cm^2/s$, mean ± S.E.) measured with DOSY NMR and mutual diffusivities ($\times10^{-6}cm^2/s$, mean ± S.E.) obtained using diffusion cells for DMSP in PBS and vitreous humor. The D_s of the reference molecule TFA is also shown for experiments done in each medium. All experiments were conducted at 37°C.

Diffusivities	PBS	Porcine vitreous	Rabbit vitreous
D_s of TFA (n = 6)	12.2 ± 0.8	12.1 ± 0.8	11.9 ± 0.5
D_s of DMSP	5.9 ± 0.7 (n = 5)	5.5 ± 0.7 (n = 6)	5.6 ± 0.6 (n = 4)
D_m of DMSP	15 ± 1.6 (n = 6)	6.2 ± 0.8 (n = 6)	9.6 ± 7.3 (n = 4)

Convection within the sample tube is a difficulty that may be encountered with DOSY NMR experiments. A heat source is applied at the bottom of the tube in cases where the sample is required to be above room temperature. The non-uniform heating may cause convection to occur, which affects the diffusion measurements. It was therefore necessary to check that convection was not an issue in these experiments, since the sample needed to be maintained at 37°C.

Provided the self diffusivity (D_{s1}) of a solute and the viscosity of the diffusion medium (μ_1) is known at a specific temperature (T_1), then it is possible to predict for a different temperature (T_2) and corresponding medium viscosity (μ_2) what the new self diffusivity (D_{s2}) of the solute would be via the following equation:

$$D_{s2} = \frac{D_{s1}\mu_1 T_2}{T_1 \mu_2} \qquad \textbf{Eq. 5}$$

If the measured D_{s2} is similar to, or does not significantly exceed the value predicted by Eq. 5, then the occurrence of convection can be ruled out. A trial experiment was conducted for one sample of DMSP dissolved in PBS (see section 2.3.2), and the DMSP D_s measured at 37 ^{o}C was $5.7 \pm 0.4\times10^{-6}$ cm^2/s. Using Eq. 5 where T_1 and T_2 are 298K and 310K respectively; μ_1 and μ_2 for PBS are 1.05cp and 0.70cp [95] respectively; and with D_{s1} of DMSP as $4.2 \pm 0.1\times10^{-6}$ cm^2/s (obtained in a separate experiment), D_{s2} was calculated to be $6.6 \pm 0.2\times10^{-6}$ cm^2/s. Since the DMSP D_s at 37 ^{o}C was lower than the value predicted by Eq. 5, it was concluded that convection was not an issue in these experiments.

3.2 In Vivo Studies

The HRA-2 image (see Figure 20) of the vitreous humor of the rabbit's left eye taken after intravitreal injection of Na-F showed a spheroidal diffusing front of the fluorophore. This indicated that the bolus takes a spheroidal shape after being deposited in the vitreous humor. The Na-F concentration profiles for both the left and right eyes are shown in Figure 21. The location of the concentration peak of each profile is the point on the optical axis that is closest to the bolus delivery. The concentration peak in each profile was closer to the anterior region of the vitreous humor. Also, the peak location appeared to be consistent in the left eye with time, but in the right eye the location retreated posteriorly as time advanced. The concentration profile at each time point decreased towards the retina and towards the anterior chamber. In the left eye, the concentration fell as time progressed. However, in the right eye the concentration continuously increased, and then fell sometime after 1.5 hr. It was interesting to note that even after four days Na-F was detected in the right eye.

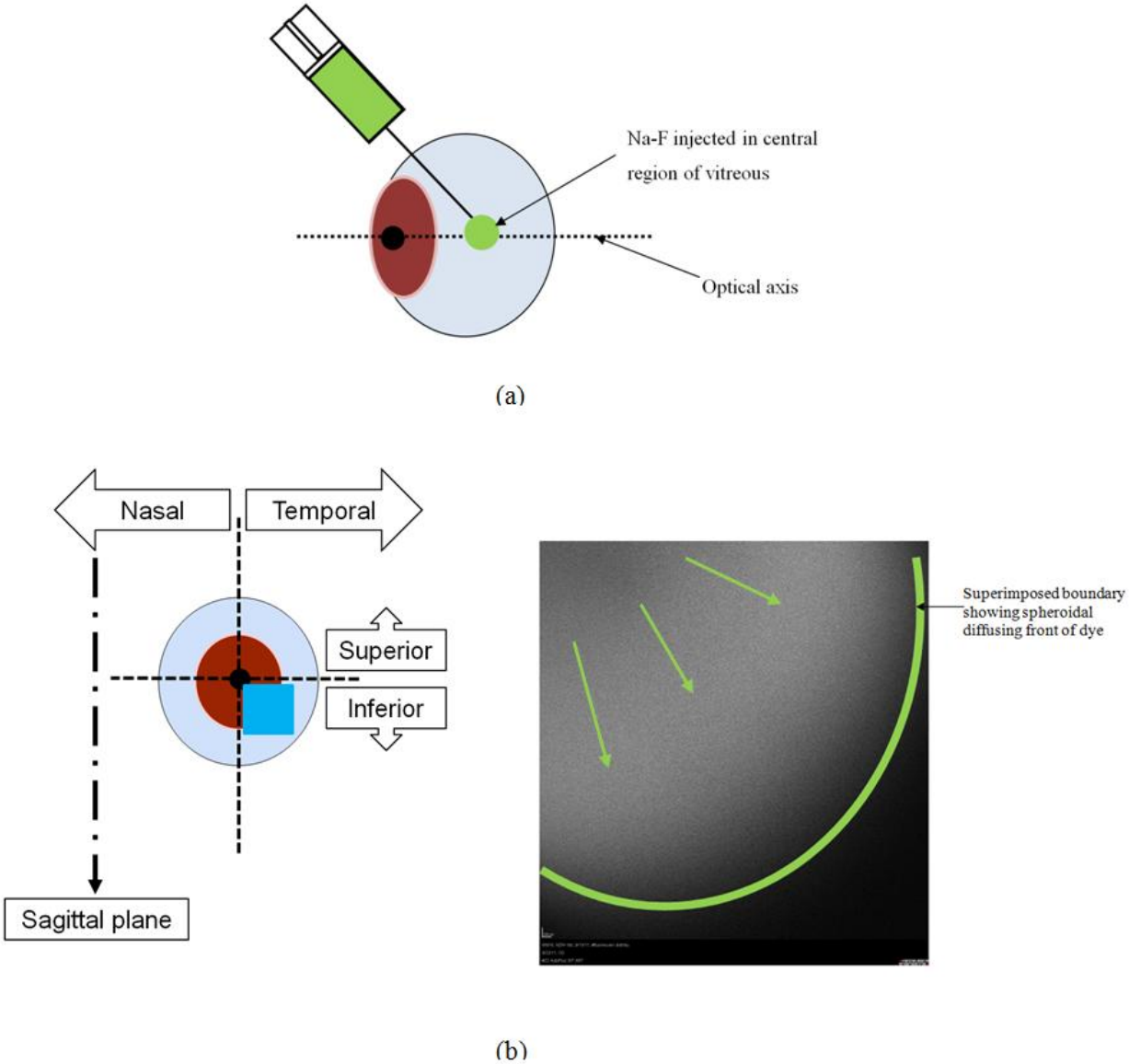

Figure 20 (a) Schematic showing side view of Na-F injection into the central vitreous humor of rabbit eye. The injection angle was approximately 40^{o} to the optical axis. (b) HRA-2 image of front view of lower temporal region of vitreous humor taken 10 minutes after injecting Na-F (right). The lighter regions represent Na-F. Arrows have been superimposed to emphasize radial outward diffusion of the dye. The blue box in the diagram to the left highlights the region of the vitreous where the image of the Na-F distribution was captured.

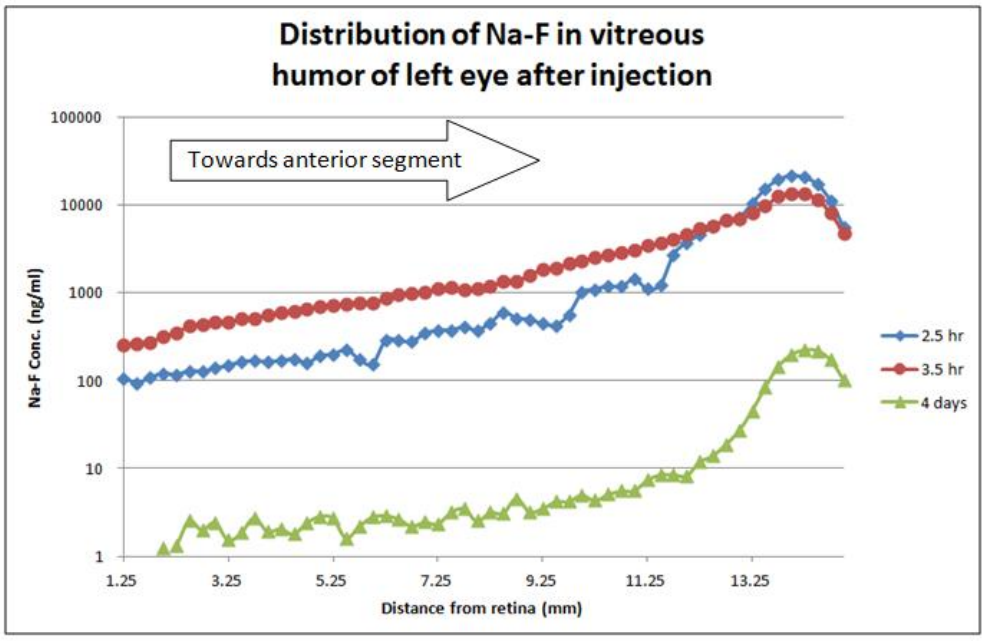

(a)

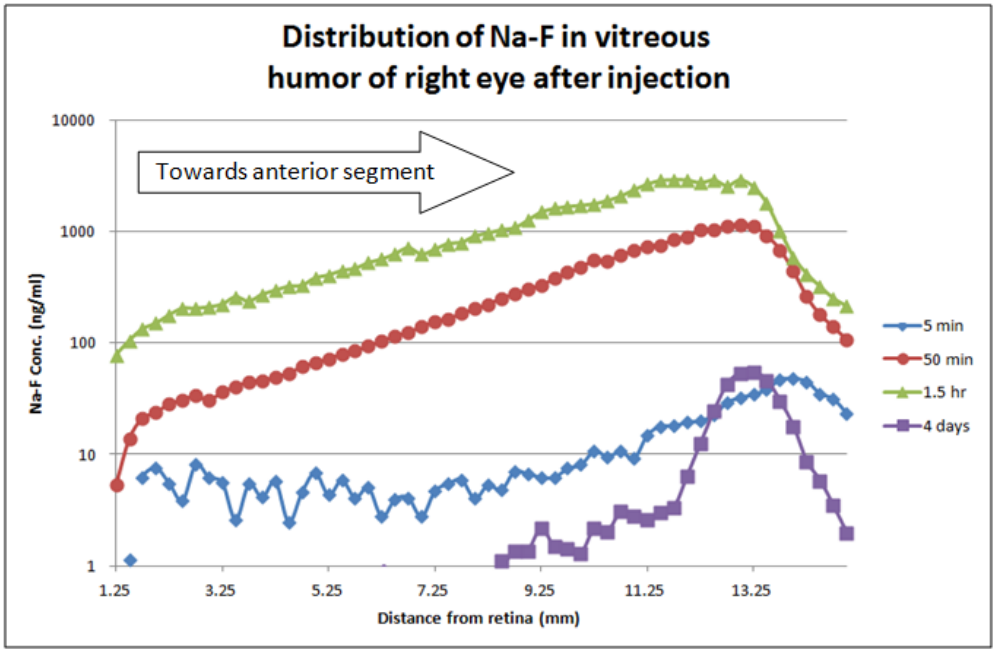

(b)

Figure 21 Na-F concentration profiles in the vitreous humor of (a) the left eye and (b) the right eye of the rabbit (n=1) obtained using the Fluorotron ™ Master

4 Discussion

4.1 Influence of Solute Size on Mutual Diffusivity and Convection

Both transscleral and intravitreal drug delivery techniques are important for the treatment of ocular diseases that affect the posterior segment of the eye. Since drugs must be transported through vitreous humor for both delivery methods, it is necessary to understand how the physicochemical properties of these drugs affect their transport in this ocular tissue. This knowledge will be useful in predicting how the properties of new compounds will affect their ability to reach the affected tissue, and, therefore, will aid in the development of new drugs. One goal of this study was to examine how solute size affects drug transport in the vitreous humor.

It was clear that the mutual diffusivity of the solutes examined was a function of both molecular weight and radius. The correlations for the linear regression in Figure 18 and Figure 19 indicated that the molecular radius was a better predictor for diffusion in PBS and porcine vitreous humor. On the other hand, the molecular weight turned out to be a better predictor for diffusion in rabbit vitreous. However, the difference between correlations for both molecular weight and radius was not significant. In studies that have examined other ocular tissues such as the sclera [50], [52], cornea [50], conjunctiva [50], and RPE [54], it was found that the molecular radius was a definite determinant of permeability across these tissues. Ambati et al. [52] found that the molecular radius was a better predictor of sclera permeability than was the molecular weight. Given that only six solutes were examined in this study, the data was insufficient to determine conclusively whether the molecular weight, or the molecular radius was the stronger diffusivity predictor. As mentioned before, theoretical correlations such as the Stoke's Einstein equation describe inverse relations between mutual diffusivity and molecular radius [72]. However, since diffusivity scales with the cube root of the molecular weight, drug diffusivity in the vitreous humor should, in theory, have a stronger dependence on the molecular radius.

There was no obvious trend in mutual diffusivity of small molecules with either molecular weight or radius. The same was true for the large molecules. One factor that could account for this was the variability inherent in the vitreous humor obtained from both porcine and rabbit eyes. The age of the animals was not controlled for, except that they were adults. As explained in section 1.5.5, the vitreous humor undergoes liquefaction with age and therefore becomes less

viscous. The diffusivity was unexpectedly high in some cases, such as for the diffusion of FD150 in porcine vitreous, and the diffusion of DMSP in rabbit vitreous. It was possible that the vitreous humor used in some of the experiments with those solutes may have come from eyes of animals that were fairly advanced in age where the vitreous viscosity is expected to be less than of that in younger adult eyes. Ambati et al. [52] noticed that the sclera permeability to FITC-dextran (70kDa) was not significantly greater than that of FD150, which to them suggested that the hydrodynamic radii of these molecules within the sclera was not identical with their molecular radii in aqueous solution. With regards to the FITC-dextrans in this study, the same might also have been true where the hydrodynamic radii of these molecules may have varied depending on the diffusion medium. This theory may also explain the unexpected observation of FD150 diffusing faster than FD40 in porcine vitreous (see Table 5).

As mentioned in section 1.6, drug transport in the eye occurs by both convection and diffusion. The Peclet number (*Pe*) can be used to determine which of the two transport mechanisms is dominant, and is defined as follows:

$$\boldsymbol{Pe = \frac{vL}{D_m}} \qquad \textbf{Eq. 6}$$

where v is the nominal flow velocity of the vitreous humor, and L is the length scale over which the transport occurs. Using a nominal flow velocity for rabbit vitreous of 3.5×10^{-7} cm/s as determined by Kim et al. [17], a length scale of 1 cm, and the mutual diffusivities obtained for the smallest (Na-F) and largest (FD150) molecules in this study (see Table 5), the corresponding Peclet numbers were calculated to be 0.05 and 0.1 respectively. These values imply that although the influence of convection becomes more pronounced for large solutes, over the range of solute size examined (up to 150,000 Daltons), diffusion is the dominant mechanism of transport in rabbit vitreous.

4.2 Diffusion in Vitreous of Different Animal Models

The viscosity of the vitreous humor is a function of the concentrations of collagen and of hyaluronan (sees section 1.5.2). The concentrations of these two macromolecules vary among

mammalian species. As mentioned before (see section 1.5.4), the vitreous space of most mammalian species, with the exception of humans and some species of monkeys, is filled with gel vitreous [38]. Balazs and Denlinger [38] reported the macromolecular composition of vitreous humor for different species. Larger species such as cattle and sheep have higher hyaluronan concentrations: 110 – 1070 µg/ml and 100 – 400 µg/ml respectively, compared to smaller species like dogs and cats: 40–60 µg/ml and 20 – 40 µg/ml respectively[38]. The same relationship is not apparent for collagen concentration, with humans having 40–120µg/ml and owl monkeys having 1250 – 2580 µg/ml.

Noulas et al. [96] reported the porcine vitreous hyaluronan and collagen concentrations to be 76 µg/ml and 150 µg/ml. Boruchoff and Woodin [97] measured lower hyaluronan and collagen concentrations of 26µg/ml and 128 µg/ml, respectively, for rabbit vitreous. With lower concentrations of these macromolecules in rabbit vitreous, the corresponding viscosity is expected to be lower than that of porcine vitreous. Consequently, with a lower viscosity, diffusivity should be greater in rabbit vitreous. However, the difference in macromolecular concentrations does not translate to a significant difference in diffusivity. It is therefore apparent that solute diffusivity is similar in both porcine and rabbit vitreous. An inference from this result is that mutual diffusivity data of other solutes obtained from either porcine or rabbit vitreous may be compared, and therefore the need to obtain data for the same vitreous system is not essential. However, whether this finding can be extended to other common vitreous models is yet to be demonstrated experimentally. It may not be prudent to extrapolate the observation of this study to other systems such as human and bovine vitreous given that the concentrations of hyaluronan and collagen are significantly different than those of porcine and rabbit vitreous. The hyaluronan concentration of the human vitreous is reported to be 192 µg/ml [5]. However, this concentration is less than that of bovine vitreous (496 ±44 µg/ml) [46]. Collagen concentration is greater in the human vitreous (300 µg/ml) compared to that in bovine vitreous (60 µg/ml) [5].

In general, the error for diffusivities in porcine vitreous was smaller than for diffusivities in rabbit vitreous. In handling the vitreous, extractions from rabbit eyes were generally observed to be less viscous than extractions from porcine eyes. The viscosity of the vitreous humor was most likely altered due to inevitable shearing as the vitreous was charged into the middle compartment using the 16 gauge needle for the diffusion experiments. It is therefore likely that rabbit vitreous

samples may have undergone more shearing due to their apparent lower viscosity which could explain the larger errors observed for diffusivity in this medium than was observed in porcine vitreous.

The mutual diffusivity can be used to give a rough estimate of the minimum time needed for a drug to take effect after being delivered which, in essence, would be the time the drug takes to penetrate from the point of delivery to the target area. The region in the vitreous humor between the drug deposition and the retina can be modeled as a semi-infinite medium. Let the distance between the drug deposition and the retina be *z*. If a drug solution or an implant is deposited in the vitreous humor, then we can use the following equation to calculate the time it would take for a point with distance *z* to obtain a concentration that is 1% of the original drug solution or of the implant's surface concentration:

$$t = \frac{z^2}{16 D_m} \qquad \textbf{Eq. 7}$$

DMSP showed the greatest disparity between its sample mean mutual diffusivity in porcine vitreous and in rabbit vitreous, with the diffusivity in the former being half of that in the latter. If the difference in the mean diffusivities had turned out to be statistically significant (no overlap in standard errors), it would be interesting to see what impact that difference can have on deductions about drug delivery in human vitreous humor. To assess this impact, let us examine a drug delivery scenario relevant to DMSP. Dexamethasone is delivered intravitreally by an implant known as Ozurdex® to treat the swelling of the macula following branched retinal vein occlusion [98]. Using DMSP as a surrogate for the dexamethasone instead, Eq. 7 can be used to estimate the time it would take for DMSP to reach the macula of the human eye from a centrally inserted intravitreal implant like Ozurdex®. Using a length scale of 0.7 cm (half the length scale of the human vitreous [14]), and the D_m of DMSP in porcine vitreous, it would take about 1 hour for the drug to reach the macula. Alternatively, the D_m of DMSP in rabbit vitreous gives a penetration time of approximately 50 minutes. The significant difference in diffusivities (see Table 5) does not translate to a significant difference in penetration time. This small difference in penetration time is not likely to be clinically relevant given that most intravitreal drug delivery systems that deliver corticosteroids last for extended periods: Ozurdex® for at least two months [98]; Retisert® for three years; and Iluvien™ for 18-36 months [21]. Also, this finding suggests

that the diffusivity obtained using either animal model can yield similar extrapolated information for the human eye.

4.3 Relation between Diffusion in PBS and in Vitreous

Mutual diffusivity in the vitreous humor was compared to that in PBS. The study showed that for both small and large molecules, the mutual diffusivity of solutes in porcine vitreous humor can be 30 – 60% of their value in PBS, whereas in rabbit vitreous the corresponding diffusivity relation can range from 40 – 65%. Ohtori and Tojo [66] found the mutual diffusivity of dexamethasone sodium m- sulfabenzoate in rabbit vitreous to be $5.1 \times 10^{-6} cm^2/s$, which was 70% of the diffusivity in water. This relation is comparable to that obtained in the current study for the mutual diffusivity of DMSP in rabbit vitreous which was 65% of that in PBS. Stay et al. [32] reported that the mutual diffusivity of small molecules ranging from 300–600 Da in the vitreous humor is 60 – 75% of that in water. However, this relation was only based on three molecules: acid 8 orange, fluorescein, and DMSB. In the current study, the mutual diffusivity of the small molecules in porcine vitreous was 30–40% of their value in PBS, while in rabbit vitreous the corresponding diffusivity ranged from 40–65% of that in PBS. The vitreous-aqueous diffusivity relation for the larger FITC-dextran molecules was found to vary significantly. The mutual diffusivity of the large molecules in porcine vitreous was 40–60% of their value in PBS, while in rabbit vitreous the corresponding diffusivity ranged from 40–50% of that in PBS. Considering the range of mutual diffusivities obtained for both vitreous models, we elected to report vitreous-aqueous diffusivity relations for both small and large sized drugs. Mutual diffusivity in the vitreous humor can be 30 – 80% of the value in PBS. This range contains that reported in [32]. Conversely, for large sized solutes, mutual diffusivity in the vitreous humor can be 40 – 60% of the value in PBS. These ranges can be used to give rough estimations of mutual diffusivities of new drugs based on their values in aqueous media such as PBS. Upper and lower bounds on the estimated mutual diffusivity can give a rough estimation for diffusion through intact vitreous (lower bound) and through more liquefied vitreous (upper bound), as in eyes of seniors where vision threatening diseases are more prevalent.

The diffusivity obtained for Na-F in PBS matched closely with that measured by Santoro et al. [99] who reported a value of $1.76 \times 10^{-5} cm^2/s$ for the transport of this same solute through a

hydrogel of which 98.5% was PBS. It was interesting to note that the mutual diffusivity measured in this study for Na-F diffusion in both porcine and rabbit vitreous was similar to that reported by Kaiser and Maurice [68] for Na-F diffusion in agar gel with a value of $6\times10^{-6}cm^2/s$. Their value has been used in mathematical models to simulate drug distribution in the vitreous humor with some good agreement between predicted and experimental profiles [36], but with the recognition that a more accurately measured value is still needed [60]. Kaiser and Maurice asserted that the diffusivity they measured is independent of agar concentration which implies that Na-F would have the same diffusivity in agar free medium. However, this study showed that there is significant difference between diffusion in the vitreous humor and in aqueous medium (PBS) with Na-F diffusivity in porcine vitreous being 36% of the value in PBS, and diffusivity of this solute in rabbit vitreous being 50% of the value in PBS. It is therefore evident that diffusion in agar gel cannot be likened to diffusion in the vitreous humor. Mutual diffusivities of solutes should therefore be determined in actual vitreous humor.

4.4 Comparison between Self Diffusivity and Mutual Diffusivity

Gisladottir et al. [41] measured the mutual diffusivity of dexamethasone in porcine vitreous to be lower than in saline. They asserted that diffusivity in the vitreous is lower than in free aqueous solution due to the difference in viscosity. Barton et al. [70] challenged this assertion by showing that self diffusivity of fluorescent dyes in the vitreous humor was essentially the same as that in PBS. However, Barton et al.'s challenge can only be valid if Gisladottir et al. had also measured self diffusivity, which is not the case. Whether the two studies are comparable is uncertain since mutual diffusivity and self diffusivity are based on different time and length scales. Very few reports have compared mutual diffusion and self diffusion in the same system in the same conditions. No study until now has examined both types of diffusion in the vitreous humor.

The self diffusivities of DMSP in both porcine and vitreous humor were virtually the same, and were also similar to that in PBS. This comparison is in agreement with Barton et al.'s study where the self diffusivities of fluorescent molecules were found to be similar in salt solutions and in porcine vitreous. Kwak et al. [77] measured the self diffusivity of phosphate ions in 20% dextran/H_2O gels to be less than in aqueous KCl solution. They explained that the restricted diffusion in the gels was associated with steric obstruction formed by the dextran polymer

network. In our study, the similarity of DMSP self diffusivity in PBS and in vitreous suggests that the network of collagen and hyaluronan presented no hindrance to self diffusion, which is consistent with the low combined concentration of these macromolecules in the vitreous (less than 1%). It should, however, be noted that the network of these macromolecules could have been significantly altered in the preparation of the vitreous-DMSP solution (see section 2.3.2.1). Otherwise, it may be inferred that the self diffusivity of a given solute in PBS can be taken as a good estimation of its value in the vitreous humor.

Table 6 shows that the mutual diffusivity was significantly greater than the self diffusivity for transport in PBS. This observation is concordant with Santoro et al.'s [99] study where the mutual diffusivity of Na-F was found to be higher than the self diffusivity for transport in PBS based hydrogels. The mutual diffusivity of Na-F found in PBS for this study ($1.6 \pm 0.7\times10^{-5}$ cm^2/s) was also higher than self diffusivity measured by Casalin et al. [100] in water ($3.9 \pm 0.4\times10^{-6}$ cm^2/s). An explanation that could account for the difference in the DMSP diffusivities measured in PBS is the difference in concentrations used in each experiment method. Diffusivity is known to become concentration dependent when solutions approach high concentrations. The DMSP sample concentration in DOSY NMR experiments was 10 mg/ml, which was four times higher than the donor concentration used in the diffusion cell experiments. The lower diffusivity measured by DOSY NMR is consistent with the higher sample concentration as diffusivity is expected to fall with increase in concentration. However, the two-fold difference in diffusivities was unexpectedly high. The effect of concentration on diffusivity is expected to be more pronounced for large sized solutes such as protein molecules since they will be influenced by solute-solute interactions to a greater extent than in the case of small sized solutes like DMSP. Keller et al. [73] measured the mutual diffusivity of hemoglobin for a wide range of protein concentrations in aqueous media, and measurements remained consistent for donor cell concentrations up to 50 mg/ml. It is therefore unlikely that the difference in DMSP concentrations (10 mg/ml versus 2.5 mg/ml) used in this study caused the significant difference observed between the two diffusivities.

Another theory that may account for the difference between the two diffusivities in PBS is the occurrence of electrostatic drag. A study by da Costa et al. [101] examined the diffusion of tetrasodium tetraphenylporphyrintetrasulfonate (Na_4TPPS) in water, and found the mutual

diffusivity to exceed the self diffusivity. It was posited that the difference is due to the electrostatic dragging effect of sodium ions on $TPPS^{4-}$. Electrostatic or ion drag forces refer to the momentum transfer resulting from the collision between a charged species having a large directed velocity, and a second charged species [102]. In the DMSP diffusion cell experiments with PBS, all three compartments contained the same concentration of cations and anions that make up the buffer. However, in addition to the constant surplus of hydrated dexamethasone phosphate (DMP) anions in the donor compartment, there was also a constant surplus of sodium cations originating from the dissolved DMSP. It may therefore be speculated that the ensuing flux of hydrated DMP anions into the middle chamber may have been supplemented by an electrostatic drag effect due to the flux of sodium cations that occurred in tandem. The drag effect could have aided the DMP anions in breaking the hydrogen bonds of the water molecules in turn enhancing mutual diffusivity.

Mutual diffusivity is not always found to exceed self diffusivity. The results of Kwak et al.'s [77] study on the transport of phosphate ions in dextran gels illustrate this case where they measured self diffusivity of the phosphate ions to be greater than the mutual diffusivity. Kwak et al. measured self diffusivity using DOSY NMR, which used a diffusion time of 60 ms that corresponded to a diffusion length of 10 μm. Mutual diffusivity was measured using 1D NMR ^{31}P NMR profiling experiments that were designed to meet the conditions of the equations that describe diffusion in a semi-infinite medium. Here, the diffusion time and diffusion length were longer, being 18 hours and 50 mm, respectively. Kwak et al. reasoned that the mutual diffusion was expected to be more sensitive to the structure of the gel than the self diffusion because of the longer diffusion length and time in the mutual diffusion experiments where the phosphate ions would need to overcome more barriers formed by the gel's structure to be transported from one position to the other.

The difference between mutual diffusivity and self diffusivity of DMSP in porcine vitreous was shown to be statistically insignificant for both transport in porcine and rabbit vitreous. These results seem to suggest that mutual diffusivity and self diffusivity are not significantly different in the vitreous humor. Nevertheless, our study highlights how significantly different the mutual diffusivity and self diffusivity can be, as in the case with DMSP diffusion in PBS. On the whole, the relation between self diffusivity and mutual diffusivity in liquids and gels is not yet

understood, and poorly investigated. It is evident, from this study and others, that the comparison between the two types of diffusivities is different for every system. Caution must therefore be exercised when comparing drug diffusivities from reports that have used different experiment techniques.

4.5 In Vivo Drug Distribution

When using mathematical models to predict the distribution of a drug after intravitreal injection, it is necessary to know what the initial shape of the deposition is, as this dictates what geometric system must be used for the mass balance (cylindrical, spherical). The Spectralis HRA-2 was used to capture an image of the bolus shortly after injection. Examination of Figure 20 reveals a spheroidal shape of the initial distribution postinjection, thus indicating that the bolus delivery can be modelled as a spherical system.

The objective of this part of the study was to measure the distribution of Na-F along the optical axis after injecting the dye in the central region of the rabbit's vitreous humor. Convective transport due to saccadic eye rotations was minimized by the sedative effect of the anaesthetics. During injection, it was often difficult to maintain the needle in the desired position and orientation (see section 2.4.3) while depressing the plunger. Based on the position of the profile peak for the early time points, it was possible to tell where along the optical axis the Na-F bolus was delivered. As can be seen from Figure 21, the concentration peaks are all closer to the anterior region indicating that the Na-F may not have been deposited in the central region of the optical axis. During the scan process, the rabbit's head must be held as stationary as possible (see Figure 15). It was possible that the distance between the lens and the right eye was not consistent between scans, which would explain why the peak location appeared to change in the right eye.

Na-F concentration decreased towards the retina and towards the anterior segment for each time point. This observation is consistent with ex vivo profiles obtained by Araie and Maurice [60] for the distribution of Na-F in rabbit eyes. The negative concentration gradients that developed on both sides of each profile peak can be explained by active outwards transport at the retina and solute migration into the anterior chamber where efflux occurs through the trabecular meshwork [6], [103]. In the left eye, concentration fell as time progressed. However, in the right eye, concentration continuously increased, and then fell sometime after 1.5 hr. This initial rise and

subsequent decrease in concentration was, most likely, because the Na-F delivery was not in the central vitreous, but rather was off to the temporal or nasal region. Consequently, Na-F would have diffused into the region of the optical axis with time leading to the initial rise in concentration, and then be removed at the blood-aqueous and blood-retinal barriers by the aforementioned mechanisms.

The data obtained in this experiment was not ideal. The off centre occurrence of the concentration peaks along the optical axis, as well as the initial rise and fall of the concentration readings in the right eye all indicate that the injection location was not central. Ocular PK models can predict intravitreal Na-F distribution for a specific injection location. Validation of these predicted profiles will not be possible if the dye cannot be injected in the desired location of the vitreous. The duration of the injection must also be considered. The initial distribution of the dye during and immediately after injection will be influenced by the induced convection that inevitably occurs as the dye flows out of the needle under pressure. This undesirable effect must be minimised by injecting at a slow, yet practical rate.

5 Conclusions and Recommendations

In summary, the present findings give some insight into understanding drug diffusion in the vitreous humor. An inverse relationship exists between mutual diffusivity in the vitreous and solute size. It was uncertain whether molecular weight or radius was the better predictor. Theoretically, mutual diffusivity should have a greater dependence on molecular radius than on molecular weight. Nevertheless, it is recommended that the effect of both properties be considered when developing new drugs for therapy of posterior segment diseases. The Peclet numbers of the smallest (Na-F) and largest (FD150) solutes examined were calculated for transport in the rabbit vitreous and they showed that diffusion is the dominant transport mechanism.

Mutual diffusivity was found to be similar in rabbit vitreous and in porcine vitreous. This observation was despite the difference in concentrations of hyaluronan and collagen between the vitreous of the two animal species. Notwithstanding the significant difference in the mean mutual diffusivities between the two animal species, drug penetration times extrapolated for the human eye based on either diffusivity were similar. Porcine and rabbit vitreous are regarded as good models for human vitreous and are popular choices for in vitro experiments mainly because they are easily accessible. Rabbits are the main candidates for in vivo ocular studies because they are easy to obtain and are manageable in an operating room for multiple experiments. Often, the choice of which species is selected depends on cost, availability of animal supply and availability of the appropriate facilities. No matter which species is used, the data obtained is always useful and gives some insight into how drugs may be distributed in the human vitreous. Recognizing this, it is difficult to recommend one species as a better model than the other.

Some studies suggest that the vitreous can be modeled essentially as water owing to the fact that this tissue is composed of 99% water. However, this work has shown definitively that diffusion in the two media is measurably different, with the average mutual diffusivities of small solutes in vitreous being 30 – 65% of that in PBS. Additionally we also report a range for the average mutual diffusivities of large solutes in vitreous to be 40 – 60% of the values in PBS. The results in these studies can be used to make a rough estimation as to what the range of mutual diffusivity of a solute would be in the vitreous humor based on measurements in PBS, which are easier to

obtain. However, the limited data available on mutual diffusivities of solutes in the vitreous of different species makes it difficult to arrive at a vitreous-aqueous diffusivity relation that applies to all solutes for diffusion in different species. More studies need to be done that examine the mutual diffusion of a larger collection of ocular drugs and drug-surrogates in the vitreous humor of different species as well as in aqueous media.

This work has presented the use of DOSY NMR as a new technique for measuring self diffusivity, or microdiffusivity of drugs in the vitreous humor. The findings of this study suggested that mutual diffusivity or macrodiffusivity, and microdiffusivity in the vitreous humor are comparable. However, in all cases of drug administration to the vitreous humor, drug diffusion is Fickian requiring the measurement of macrodiffusivity. In light of this, it would be more rigorous to obtain the macrodiffusivity directly where possible. Nonetheless, knowledge of the microdiffusivity of probe molecules in the vitreous is still useful as it can be used to shed light on the macromolecular matrix structure of this gel as was done for other similar systems [84].

The Spectralis HRA-2 was used for the first time to obtain imagery of a fluorophore deposition after intravitreal injection. The image showed that the bolus and its subsequent distribution can be modeled by a spherical system. A method has been presented that uses the Fluorotron Master™ to measure in vivo the time dependent change in intravitreal concentration of Na-F along the optical axis postinjection. This methodology would be useful in providing data to which predicted profiles can be compared to for model validation. However, injecting at the desired region of the vitreous is often difficult to achieve as was manifested in the concentration profiles. There needs to be an improved method of injection, so that any unwanted movement of the needle is minimized while depressing the plunger to administer the dye. An angle marker should be used so that the needle is always aligned and parallel to it to ensure that the required angle of injection is maintained as best as possible. Also, the injector's hand should be supported by some means to minimize free movement. A needle having a length no longer than half an inch should be used. The reduced length will prevent bending of the needle that occurs when trying to pierce the sclera, and will also help in maintaining the required injection angle. During the scan step of the fluorophotometry, the hands of the person holding the rabbit's head should be

supported, as this will aid in maintaining the distance between the eye and the lens of the Fluorotron Master™.

6 Nomenclature

DMSP	Dexamethasone Sodium Phosphate
DOSY NMR	Diffusion Ordered Nuclear Magnetic Resonance Spectroscopy
D_m	Mutual Diffusivity
D_s	Self Diffusivity
FCS	Fluorescence Correlation Spectroscopy
FD150	FITC-conjugated dextrans(150kDa)
FD4	FITC-conjugated dextrans(4kDa)
FD40	FITC-conjugated dextrans(40kDa)
FITC	Fluorescein Isothiocyanate
FM	Filter Membranes
GAG	Glycosaminoglycan
Gd-DTPA	Gadolinium-diethylenetriaminopentaacetic Acid
$K_{o/w}$	Octanol-Water Partition Coefficient
MR	Molecular Radius
MRI	Magnetic Resonance Imaging
MW	Molecular Weight
Na-F	Sodium Fluorescein
PBS	Phosphate Buffered Saline

PEG	Poly(ethylene glycol)
Pe	Peclet Number
PVH	Porcine Vitreous Humor
RCS	Retina/Choroid/Sclera
RPE	Retina Pigment Epithelium
RVH	Rabbit Vitreous Humor
TFA	Trifluoroacetic Acid
TM	Timolol Maleate
UV	Ultra Violet
Δ	Time between successive gradient pulses
δ	Duration of the magnetic field gradient strength
γ	Gyromagnetic ratio specific to a spin-active nucleus
R	Ratio of a NMR signal with a diffusion-sensitizing magnetic field gradient strengths to that without

7 Appendices

Appendix i Concentration Calibration Curves

The following calibration curves were used to convert the UV-visible spectrophotometer readings to solute concentration for samples collected from the receptor cell in the diffusion cell experiments. A different batch of FD150 was used for the experiments with rabbit vitreous, so a new calibration curve (batch 2) was prepared.

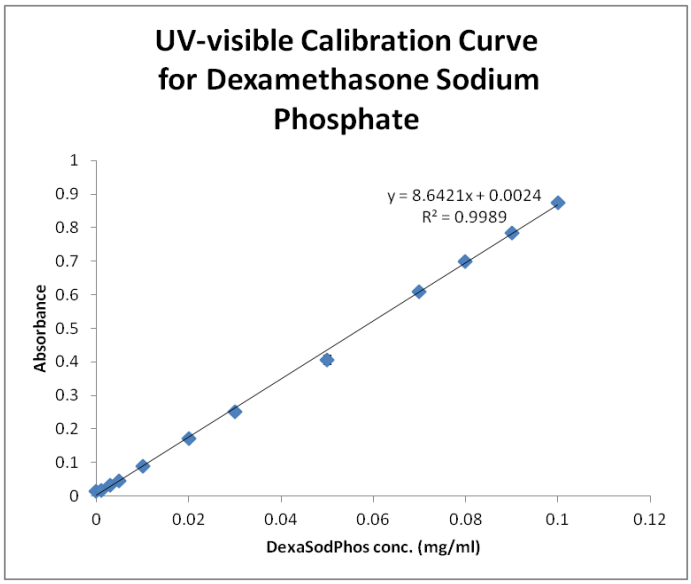

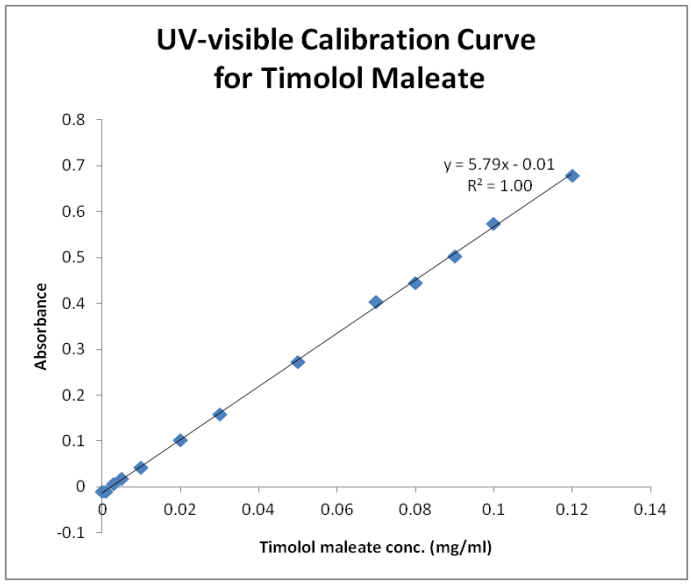

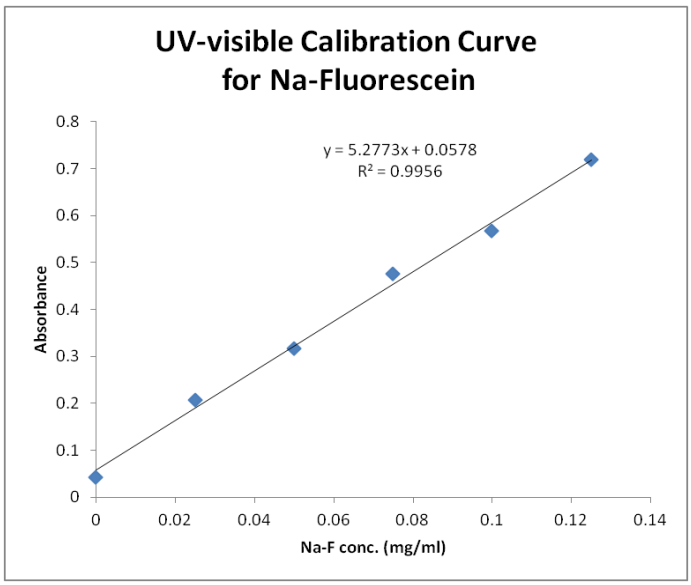

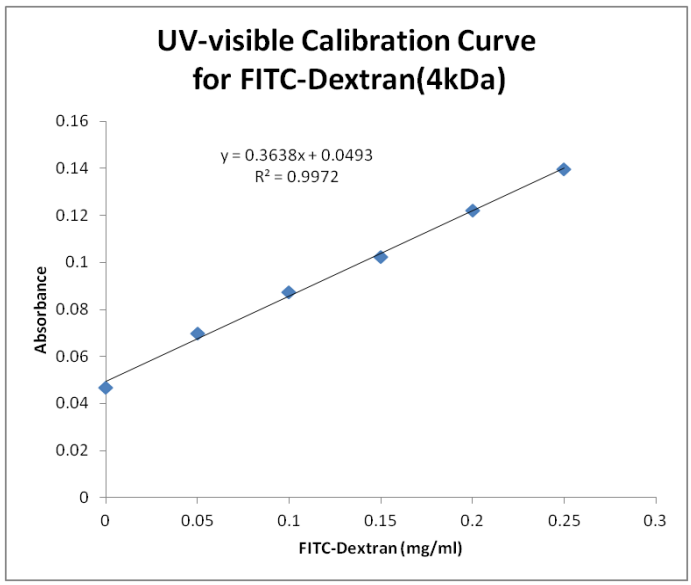

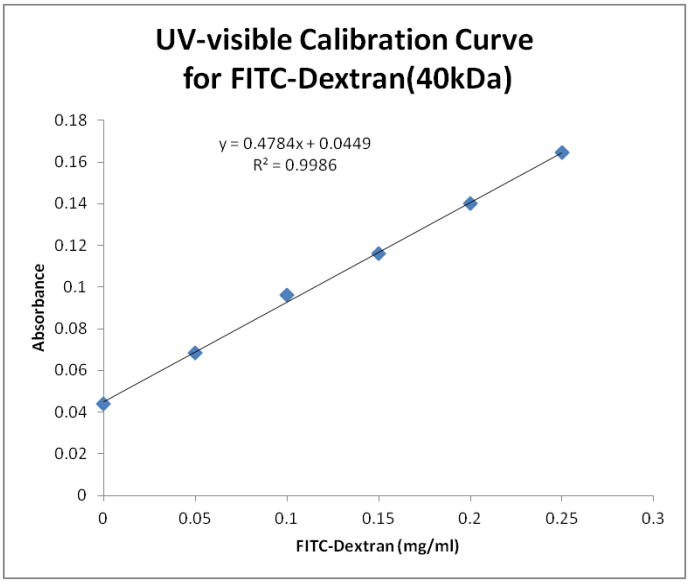
UV-visible Calibration Curve
for FITC-Dextran(40kDa)
y = 0.4784x + 0.0449
R² = 0.9986
Absorbance
FITC-Dextran (mg/ml)
0.18
0.16
0.14
0.12
0.1
0.08
0.06
0.04
0.02
0
0
0.05
0.1
0.15
0.2
0.25
0.3

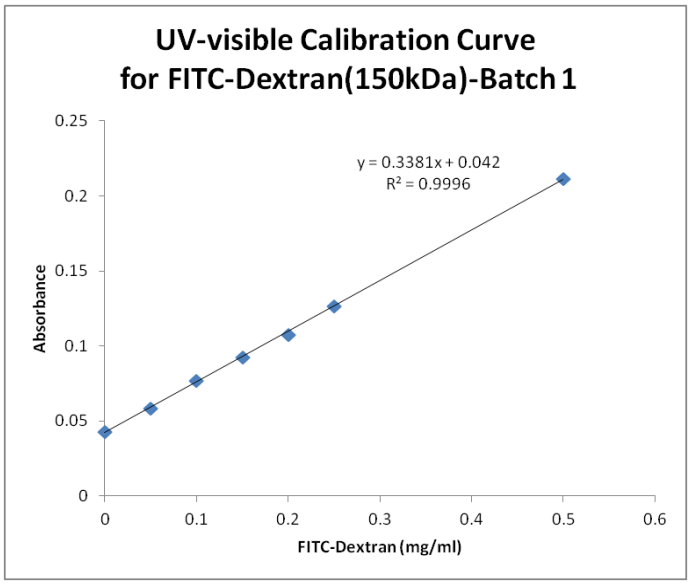
UV-visible Calibration Curve
for FITC-Dextran(150kDa)-Batch 1
y = 0.3381x + 0.042
R² = 0.9996
Absorbance
FITC-Dextran (mg/ml)
0.25
0.2
0.15
0.1
0.05
0
0
0.1
0.2
0.3
0.4
0.5
0.6

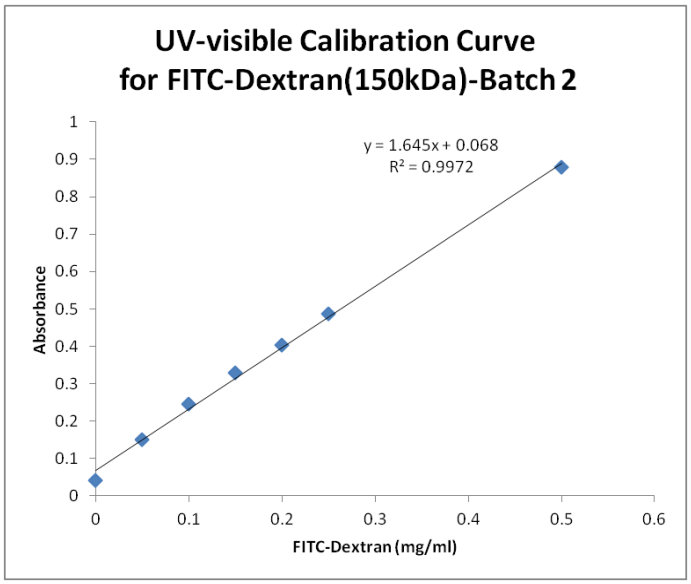
UV-visible Calibration Curve
for FITC-Dextran(150kDa)-Batch 2
y = 1.645x + 0.068
R² = 0.9972
Absorbance
FITC-Dextran (mg/ml)
1
0.9
0.8
0.7
0.6
0.5
0.4
0.3
0.2
0.1
0
0
0.1
0.2
0.3
0.4
0.5
0.6

Appendix ii Concentration Profile Curves

All concentration profile curves of solutes examined are reported for diffusion through PBS, porcine vitreous and rabbit vitreous. Only the steady state portion of each curve is shown. The associated normal probability plot that was used to check the linear fit of the steady state region is also shown for each curve.

Aii-1 Mutual Diffusion in PBS

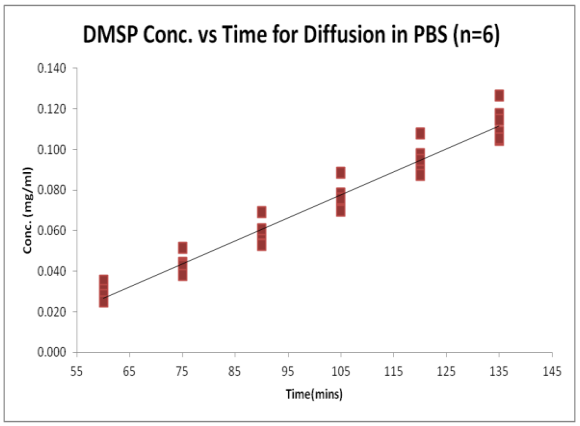

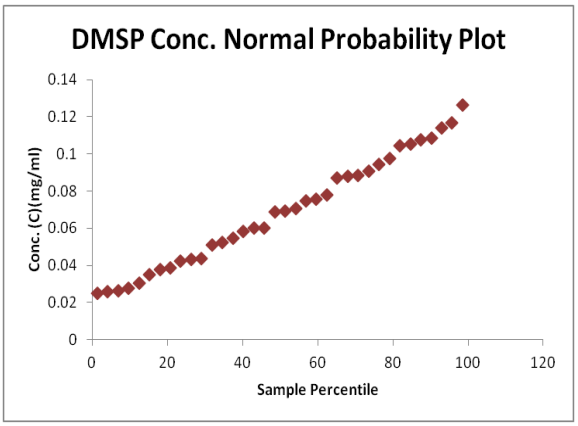

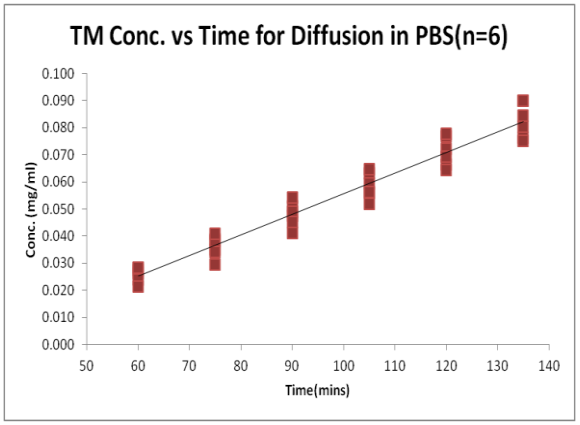

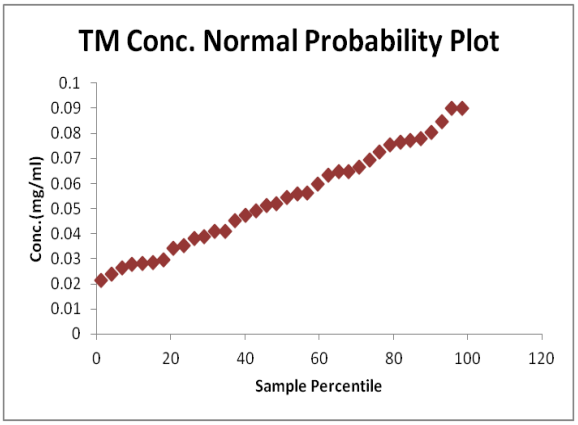

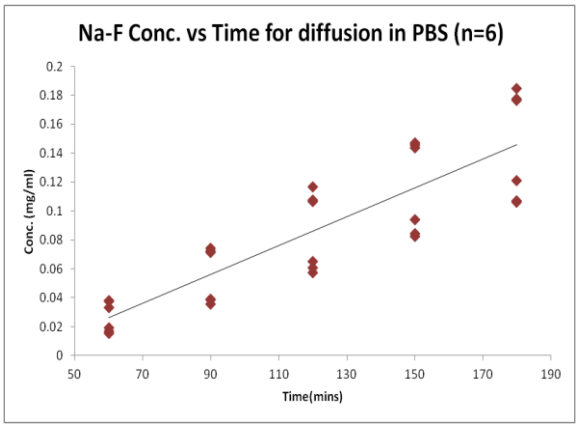

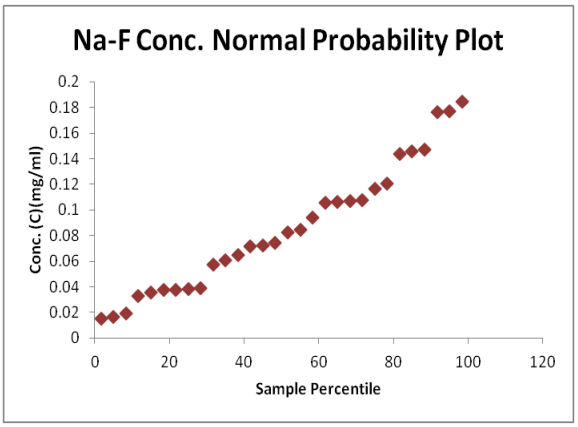

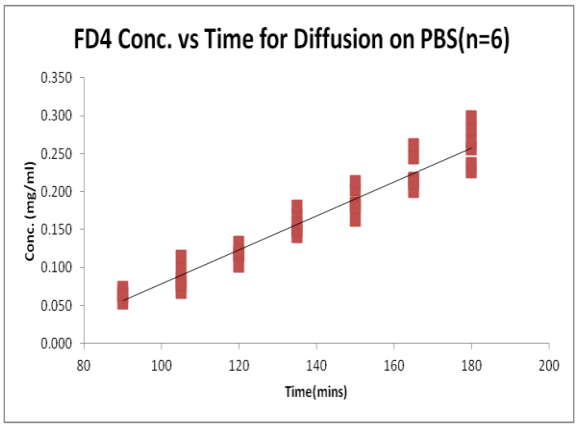
FD4 Conc. vs Time for Diffusion on PBS(n=6)
Conc. (mg/ml)
0.350
0.300
0.250
0.200
0.150
0.100
0.050
0.000
80
100
120
140
160
180
200
Time(mins)

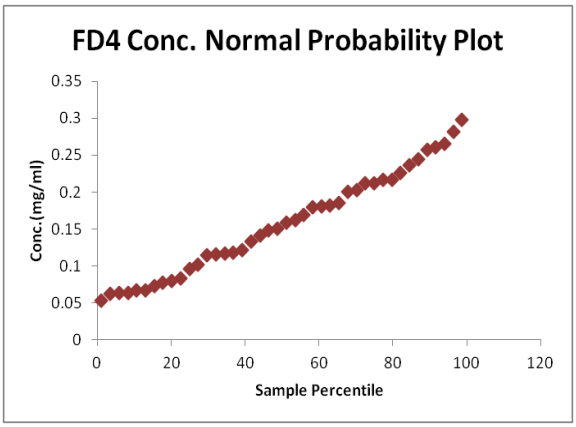
FD4 Conc. Normal Probability Plot
Conc.(mg/ml)
0.35
0.3
0.25
0.2
0.15
0.1
0.05
0
0
20
40
60
80
100
120
Sample Percentile

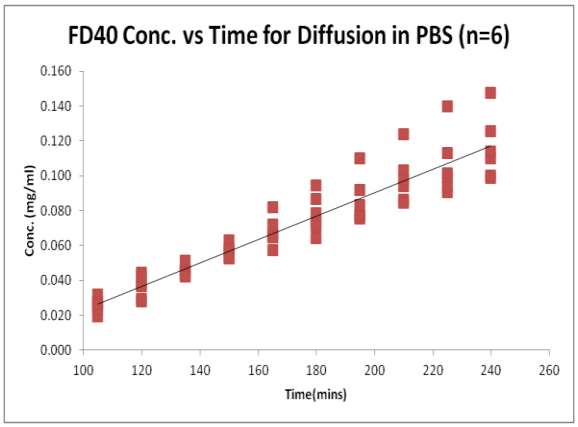
FD40 Conc. vs Time for Diffusion in PBS (n=6)
Conc. (mg/ml)
0.160
0.140
0.120
0.100
0.080
0.060
0.040
0.020
0.000
100
120
140
160
180
200
220
240
260
Time(mins)

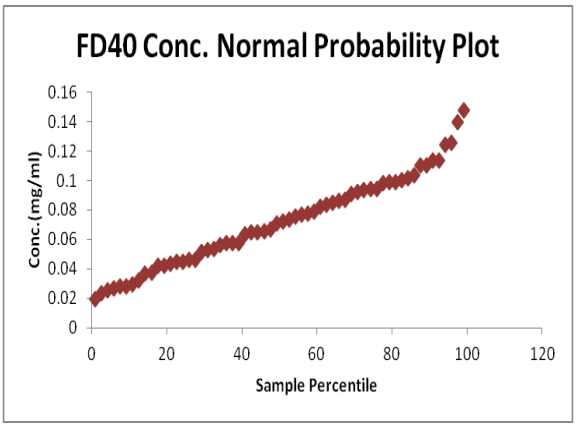
FD40 Conc. Normal Probability Plot
Conc.(mg/ml)
0.16
0.14
0.12
0.1
0.08
0.06
0.04
0.02
0
0
20
40
60
80
100
120
Sample Percentile

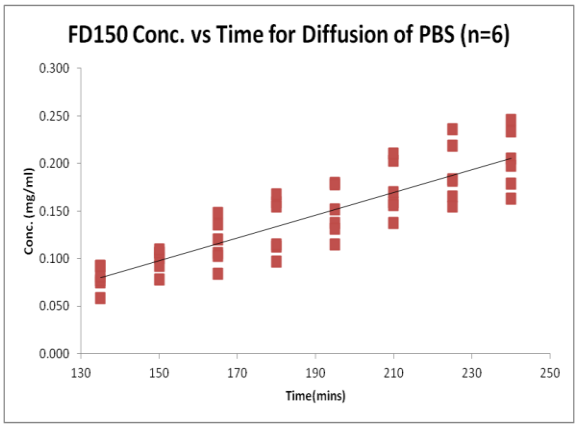
FD150 Conc. vs Time for Diffusion of PBS (n=6)
Conc. (mg/ml)
0.300
0.250
0.200
0.150
0.100
0.050
0.000
130
150
170
190
210
230
250
Time(mins)

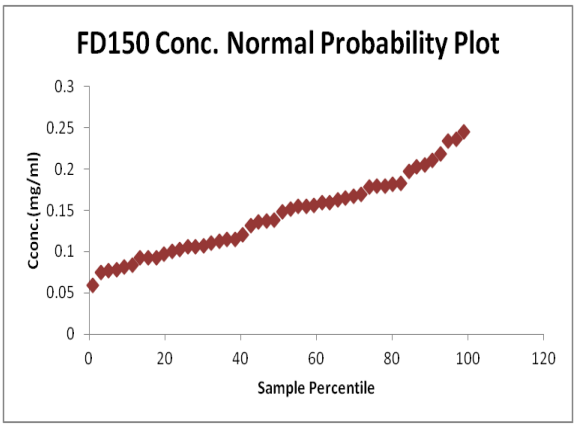
FD150 Conc. Normal Probability Plot
Cconc.(mg/ml)
0.3
0.25
0.2
0.15
0.1
0.05
0
0
20
40
60
80
100
120
Sample Percentile

Aii-2 Mutual Diffusion in Porcine Vitreous Humor

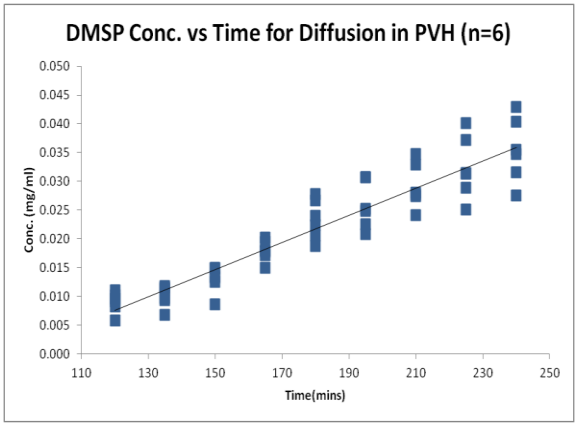

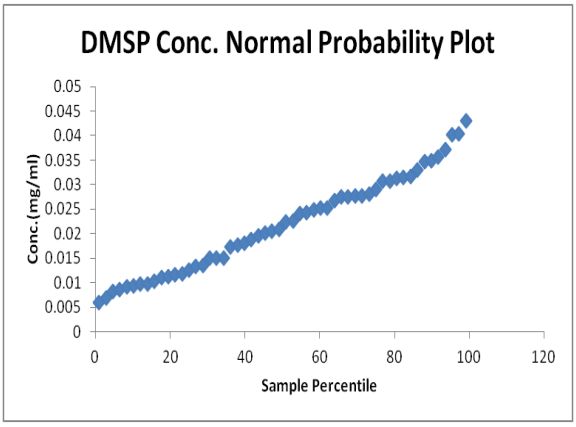

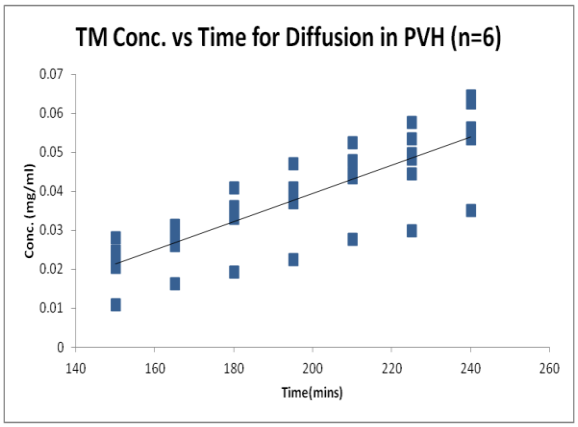

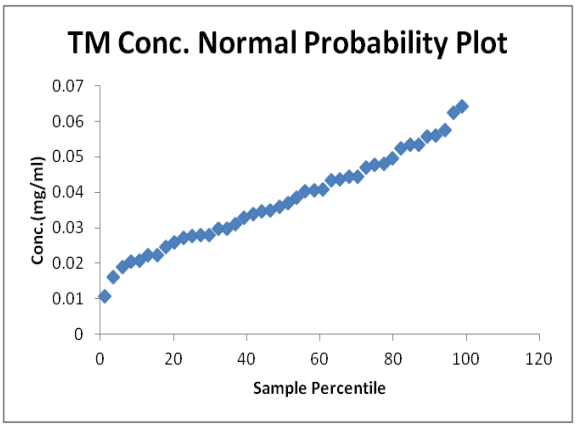

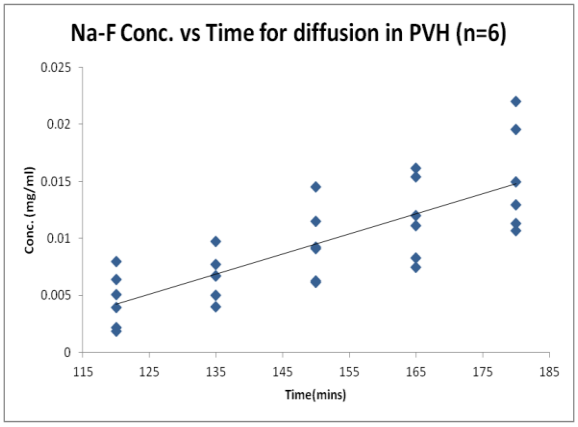

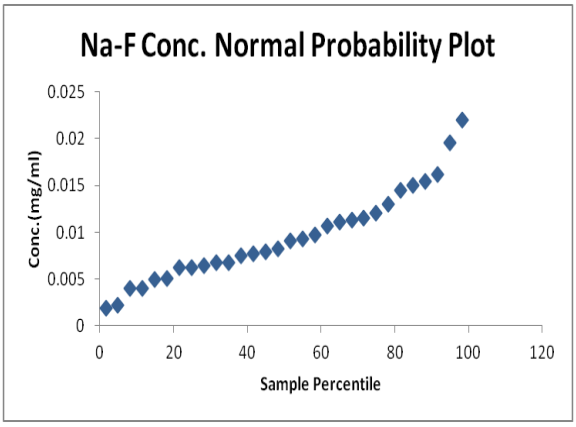

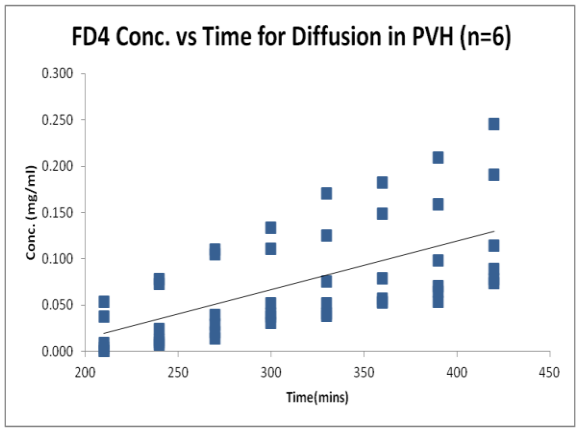
FD4 Conc. vs Time for Diffusion in PVH (n=6)
Conc. (mg/ml)
0.300
0.250
0.200
0.150
0.100
0.050
0.000
200
250
300
350
400
450
Time(mins)

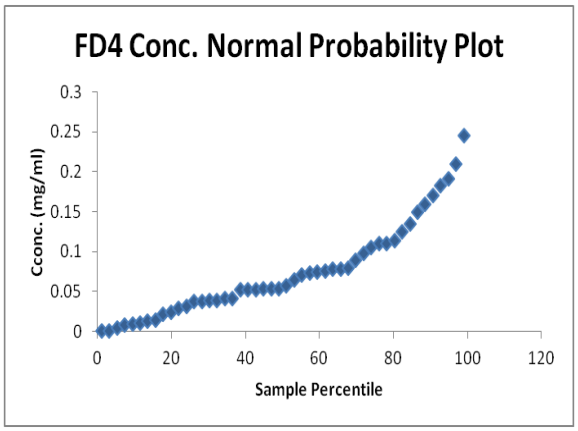
FD4 Conc. Normal Probability Plot
Cconc. (mg/ml)
0.3
0.25
0.2
0.15
0.1
0.05
0
0
20
40
60
80
100
120
Sample Percentile

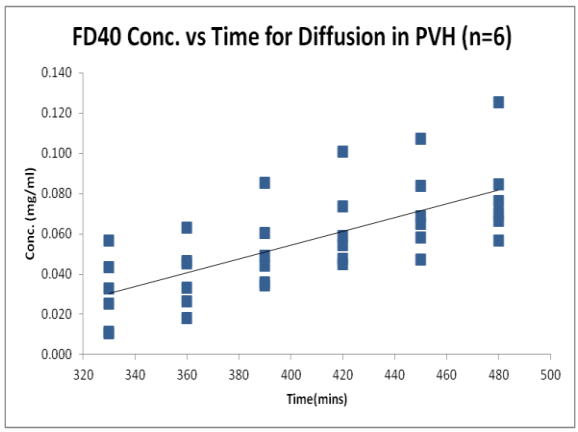
FD40 Conc. vs Time for Diffusion in PVH (n=6)
Conc. (mg/ml)
0.140
0.120
0.100
0.080
0.060
0.040
0.020
0.000
320
340
360
380
400
420
440
460
480
500
Time(mins)

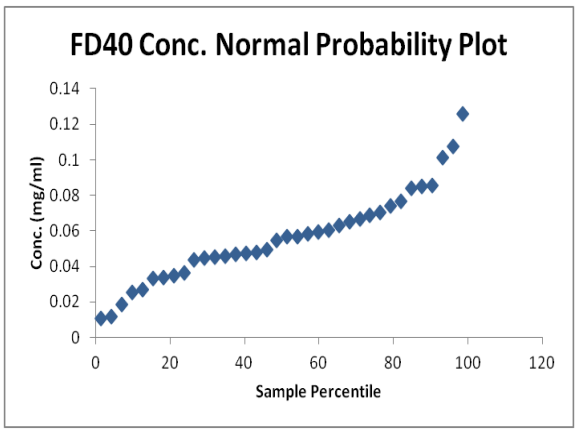
FD40 Conc. Normal Probability Plot
Conc. (mg/ml)
0.14
0.12
0.1
0.08
0.06
0.04
0.02
0
0
20
40
60
80
100
120
Sample Percentile

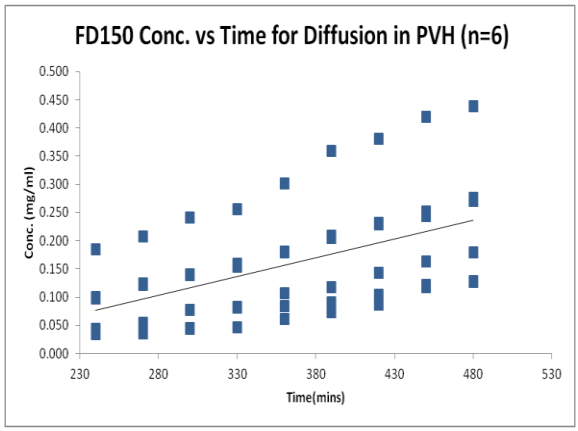
FD150 Conc. vs Time for Diffusion in PVH (n=6)
Conc. (mg/ml)
0.500
0.450
0.400
0.350
0.300
0.250
0.200
0.150
0.100
0.050
0.000
230
280
330
380
430
480
530
Time(mins)

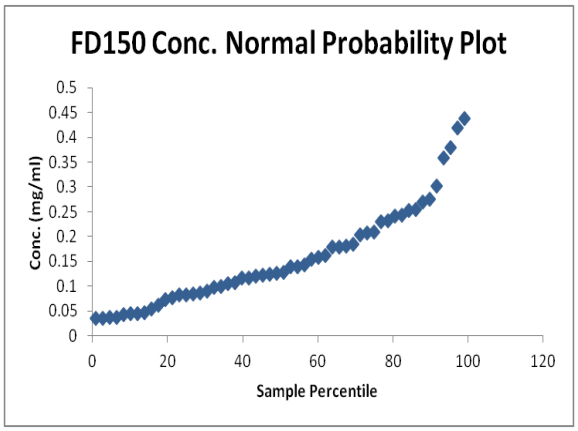
FD150 Conc. Normal Probability Plot
Conc. (mg/ml)
0.5
0.45
0.4
0.35
0.3
0.25
0.2
0.15
0.1
0.05
0
0
20
40
60
80
100
120
Sample Percentile

Aii-3 Mutual Diffusion in Rabbit Vitreous Humor

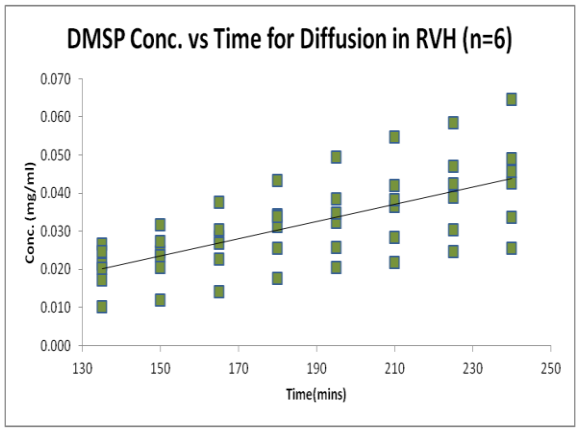

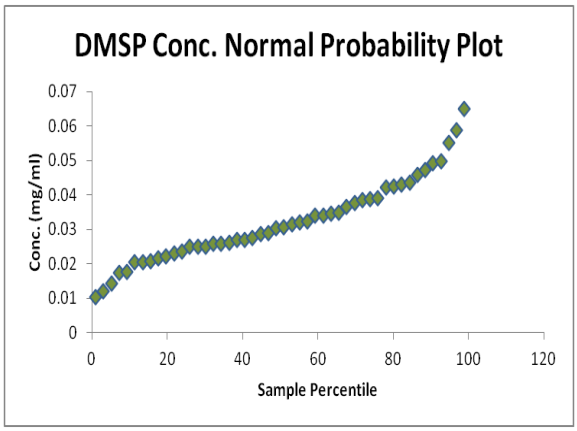

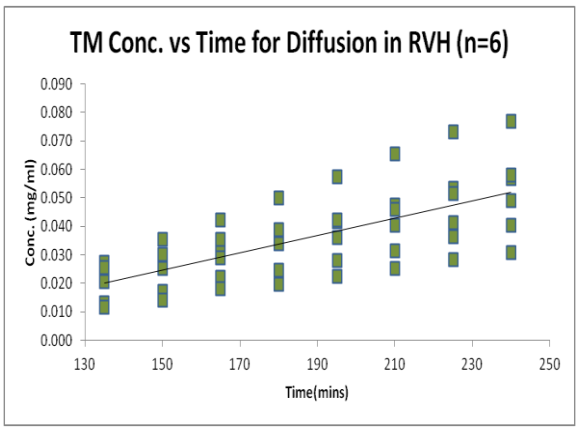

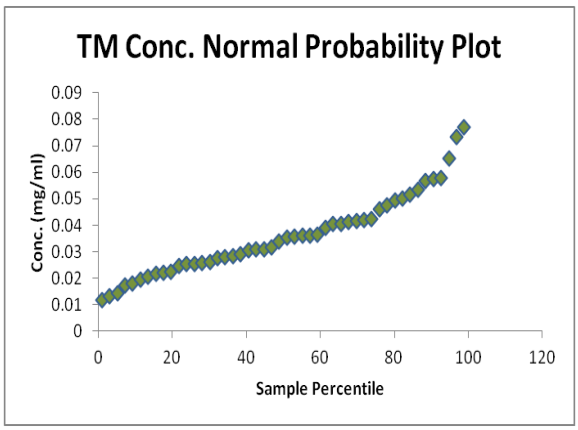

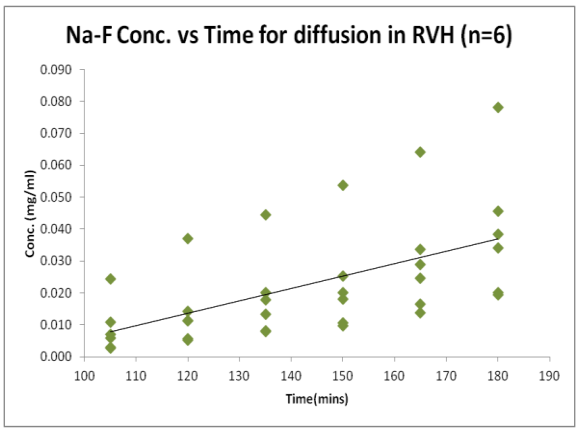

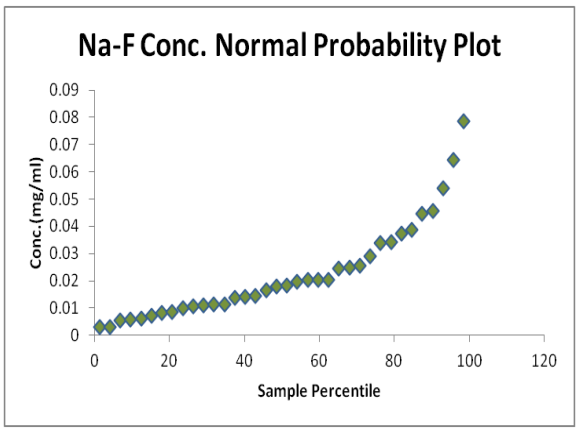

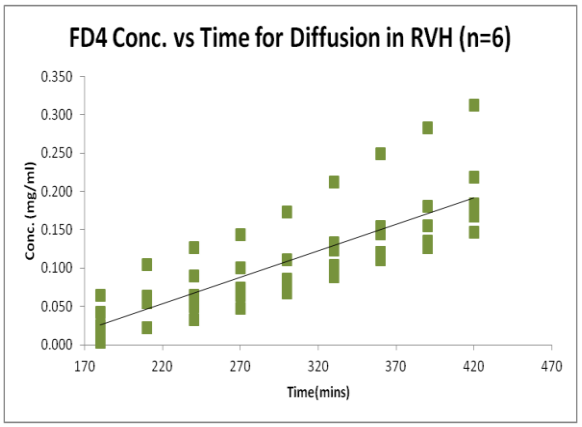
FD4 Conc. vs Time for Diffusion in RVH (n=6)
Conc. (mg/ml)
0.350
0.300
0.250
0.200
0.150
0.100
0.050
0.000
170
220
270
320
370
420
470
Time(mins)

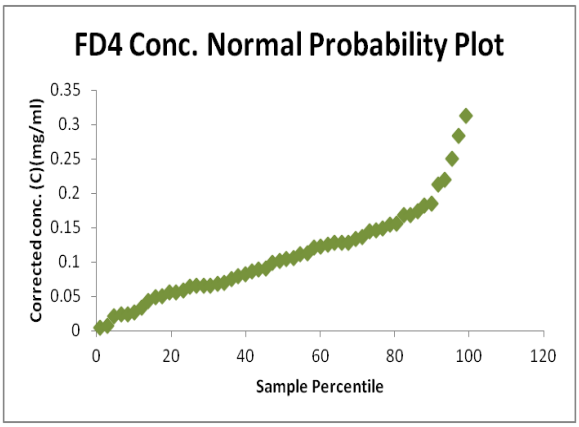
FD4 Conc. Normal Probability Plot
Corrected conc. (C)(mg/ml)
0.35
0.3
0.25
0.2
0.15
0.1
0.05
0
0
20
40
60
80
100
120
Sample Percentile

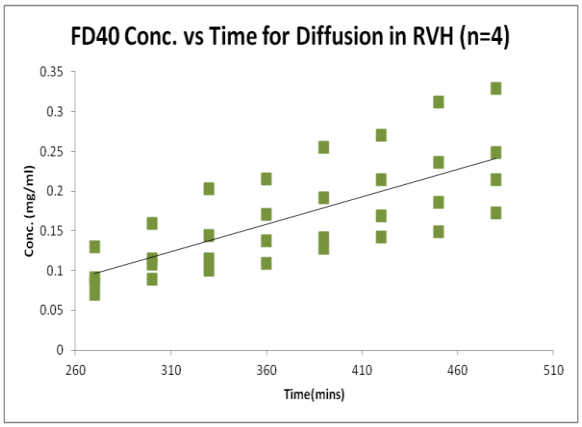
FD40 Conc. vs Time for Diffusion in RVH (n=4)
Conc. (mg/ml)
0.35
0.3
0.25
0.2
0.15
0.1
0.05
0
260
310
360
410
460
510
Time(mins)

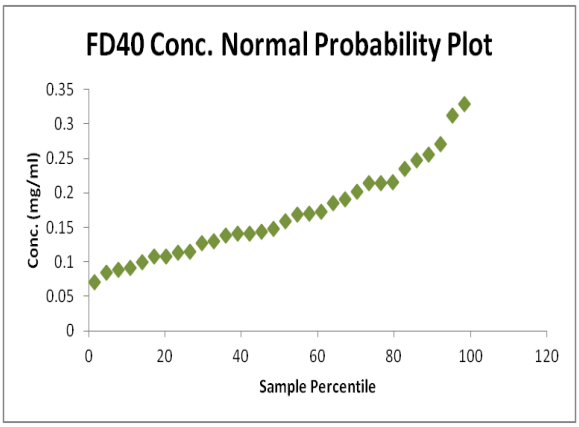
FD40 Conc. Normal Probability Plot
Conc. (mg/ml)
0.35
0.3
0.25
0.2
0.15
0.1
0.05
0
0
20
40
60
80
100
120
Sample Percentile

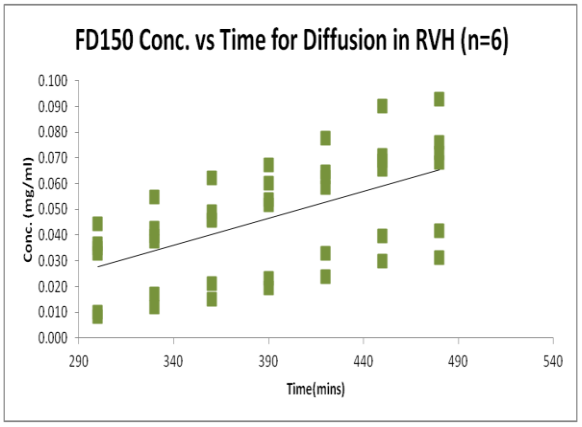
FD150 Conc. vs Time for Diffusion in RVH (n=6)
Conc. (mg/ml)
0.100
0.090
0.080
0.070
0.060
0.050
0.040
0.030
0.020
0.010
0.000
290
340
390
440
490
540
Time(mins)

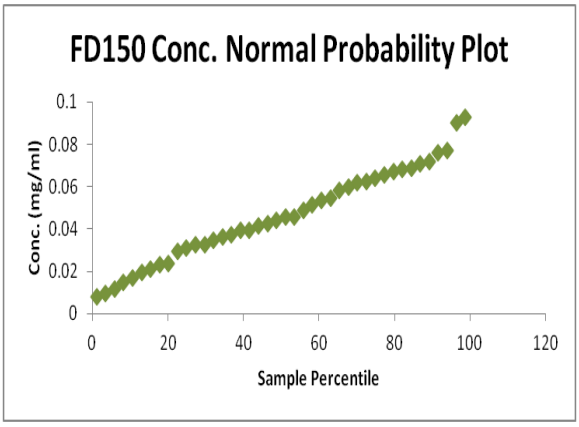
FD150 Conc. Normal Probability Plot
Conc. (mg/ml)
0.1
0.08
0.06
0.04
0.02
0
0
20
40
60
80
100
120
Sample Percentile

Appendix iii Shake Flask Method

A 1.5 ml vial was filled with 500µL of n-octanol and 500µL of 0.2mg/ml of a solution of the FITC-Dextran in PBS. The vial was vortexed for approximately one minute. After allowing the two phases to separate, 100 µL of the PBS phase was withdrawn with a micropipette and assayed using UV-visible spectrophotometry. The dye concentration in the n-octanol phase was then determined by mass balance. The ratio of the dye concentration in the n-octanol phase to the dye concentration in the PBS phase gave the $K_{o/w}$. The $K_{o/w}$ of each dye was taken as the average of n=3.

Appendix iv DOSY NMR Data

This appendix shows examples of the DOSY NMR spectrum (Figure 22), the Stejskal-Tanner plots (Figure 23) and the resulting DOSY NMR spectra (Figure 24) that were obtained for a rabbit vitreous solution sample containing a coaxial insert with a solution of TFA in D_2O. A chemical shift spectrum for each DOSY NMR experiment is obtained. All spectra were identical because the only two species with ^{19}F were TFA and DMSP. The Stejskal-Tanner plots are similar for each experiment with the degree of fitting differs among samples.

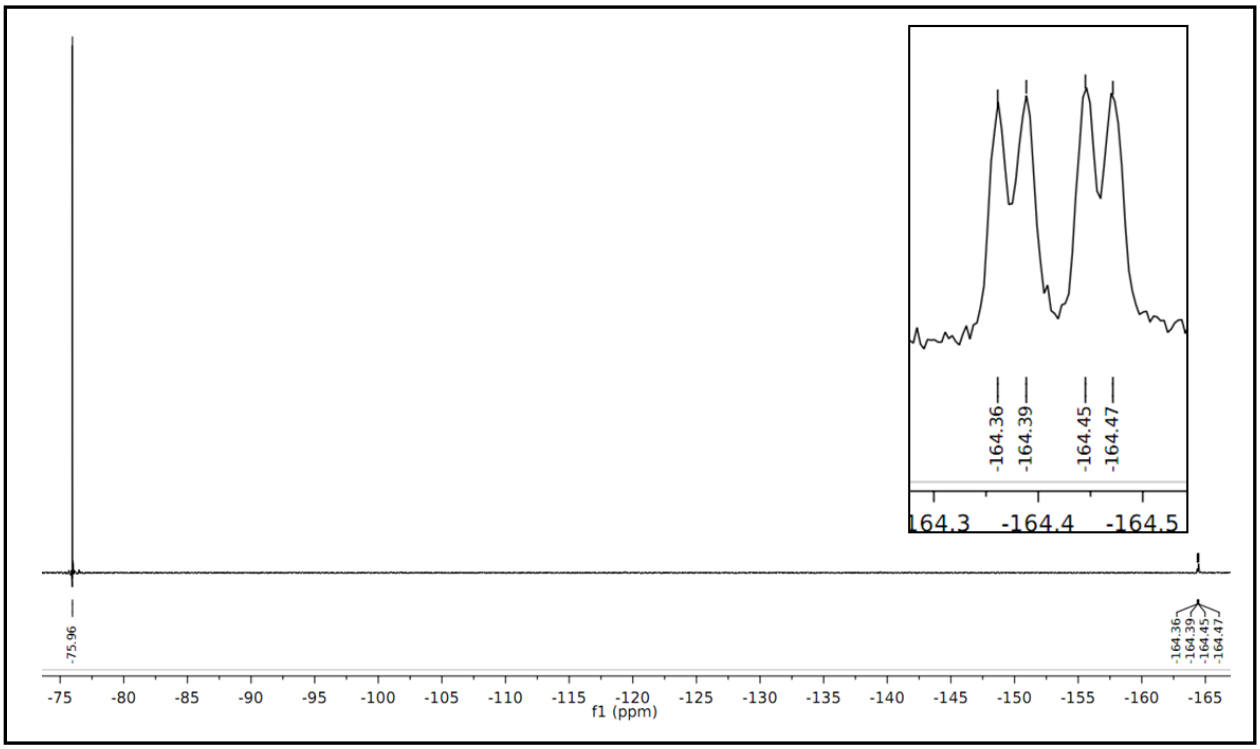

Figure 22 Chemical shift spectrum for a sample of DMPS solution in rabbit vitreous shows the TFA (in the coaxial insert) detected at 76ppm and DMSP at 164ppm (magnified in inset).The higher signal intensity for TFA corresponds to its higher concentration compared to DMSP. The multiple peaks in the inset are due to the influence of other chemical species in the DMSP compound that surround the ^{19}F, causing the drug to register at slightly different shifts.

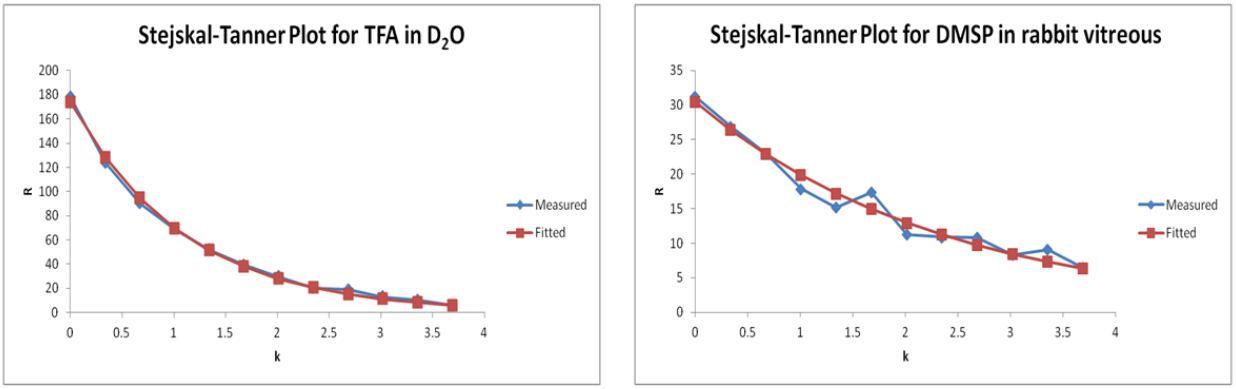

a b

Figure 23 Stejskal-Tanner Plots for (a) TFA in D_2O and (b) DMSP in rabbit vitreous

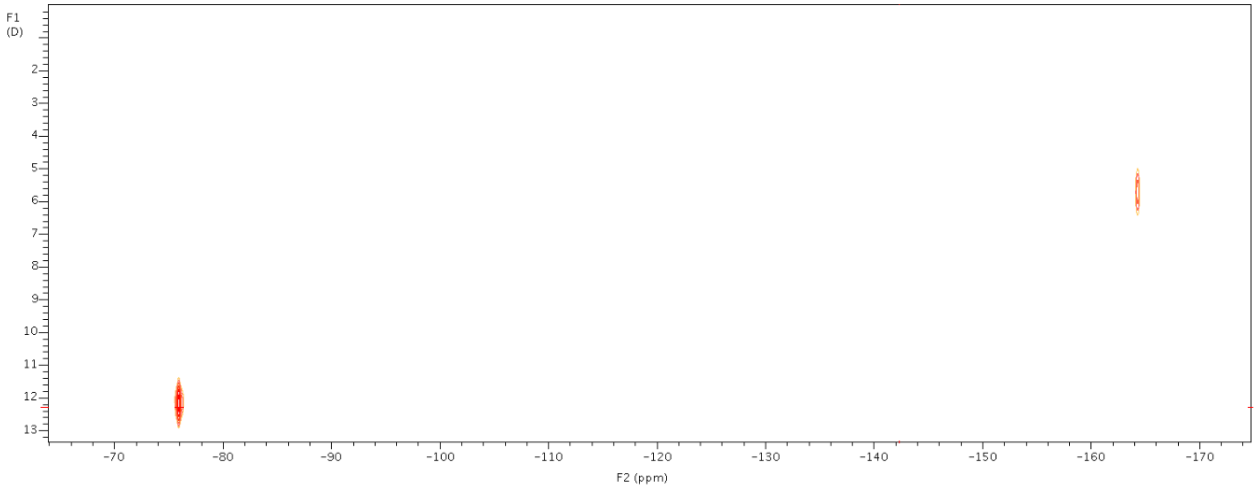

Figure 24 DOSY NMR spectrum for a rabbit vitreous-DMSP solution sample based on the fitted Stejskal-Tanner plots in Figure 23. The x-axis shows the chemical shift of the species detected, and the y axis shows the corresponding D_s

Appendix v Statistical Analysis using t-tests

Av-1 Comparing sample mean mutual diffusivities obtained in different diffusion media

For each solute, a t-test was done to assess whether the mutual diffusivities obtained in porcine and in rabbit vitreous were statistically different. The steps are as follows:

1. The parameters of interest are the population mean mutual diffusivities for the two vitreous models, say, μ_1 and μ_2, and we are interested in determining whether $\mu_1 - \mu_2 = 0$.
2. Null hypothesis: $\mu_1 - \mu_2 = 0$, or $\mu_1 = \mu_2$
3. Alternative hypothesis: $\mu_1 \neq \mu_2$
4. Confidence interval = 95%, or significance level $\alpha = 0.05$
5. For the mean of sample 1($\overline{x}_1$) and of sample 2 ($\overline{x}_2$), and associated standard errors SE_1 and SE_2, respectively, the test statistic is
$$t_0^* = \frac{\overline{x}_1 - \overline{x}_2 - (\mu_1 - \mu_2)}{\sqrt{(SE_1^2 + SE_2^2)}}$$
6. The degrees of freedom (ν) on t_0^* are found from
$$\nu = \frac{(SE_1^2 + SE_2^2)^2}{\frac{SE_1^4}{n_1 - 1} + \frac{SE_2^4}{n_2 - 1}}$$
7. With the sample mean diffusivity in rabbit vitreous as $\overline{x}_1$, and the sample mean diffusivity in porcine vitreous as $\overline{x}_2$, the t-test statistics were determined (see Table 7). If $t_0^* < t_{\alpha/2,\nu}$ (obtained from standard t – distribution table), we fail to reject the null hypothesis, which infers that the difference between the sample mean D_m in rabbit vitreous and the sample mean D_m in porcine vitreous is not statistically significant. As Table 7 shows, this result applied to all solutes.

Table 7 Comparison of sample mean diffusivities in porcine and rabbit vitreous using t-tests.

	Pig vitreous			Rabbit vitreous			t-test variables		
Molecule	*n*	D_m x 10^6	*SE* x 10^6	*n*	D_m x 10^6	*SE* x 10^6	t_0^*	ν	$t_{\alpha/2,\nu}$
Na-F	6	5.7	1.6	6	6.4	3.1	0.210	7.5	2.447
Timolol Maleate	6	5.9	1.5	6	8.0	3.7	0.509	6.7	2.447
DMSP	6	6.2	0.8	4	9.6	7.3	0.651	5.1	2.571
FD4	6	3.1	1.2	6	3.8	1.0	0.439	9.4	2.262
FD40	6	2.2	0.8	4	4.1	2.2	0.809	3.8	3.182
FD150	6	4.4	3.2	6	3.3	1.9	-0.307	8.2	2.306

Av-2 Comparing sample means of mutual and self diffusivities obtained in different diffusion media

The same steps, as described in section Av-1, were repeated to compare the sample mean D_m and sample mean D_s of DMSP obtained in PBS and vitreous humor. The results of the t-tests are reported in Table 8.

Table 8 Comparison of sample means of D_m and D_s in PBS and vitreous using t-tests.

	Self diffusivity			Mutual diffusivity			t-test variables		
Medium	*n*	D_m x 10^6	SE x 10^6	*n*	D_m x 10^6	*SE* x 10^6	t_0^*	ν	$t_{\alpha/2,\nu}$
PBS	5	5.9	0.7	6	15	1.6	5.211	6.8	2.447
Pig vitreous	6	5.5	0.7	6	6.2	0.8	0.659	9.8	2.262
Rabbit vitreous	4	5.6	0.6	4	9.6	7.3	0.546	3.0	3.182

8 References

[1] V. M. Centre.com, “The Eye and Vision.” [Online]. Available: http://www.virtualmedicalcentre.com/anatomy/the-eye-and-vision/28. [Accessed: 10-Jun-2012].

[2] A. Lens, *Ocular anatomy and physiology*. Thorofare, NJ: SLACK, 2008.

[3] H. F. Edelhauser and J. L. Ubels, “The Cornea and the Sclera,” in *Adler’s physiology of the eye : clinical application*, St. Louis: Mosby, 2003, pp. 47–114.

[4] M. J. Hogan, *Histology of the human eye;: an atlas and textbook [by] Michael J. Hogan, Jorge A. Alvarado, and Joan Esperson Weddell.* Philadelphia|bSaunders|c1971: Saunders|c1971, 1971.

[5] J. Sebag, “Macromolecular structure of the corpus vitreus,” *Progress in Polymer Science (Oxford)*, vol. 23, no. 3, pp. 415–446, 1998.

[6] Y. E. Choonara, V. Pillay, M. P. Danckwerts, T. R. Carmichael, and L. C. Du Toit, “A review of implantable intravitreal drug delivery technologies for the treatment of posterior segment eye diseases,” *Journal of Pharmaceutical Sciences*, vol. 99, no. 5, pp. 2219–2239, 2010.

[7] R. K. Balachandran and V. H. Barocas, “Computer modeling of drug delivery to the posterior eye: Effect of active transport and loss to choroidal blood flow,” *Pharmaceutical Research*, vol. 25, no. 11, pp. 2685–2696, 2008.

[8] “Vision Problems in the U.S.: Prevalence of Adult Vision Impariment and Age-Related Eye Disease in America,” *Preventative Blindness America*, 05-Sep-2012. [Online]. Available: http://www.visionproblemsus.org/amd.html.

[9] “Facts and Statistics,” *Canadian National Institute for the Blind*, 05-Sep-2012. [Online]. Available: http://www.cnib.ca/en/your-eyes/eye-conditions/amd/resources/facts-stats/Pages/default.aspx.

[10] D. S. Friedman, B. J. O’Colmain, B. Muñoz, S. C. Tomany, C. McCarty, P. T. V. M. DeJong, B. Nemesure, P. Mitchell, J. Kempen, and N. Congdon, “Prevalence of Age-Related Macular Degeneration in the United States,” *Archives of Ophthalmology*, vol. 122, no. 4, pp. 564–572, 2004.

[11] S. Macha and A. K. Mitra, “Ocular pharmacokinetics in rabbits using a novel dual probe microdialysis technique,” *Experimental Eye Research*, vol. 72, no. 3, pp. 289–299, 2001.

[12] F. Boscia, “Current approaches to the management of diabetic retinopathy and diabetic macular oedema,” *Drugs*, vol. 70, no. 16, pp. 2171–2200, 2010.

[13] K. D. Schweitzer, A. Eneh, and J. Gale, “Practice patterns of Canadian vitreoretinal specialists in diabetic macular edema treatment,” *Canadian Journal of Ophthalmology*, vol. 46, no. 3, pp. 227–231, 2011.

[14] J. Xu, J. J. Heys, V. H. Barocas, and T. W. Randolph, “Permeability and diffusion in vitreous humor: Implications for drug delivery,” *Pharmaceutical Research*, vol. 17, no. 6, pp. 664–669, 2000.

[15] J. Park, P. M. Bungay, R. J. Lutz, J. J. Augsburger, R. W. Millard, A. S. Roy, and R. K. Banerjee, “Evaluation of coupled convective-diffusive transport of drugs administered by intravitreal injection and controlled release implant,” *Journal of Controlled Release*, vol. 105, no. 3, pp. 279–295, 2005.

[16] D. H. Geroski and H. F. Edelhauser, “Drug delivery for posterior segment eye disease,” *Investigative Ophthalmology and Visual Science*, vol. 41, no. 5, pp. 961–964, 2000.

[17] H. Kim, M. J. Lizak, G. Tansey, K. G. Csaky, M. R. Robinson, P. Yuan, N. S. Wang, and R. J. Lutz, “Study of ocular transport of drugs released from an intravitreal implant using magnetic resonance imaging,” *Annals of Biomedical Engineering*, vol. 33, no. 2, pp. 150–164, 2005.

[18] D. Maurice, “Review: practical issues in intravitreal drug delivery,” *J Ocul Pharmacol Ther*, vol. 17, no. 4, pp. 393–401, Aug. 2001.

[19] F. E. Kane, J. Burdan, A. Cutino, and K. E. Green, “Iluvien^{TM}: A new sustained delivery technology for posterior eye disease,” *Expert Opinion on Drug Delivery*, vol. 5, no. 9, pp. 1039–1046, 2008.

[20] S. H. Kim, R. J. Lutz, N. S. Wang, and M. R. Robinson, “Transport barriers in transscleral drug delivery for retinal diseases,” *Ophthalmic Research*, vol. 39, no. 5, pp. 244–254, 2007.

[21] S. S. Lee, P. M. Hughes, and M. R. Robinson, “Recent advances in drug delivery systems for treating ocular complications of systemic diseases,” *Current Opinion in Ophthalmology*, vol. 20, no. 6, pp. 511–519, 2009.

[22] D. H. Geroski and H. F. Edelhauser, “Transscleral drug delivery for posterior segment disease,” *Advanced Drug Delivery Reviews*, vol. 52, no. 1, pp. 37–48, 2001.

[23] M. A. Bonini-Filho, R. Jorge, J. C. Barbosa, D. Calucci, J. A. Cardillo, and R. A. Costa, “Intravitreal injection versus sub-tenon’s infusion of triamcinolone acetonide for refractory diabetic macular edema: A randomized clinical trial,” *Investigative Ophthalmology and Visual Science*, vol. 46, no. 10, pp. 3845–3849, 2005.

[24] N. Ohguro, A. A. Okada, and Y. Tano, “Trans-Tenon’s retrobulbar triamcinolone infusion for diffuse diabetic macular edema [2],” *Graefe’s Archive for Clinical and Experimental Ophthalmology*, vol. 242, no. 5, pp. 444–445, 2004.

[25] A. A. Okada, T. Wakabayashi, E. Kojima, Y. Asano, and T. Hida, "Trans-Tenon's retrobulbar triamcinolone infusion for small choroidal neovascularisation [5]," *British Journal of Ophthalmology*, vol. 88, no. 8, pp. 1097–1098, 2004.

[26] A. A. Okada, T. Wakabayashi, Y. Morimura, S. Kawahara, E. Kojima, Y. Asano, and T. Hida, "Trans-Tenon's retrobulbar triamcinolone infusion for the treatment of uveitis," *British Journal of Ophthalmology*, vol. 87, no. 8, pp. 968–971, 2003.

[27] T. W.-Y. Lee and J. R. Robinson, "Drug Delivery to the Posterior Segment of the Eye III: The Effect of Parallel Elimination Pathway on the Vitreous Drug Level after Subconjunctival Injection," *Journal of Ocular Pharmacology and Therapeutics*, vol. 20, no. 1, pp. 55–64, 2004.

[28] C. A. Tabatabay, D. J. D'Amico, L. A. Hanninen, and K. R. Kenyon, "Experimental drusen formation induced by intravitreal aminoglycoside injection," *Archives of Ophthalmology*, vol. 105, no. 6, pp. 826–830, 1987.

[29] S. C. Pflugfelder, E. Hernandez, and S. J. Fliesler, "Intravitreal vancomycin. Retinal toxicity, clearance, and interaction with gentamicin," *Archives of Ophthalmology*, vol. 105, no. 6, pp. 831–837, 1987.

[30] K. Tojo, "A pharmacokinetic model for ocular drug delivery," *Chemical and Pharmaceutical Bulletin*, vol. 52, no. 11, pp. 1290–1294, 2004.

[31] J. Kathawate and S. Acharya, "Computational modeling of intravitreal drug delivery in the vitreous chamber with different vitreous substitutes," *International Journal of Heat and Mass Transfer*, vol. 51, no. 23–24, pp. 5598–5609, 2008.

[32] M. S. Stay, J. Xu, T. W. Randolph, and V. H. Barocas, "Computer simulation of convective and diffusive transport of controlled-release drugs in the vitreous humor," *Pharmaceutical Research*, vol. 20, no. 1, pp. 96–102, 2003.

[33] M. K. Krishnamoorthy, J. Park, J. J. Augsburger, and R. K. Banerjee, "Effect of retinal permeability, diffusivity, and aqueous humor hydrodynamics on pharmacokinetics of drugs in the eye," *Journal of Ocular Pharmacology and Therapeutics*, vol. 24, no. 3, pp. 255–267, 2008.

[34] P. J. Missel, "Hydraulic flow and vascular clearance influences on intravitreal drug delivery," *Pharmaceutical Research*, vol. 19, no. 11, pp. 1636–1647, 2002.

[35] P. J. Missel, M. Horner, and R. Muralikrishnan, "Simulating dissolution of intravitreal triamcinolone acetonide suspensions in an anatomically accurate rabbit eye model," *Pharmaceutical Research*, vol. 27, no. 8, pp. 1530–1546, 2010.

[36] S. Friedrich, Y.-L. Cheng, and B. Saville, "Finite element modeling of drug distribution in the vitreous humor of the rabbit eye," *Annals of Biomedical Engineering*, vol. 25, no. 2, pp. 303–314, 1997.

[37] T. W. Olsen, X. Feng, K. Wabner, S. R. Conston, D. H. Sierra, D. V. Folden, M. E. Smith, and J. D. Cameron, "Cannulation of the Suprachoroidal Space: A Novel Drug Delivery Methodology to the Posterior Segment," *American Journal of Ophthalmology*, vol. 142, no. 5, 2006.

[38] E. Balazs and J. Denlinger, "The Vitreus," in *The eye.*, New York,|bAcademic Press,|c1962-[67]: Academic Press, 196267, pp. 533–575.

[39] T. W. Olsen, H. F. Edelhauser, J. I. Lim, and D. H. Geroski, "Human scleral permeability: Effects of age, cryotherapy, transscleral diode laser, and surgical thinning," *Investigative Ophthalmology and Visual Science*, vol. 36, no. 9, pp. 1893–1903, 1995.

[40] S. Duke-Elder, *System of ophthalmology.*, vol. 4, 15 vols. London|bH. Kimpton|c(1958-76).: H. Kimpton|c(1958-76)., 195876.

[41] S. Gisladottir, T. Loftsson, and E. Stefansson, "Diffusion characteristics of vitreous humour and saline solution follow the Stokes Einstein equation," *Graefe's Archive for Clinical and Experimental Ophthalmology*, vol. 247, no. 12, pp. 1677–1684, 2009.

[42] N. Soman and R. Banerjee, "Artificial vitreous replacements," *Bio-Medical Materials and Engineering*, vol. 13, no. 1, pp. 59–74, 2003.

[43] "Vitreous," in *Adler's physiology of the eye : clinical application*, St. Louis: Mosby, 2003, pp. 293–316.

[44] "Vitreous Aging," in *Principles and practice of ophthalmology : basic sciences*, Philadelphia: Saunders, 1994, pp. 712–713.

[45] C. W. Oyster, *The human eye : structure and function*. Sunderland, Mass.: Sinauer Associates, 1999.

[46] T. Gherezghiher, M. C. Koss, R. E. Nordquist, and C. P. Wilkinson, "Analysis of vitreous and aqueous levels of hyaluronic acid: Application of high-performance liquid chromatography," *Experimental Eye Research*, vol. 45, no. 2, pp. 347–349, Aug. 1987.

[47] J. Sebag and E. A. Balazs, "Morphology and ultrastructure of human vitreous fibers," *Investigative Ophthalmology and Visual Science*, vol. 30, no. 8, pp. 1867–1871, 1989.

[48] U. B. G. Laurent and J. R. E. Fraser, "Turnover of hyaluronate in the aqueous humour and vitreous body of the rabbit," *Experimental Eye Research*, vol. 36, no. 4, pp. 493–504, 1983.

[49] A. Edwards and M. R. Prausnitz, "Fiber Matrix Model of Sclera and Corneal Stroma for Drug Delivery to the Eye," *AIChE Journal*, vol. 44, no. 1, pp. 214–225, 1998.

[50] M. R. Prausnitz, "Permeability of cornea, sciera, and conjunctiva: A literature analysis for drug delivery to the eye," *Journal of Pharmaceutical Sciences*, vol. 87, no. 12, pp. 1479–1488, 1998.

[51] N. P. S. Cheruvu and U. B. Kompella, “Bovine and porcine transscleral solute transport: Influence of lipophilicity and the choroid-Bruch’s layer,” *Investigative Ophthalmology and Visual Science*, vol. 47, no. 10, pp. 4513–4522, 2006.

[52] J. Ambati, C. S. Canakis, J. W. Miller, E. S. Gragoudas, A. Edwards, D. J. Weissgold, I. Kim, F. C. Delori, and A. P. Adamis, “Diffusion of high molecular weight compounds through sclera,” *Investigative Ophthalmology and Visual Science*, vol. 41, no. 5, pp. 1181–1185, 2000.

[53] A. A. Hussain, L. Rowe, and J. Marshall, “Age-related alterations in the diffusional transport of amino acids across the human Bruch’s-choroid complex,” *Journal of the Optical Society of America A: Optics and Image Science, and Vision*, vol. 19, no. 1, pp. 166–172, 2002.

[54] L. Pitkänen, V.-P. Ranta, H. Moilanen, and A. Urtti, “Permeability of retinal pigment epithelium: Effects of permeant molecular weight and lipophilicity,” *Investigative Ophthalmology and Visual Science*, vol. 46, no. 2, pp. 641–646, 2005.

[55] H. Lund-Andersen, B. Krogsaa, M. La Cour, and J. Larsen, “Quantitative vitreous fluorophotometry applying a mathematical model of the eye,” *Investigative Ophthalmology and Visual Science*, vol. 26, no. 5, pp. 698–710, 1985.

[56] C. B. Engler, B. Sander, M. Larsen, P. Dalgaard, and H. Lund-Andersen, “Fluorescein transport across the human blood-retina barrier in the direction vitreous to blood: Quantitative assessment in vivo,” *Acta Ophthalmologica*, vol. 72, no. 6, pp. 655–662, 1994.

[57] R. C. Zeimer, N. P. Blair, and J. G. Cunha-Vaz, “Pharmacokinetic interpretation of vitreous fluorophotometry.,” *Investigative Ophthalmology & Visual Science*, vol. 24, no. 10, pp. 1374 –1381, Oct. 1983.

[58] S. A. Molokhia, E.-K. Jeong, W. I. Higuchi, and S. K. Li, “Transscleral iontophoretic and intravitreal delivery of a macromolecule: Study of ocular distribution in vivo and postmortem with MRI,” *Experimental Eye Research*, vol. 88, no. 3, pp. 418–425, 2009.

[59] K. Tojo and A. Isowaki, “Pharmacokinetic model for in vivo/in vitro correlation of intravitreal drug delivery,” *Advanced Drug Delivery Reviews*, vol. 52, no. 1, pp. 17–24, 2001.

[60] M. Araie and D. M. Maurice, “The loss of fluorescein, fluorescein glucuronide and fluorescein isothiocyanate dextran from the vitreous by the anterior and retinal pathways,” *Experimental Eye Research*, vol. 52, no. 1, pp. 27–39, 1991.

[61] S. S. Hayreh, “Posterior drainage of the intraocular fluid from the vitreous,” *Experimental Eye Research*, vol. 5, no. 2, pp. 123–144, IN13–IN16, Apr. 1966.

[62] J. H. Siggers and C. R. Ethier, “Fluid mechanics of the eye,” *Annual Review of Fluid Mechanics*, vol. 44, pp. 347–372, 2011.

[63] R. Repetto, J. H. Siggers, and A. Stocchino, “Mathematical model of flow in the vitreous humor induced by saccadic eye rotations: Effect of geometry,” *Biomechanics and Modeling in Mechanobiology*, vol. 9, no. 1, pp. 65–76, 2010.

[64] A. Stocchino, R. Repetto, and J. H. Siggers, “Mixing processes in the vitreous chamber induced by eye rotations,” *Physics in Medicine and Biology*, vol. 55, no. 2, pp. 453–467, 2010.

[65] R. Repetto, A. Tatone, A. Testa, and E. Colangeli, “Traction on the retina induced by saccadic eye movements in the presence of posterior vitreous detachment,” *Biomechanics and Modeling in Mechanobiology*, vol. 10, no. 2, pp. 191–202, 2011.

[66] A. Ohtori and K. Tojo, “In vivo/in vitro correlation of intravitreal delivery of drugs with the help of computer simulation,” *Biol. Pharm. Bull*, vol. 17, no. 2, pp. 283–290, Feb. 1994.

[67] K. Tojo, K. Nakagawa, Y. Morita, and A. Ohtori, “A pharmacokinetic model of intravitreal delivery of ganciclovir,” *European Journal of Pharmaceutics and Biopharmaceutics*, vol. 47, no. 2, pp. 99–104, 1999.

[68] R. J. Kaiser and D. M. Maurice, “The diffusion of fluorescein in the lens,” *Experimental Eye Research*, vol. 3, no. 2, pp. 156–IN2, Jun. 1964.

[69] C. S. Dias and A. K. Mitra, “Vitreal elimination kinetics of large molecular weight FITC-labeled dextrans in albino rabbits using a novel microsampling technique,” *Journal of Pharmaceutical Sciences*, vol. 89, no. 5, pp. 572–578, 2000.

[70] K. A. Barton, Y.-B. Shui, J. M. Petrash, and D. C. Beebe, “Comment on: The Stokes-Einstein equation and the physiological effects of vitreous surgery [1],” *Acta Ophthalmologica Scandinavica*, vol. 85, no. 3, pp. 339–340, 2007.

[71] E. L. Cussler, *Diffusion, mass transfer in fluid systems*. New York: Cambridge University Press, 1984.

[72] R. S. Brodkey, *Transport phenomena : a unified approach*. New York: McGraw-Hill, 1988.

[73] K. H. Keller, E. R. Canales, and S. I. Yum, “Tracer and mutual diffusion coefficients of proteins.,” *The Journal of physical chemistry*, vol. 75, no. 3, pp. 379–387, 1971.

[74] R. Mills, “The intradiffusion and derived frictional coefficients for benzene and cyclohexane in their mixtures at 25°,” *Journal of Physical Chemistry*, vol. 69, no. 9, pp. 3116–3119, 1965.

[75] J. G. Albright and R. Mills, “A study of diffusion in the ternary system, labeled urea-urea-water, at 25° by measurements of the intradiffusion coefficients of urea,” *Journal of Physical Chemistry*, vol. 69, no. 9, pp. 3120–3126, 1965.

[76] N. K. Reitan, A. Juthajan, T. Lindmo, and C. De Lange Davies, "Macromolecular diffusion in the extracellular matrix measured by fluorescence correlation spectroscopy," *Journal of Biomedical Optics*, vol. 13, no. 5, 2008.

[77] S. Kwak, M. T. P. Viet, and M. Lafleur, "Self- and mutual-diffusion coefficients measurements by 31P NMR 1D profiling and PFG-SE in dextran gels," *Journal of Magnetic Resonance*, vol. 162, no. 1, pp. 198–205, 2003.

[78] *NMR spectroscopy in pharmaceutical analysis*. Boston: Elsevier, 2008.

[79] C. S. Johnson Jr., "Diffusion ordered nuclear magnetic resonance spectroscopy: Principles and applications," *Progress in Nuclear Magnetic Resonance Spectroscopy*, vol. 34, no. 3–4, pp. 203–256, 1999.

[80] E. Durand, M. Clemancey, J.-M. Lancelin, J. Verstraete, D. Espinat, and A.-A. Quoineaud, "Aggregation states of asphaltenes: Evidence of two chemical behaviors by 1H diffusion-ordered spectroscopy nuclear magnetic resonance," *Journal of Physical Chemistry C*, vol. 113, no. 36, pp. 16266–16276, 2009.

[81] K. F. Morris and C. S. Johnson Jr., "Resolution of discrete and continuous molecular size distributions by means of diffusion-ordered 2D NMR spectroscopy," *Journal of the American Chemical Society*, vol. 115, no. 10, pp. 4291–4299, 1993.

[82] D. P. Hinton and C. S. Johnson Jr., "Diffusion ordered 2D NMR spectroscopy of phospholipid vesicles: Determination of vesicle size distributions," *Journal of Physical Chemistry*, vol. 97, no. 35, pp. 9064–9072, 1993.

[83] S. Kwak and M. Lafleur, "NMR self-diffusion of molecular and macromolecular species in Dextran solutions and gels," *Macromolecules*, vol. 36, no. 9, pp. 3189–3195, 2003.

[84] S. D. McConaughy, S. E. Kirkland, N. J. Treat, P. A. Stroud, and C. L. McCormick, "Tailoring the network properties of Ca 2+ crosslinked Aloe vera polysaccharide hydrogels for in situ release of therapeutic agents," *Biomacromolecules*, vol. 9, no. 11, pp. 3277–3287, 2008.

[85] R. Colsenet, O. Söderman, and F. Mariette, "Pulsed field gradient NMR study of poly(ethylene glycol) diffusion in whey protein solutions and gels," *Macromolecules*, vol. 39, no. 3, pp. 1053–1059, 2006.

[86] G. Lafitte, K. Thuresson, and O. Söderman, "Mixtures of mucin and oppositely charged surfactant aggregates with varying charge density. Phase behavior, association, and dynamics," *Langmuir*, vol. 21, no. 16, pp. 7097–7104, 2005.

[87] D. Burstein, M. L. Gray, A. L. Hartman, R. Gipe, and B. D. Foy, "Diffusion of small solutes in cartilage as measured by nuclear magnetic resonance (NMR) spectroscopy and imaging," *Journal of Orthopaedic Research*, vol. 11, no. 4, pp. 465–478, 1993.

[88] B. Antalek, “Using PGSE NMR for chemical mixture analysis: Quantitative aspects,” *Concepts in Magnetic Resonance Part A: Bridging Education and Research*, vol. 30, no. 5, pp. 219–235, 2007.

[89] V. Martínez, M. I. Maguregui, R. M. Jiménez, and R. M. Alonso, “Determination of the pK(a) values of β-blockers by automated potentiometric titrations,” *Journal of Pharmaceutical and Biomedical Analysis*, vol. 23, no. 2–3, pp. 459–468, 2000.

[90] J.-P. Sylvestre, R. H. Guy, and M. B. Delgado-Charro, “In Vitro optimization of dexamethasone phosphate delivery by iontophoresis,” *Physical Therapy*, vol. 88, no. 10, pp. 1177–1185, 2008.

[91] R. Hayward, K. J. Saliba, and K. Kirk, “The pH of the digestive vacuole of Plasmodium falciparum is not associated with chloroquine resistance,” *Journal of Cell Science*, vol. 119, no. 6, pp. 1016–1025, 2006.

[92] H. Todo, E. Kimura, Y. Yasuno, Y. Tokudome, F. Hashimoto, Y. Ikarashi, and K. Sugibayashi, “Permeation pathway of macromolecules and nanospheres through skin,” *Biological and Pharmaceutical Bulletin*, vol. 33, no. 8, pp. 1394–1399, 2010.

[93] K. Patel, H. Patel, J. Patel, and G. Deshmuk, “Formulation and Evaluation of Transdermal Drug Delivery System of Timolol Maleate as a Model Drug,” *Americal Journal of Pharmatech Research*, vol. 1, no. 1, pp. 7–17, 2011.

[94] S. Einmahl, M. Zignani, E. Varesio, J. Heller, J. L. Veuthey, C. Tabatabay, and R. Gurny, “Concomitant and controlled release of dexamethasone and 5-fluorouracil from poly(ortho ester),” *International Journal of Pharmaceutics*, vol. 185, no. 2, pp. 189–198, 1999.

[95] Fluxion, “Viscosity: Understanding effects of viscosity in the BioFlux system,” 23-Jul-2012. [Online]. Available: http://www.iul-instruments.de/pdf/168_BioFlux_Viscosity_TechNote-1038-01.pdf.

[96] A. V. Noulas, A. D. Theocharis, E. Feretis, N. Papageorgakopoulou, N. K. Karamanos, and D. A. Theocharis, “Pig vitreous gel: Macromolecular composition with particular reference to hyaluronan-binding proteoglycans,” *Biochimie*, vol. 84, no. 4, pp. 295–302, 2002.

[97] S. A. BORUCHOFF and A. M. WOODIN, “Viscosity and composition of solutions derived from rabbit vitreous humour.,” *The British journal of ophthalmology*, vol. 40, no. 2, pp. 113–118, 1956.

[98] “Ozurdex(dexamethasone intravitreat implant)0.7mg,” 30-Jul-2012. [Online]. Available: http://www.ozurdex.com/HowItWorks.aspx.

[99] M. Santoro, P. Marchetti, F. Rossi, G. Perale, F. Castiglione, A. Mele, and M. Masi, “Smart approach to evaluate drug diffusivity in injectable agar-carbomer hydrogels for drug delivery,” *Journal of Physical Chemistry B*, vol. 115, no. 11, pp. 2503–2510, 2011.

[100] T. Casalini, M. Salvalaglio, G. Perale, M. Masi, and C. Cavallotti, “Diffusion and aggregation of sodium fluorescein in aqueous solutions,” *Journal of Physical Chemistry B*, vol. 115, no. 44, pp. 12896–12904, 2011.

[101] V. C. P. Da Costa, A. C. F. Ribeiro, A. J. F. N. Sobral, V. M. M. Lobo, O. Annunziata, C. I. A. V. Santos, S. A. Willis, W. S. Price, and M. A. Esteso, “Mutual and self-diffusion of charged porphyrines in aqueous solutions,” *Journal of Chemical Thermodynamics*, vol. 47, pp. 312–319, 2012.

[102] W. Z. Collison and M. J. Kushner, “Ion drag effects in inductively coupled plasmas for etching,” *Applied Physics Letters*, vol. 68, no. 7, pp. 903–905, 1996.

[103] J. Barar, A. R. Javadzadeh, and Y. Omidi, “Ocular novel drug delivery: Impacts of membranes and barriers,” *Expert Opinion on Drug Delivery*, vol. 5, no. 5, pp. 567–581, 2008.